The Enantioselective Hydrogenation of Pyruvate Esters over Cinchona Alkaloid Modified Platinum Catalysts

Thesis submitted in accordance with the requirements of the University of Cardiff for the degree of Doctor of Philosophy by

Robert Leyshon Jenkins

September 2007

ProQuest LLC
789 East Eisenhower Parkway
P.O. Box 1346
Ann Arbor, MI 48106-1346

Acknowledgements

I have many, many people to thank for helping me to complete this thesis and the work it contains. Firstly to Graham Hutchings, to who I am very grateful for all the help and support given to me over the last 10 years. Secondly many thanks to Paul McMorn, Richard Wells, Nick Dummer and Horse McGuire for helpful advice and guidance. Additionally thanks must go to Gary Attard for the many fruitful debates and whose enthusiasm for the subject is second to none.

Thanks to my support staff colleagues Trish, John, Alun, Ricky, G, Rob A , Jim, Sham, Robin, Dave, Gary, Jamie, J. C., and Mal for their help and many 'favours'.

A special thank you to Nick Tomkinson, Mike Coogan and Dave Willock for their help and advice. Also a thank you to Dave Knight for his support.

A big thank you to my parents and parents in law for your love and support, Dad I wish you were here to see me complete this thesis. We all miss you very much.

My sincerest thanks and love go to Helen, Aaron and Joseph who have sacrificed much to enable me to finish this thesis, your love, encouragement and understanding have helped me tremendously and I am forever in your debt.

Publications

The work in this thesis has led to the following publications:

Enantioselective hydrogenation of pyruvate esters in the mesoporous environment of Pt-MCM-41: J. Hall, J.E. Halder, G.J. Hutchings, R.L. Jenkins, P. Johnston, P. McMorn, P.B.Wells and R.P.K. Wells, *Topics in Catalysis.*, **11-12** (2000) 351.

Continuous stable enantioselective hydrogenation of alkyl pyruvate esters using pre-modified cinchonide platinum catalysts: R.L. Jenkins, P. McMorn and G.J. Hutchings, *Catal. Lett.*, **100** (3-4) (2005) 255.

Unexpected inversion of enantioselectivity during the hydrogenation of ethyl pyruvate using hydroquinidine-4-chlorobenzoate and hydroquinine-4-chlorobenzoate modified Pt/Al_2O_3: R.L. Jenkins, N. Dummer, X. Li, S.M. Bawaked, P. McMorn, R.P. Wells, A. Burrows, C.J. Kiely and G.J. Hutchings, *Catal. Lett.*, **110** (1-2) (2006) 135.

Abstract

The enantioselective hydrogenation of pyruvate esters has been investigated over cinchona alkaloid modified platinum catalysts. Three topics have been examined:

(i) AlMCM-41 as a novel support for the platinum catalysed enantioselective hydrogenation of ethyl pyruvate.

(ii) The enantioselective hydrogenation of pyruvate esters over cinchonidine pre-modified Pt/γ-Al_2O_3 catalysts in a continuous flow reactor.

(iii) An investigation into the modifier concentration dependence on the sense of enantioselectivity in ethyl pyruvate hydrogenation exhibited by derivatives of hydroquinidine and hydroquinine.

A series of Pt-AlMCM-41 catalysts were synthesised using both *C16*- and *C18*- alkyl chain surfactant templates with platinum loadings approaching 2 wt/%.

High resolution transmission electron microscopy (HRTEM) data confirmed retention of the mesoporous structure in the active catalysts and gave information on the platinum particle size and their location within the mesopore. High resolution magic angle spinning (HRMAS) ^{27}Al NMR was used to study the movement of aluminium within the mesoporous structure during the different preparation stages. The resultant platinum catalysts afforded enantioselectivities comparable to that obtained with the standard reference catalyst EUROPT-1 (6.3% Pt/silica), at rates moderated by an order of magnitude by mass transfer limitations. This is the first report of an enantioselective hydrogenation occurring in a mesopore.

The hydrogenation of pyruvate esters over cinchonidine pre-modified catalysts in a continuous flow reactor operating at ambient temperature and pressure (0.25 bar/g) has

been investigated. With dichloromethane as a solvent sustained enantiomeric excess of > 70% was maintained at very low cinchonidine/platinum ratios and are comparable to the enantioselectivity achieved when the reaction is conducted in the same solvent at autogeneous pressures (50 bar). When dichloromethane is used as a reaction solvent conversion is seen to decrease with time on line and is considered to be the result of polymer formation on the catalyst surface. The pre-treatment of the catalyst bed with (*R*)-ethyl lactate prior to the introduction of methyl pyruvate is detrimental to the catalytic system with an 18 % drop in enantioselectivity, potentially the result of an unfavourable interaction between lactate and modifier.

In the enantioselective hydrogenation of ethyl pyruvate over hydroquinidine-4-chlorobenzoate modified Pt/γ-Al_2O_3 the sense of enantioselectivity is a function of modifier concentration. At low concentration (*S*)-ethyl lactate is preferentially formed while at high concentration (*R*)-ethyl lactate is the preferred enantiomer with an enantiomeric swing of 40% across the modifier range tested. The opposite trend with a similar magnitude was observed with hydroquinine-4-chlorobenzoate. The effect is sensitive to the way in which the Pt/γ-Al_2O_3 catalyst is prepared with reduction temperature determining if inversion of enantioselectivity was observed. The same experiments conducted over platinum silica and platinum graphite catalysts failed to demonstrate the same modifier concentration dependence on the sense of enantioselectivity.

Abbreviations

BET	Brunauer, Emmet and Teller
BJH	Barret, Joyner and Halenda
CFR	Continuous Flow Reactor
CH_2Cl_2/DCM	Dichloromethane
cm^3	Cubic Centimetre
e.e.	Enantiomeric Excess
g	Gram
GHSV	Gas Hourly Space Velocity
GC	Gas Chromatography
h	Hour
HPLC	High Performance Liquid Chromatography
HRTEM	High Resolution Transmission Electron Microscopy
ICP-MS	Inductively Coupled Plasma Mass Spectrometry
K	Kelvin
MAS-NMR	Magic Angle Spinning Nuclear Magnetic Resonance
min	Minutes
NMR	Nuclear Magnetic Resonance
ppm	Parts Per Million
Pt	Platinum
s	Seconds
TGA	Thermal Gravimetric Analysis
UV/Vis	Ultra Violet / Visible
XRD	X-ray Diffraction

Table of Contents

Chapter One

Chapter One Introduction

1.1 Introduction

1.1.1 Historical perspective

It was in the early nineteenth century that the first reports of catalysis were documented. Michael Faraday reported that it was possible to maintain the oxidation of ethanol vapour in the presence of porous platinum. It was with the same metal that J.W. Dobereiner discovered that hydrogen oxidation could be achieved at room temperature. Peregrine Philips patented the role of platinum in the oxidation of sulphur dioxide in 1831; this patent was to form the basis of the contact process, the industrial manufacture of sulphuric acid.

The first attempt at rationalising these unusual observations was made in 1836 by J. J. Berzelius [1] who explained the effect as follows:

'I shall call it the catalytic power of substances, and the decomposition by means of this power catalysis, just as we use the word analysis to denote the separation of the component parts of bodies by means of chemical forces. Catalytic power actually means that substances are able to awake affinities, which are asleep at this temperature by their mere presence and not by their own affinity'.

Thus 'by waking affinities which are asleep' a catalyst breaks down the barriers, which would otherwise inhibit the reaction between molecules.

1.2 Definitions and terms

1.2.1 Catalyst

A catalyst can be defined as a substance, which increases the rate at which a chemical reaction approaches equilibrium without being consumed in the process.

The primary effect of a catalyst is to increase the rate at which the reaction proceeds; a catalyst cannot be used to initiate a reaction that is not thermodynamically feasible. The enthalpy of a reaction as well as other thermodynamic factors are a function of the nature of the reactants and products and cannot be modified through the presence of a catalyst. However, kinetic factors such as the rate constant, activation energy and the nature of the transition state are characteristics of a reaction, which can be influenced through the presence of a catalyst.

The Arrhenius equation below (Equation 1.1) outlines the parameters that influence the rate of reaction at a given temperature.

$$k = A \exp(-E_a/RT) \qquad \text{Equation 1.1}$$

Where:

K = rate constant

A = collision frequency

Ea = activation energy

T = temperature of reaction

R = gas constant

The value of the collision frequency, A, for a catalysed reaction is much less than that observed in an un-catalysed reaction since the number of collisions between reactant

molecules and the catalytic site are relatively small in number compared to those collisions which occur solely between reactant molecules. Thus, if a catalysed reaction is to compete with an un-catalysed reaction in terms of rate, the resultant activation energy of the catalysed reaction must be substantially lower than that observed in the absence of the catalyst. A catalyst therefore increases the rate of reaction through a decrease in activation energy; that is, a catalyst provides a more energetically favourable pathway by which the reaction can proceed. The final part of the above definition states that the catalyst is not consumed during the reaction and will therefore continue to operate indefinitely. However, in practice this is seldom the case, as many catalysts are prone to some form of degradation be it through sintering, leaching or coking.

1.2.2 Catalyst type

It is possible to divide the area of catalysis into three discrete categories, homogeneous, heterogeneous and enzymatic catalysis:

1.2.2.1 Homogeneous catalysis

When a catalyst is used in a reaction and is of the same phase as the reactant(s) and no phase boundary is present it is termed homogeneous catalysis. This type of catalysis can take place in the gas phase, for example in the nitrous oxide catalysed oxidation of sulphur dioxide, or in the liquid phase, in the base catalysed hydrolysis of an ester.

1.2.2.2 Heterogeneous catalysis

Catalysis becomes heterogeneous when the addition of a catalyst to a reaction increases the number phases present in the system i.e. a phase boundary separates the catalyst from

the reactants and the reaction occurs at an interface. A number of different phase combinations can occur in heterogeneous catalysis, as shown in Table 1.1.

Table 1.1 The different phase combinations of heterogeneous catalysis.

Catalyst phase	Reactant phase	Catalysed Reaction
Liquid	Gas	Alkene polymerisation catalysed by H_3PO_4 [2]
Solid	Liquid	Decomposition of H_2O_2 catalysed by gold [3]
Solid	Gas	Synthesis of ammonia catalysed by iron [4]

1.2.2.3 Enzymatic catalysis

Enzymatic catalysis is the catalysis of natural processes or the mimicking of these natural processes. Enzymes are complex organic molecules, usually proteins, with molecular weights ranging between 6000 and 600,000 amu; the catalytic enzyme process is neither homogeneous nor heterogeneous in character but lies somewhere in between the two.

1.2.3 Catalytic cycle

The catalytic properties of solid surfaces arise from their ability to interact with reactant molecules. The process of interaction is called *adsorption*. As a result of this interaction, new chemical species are formed and new reaction pathways become accessible (Figure 1.1). Molecules that react at the catalyst surface via the gas or liquid phase are termed substrates and during the process of adsorption, substrate molecules that accumulate at the solid surface (adsorbent) are termed adsorbates. The process by which molecules leave the solid surface either unchanged (as substrate) or chemically changed (as product) is termed *desorption*.

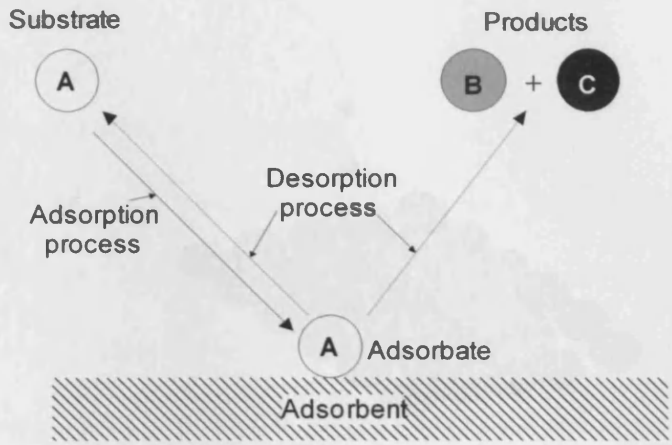

Figure 1.1 Graphical representation of the adsorption and desorption processes

1.2.4 Adsorption

Chemical adsorption or chemisorption involves the formation of a chemical bond between the adsorbent and the adsorbate. Physical adsorption or physisorption involves only weak van der Waals interactions between the adsorbent and adsorbate; such weak interactions do not directly contribute to catalysis.

Thus, in any catalytic surface reaction, the essential components of the mechanism are the chemisorption of substrate molecules and desorption of products. Chemisorption of a substrate is a necessity to explain the ability of a catalyst to facilitate its conversion to products. There are two modes of chemisorption:

1.2.4.1 Dissociative adsorption

Many molecules are unable to interact with the 'free valencies' of a metal surface without undergoing bond cleavage on adsorption. This type of chemisorption is termed dissociative adsorption; molecular hydrogen is a substrate molecule that undergoes this type of chemisorption at a transition metal surface (Figure 1.2).

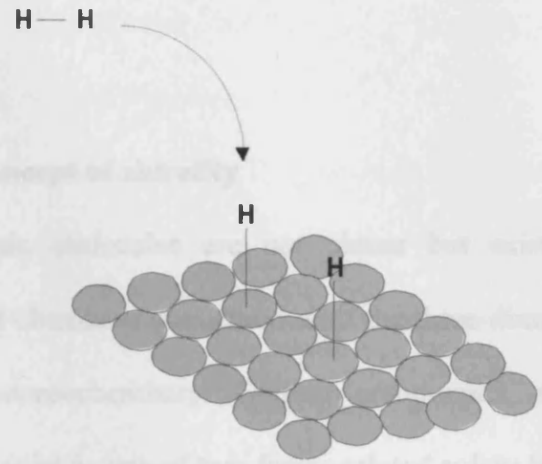

Figure 1.2 Dissociative adsorption of molecular hydrogen at a transition metal surface.

1.2.4.2 Associative adsorption

Substrate molecules that possess a lone pair of electrons such as ammonia, or an electron rich π-bond system such as that found in ethene can adsorb onto a metal surface without undergoing dissociation. This form of chemisorption is termed associative adsorption and is accompanied with molecular orbital rehybridisation within the substrate molecule. For example, when ethene associately adsorbs onto a metal surface its carbon atoms undergo molecular orbital rehybridisation to adopting a sp^3 configuration. (Figure 1.3).

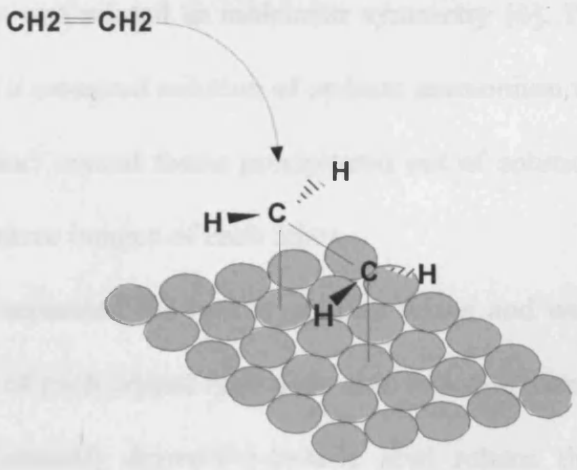

Figure 1.3 Associative adsorption of an ethene molecule at a transition metal surface.

1.3 Chirality

1.3.1 The origin and concept of chirality

The majority of organic molecules are not planar but exist as three-dimensional structures; the branch of chemistry concerned with the three-dimensional nature of these molecules is termed stereochemistry. Certain compounds, which have the same molecular formula, can exist in one of two forms related solely by the fact they are non-superimpossable mirror images of each other. These molecules are said to be chiral and are known as enantiomers (or enantiomeric with respect to each other); a mixture of enantiomers present in a 1:1 ratio is termed a racemic mixture, while the enrichment of a particular enantiomer is measured by its enantiomeric excess (e.e.) A simple example of a chiral molecule is given in Figure 1.4.

The concept of chirality and that of enantiomers was first proposed by Jean-Baptiste Biot in 1815. Biot [5] made the remarkable observation that when plane polarized light waves oscillating in a single plane, passed through certain compound containing solutions, the plane of polarization was rotated. It was several decades later, in 1848, that Louis Pasteur proposed that chirality was related to molecular symmetry [6]. Pasteur discovered that when he recrystallised a saturated solution of sodium ammonium tartrate at temperatures below 28 °C, two distinct crystal forms precipitated out of solution, these crystals were non-superimposable mirror images of each other.

Pasteur painstakingly separated the two crystalline forms and was able to demonstrate that separate solutions of each crystal type were able to rotate plane polarized light in the opposite directions; (natural) *dextro*-(+)-tartaric acid rotates the plane to the right whereas the other form, (-)-tartaric acid, rotated the plane in the opposite direction.

Pasteur postulated that the molecular structures of (+) - and (-)-tartaric acid must be related to their three-dimensional structure.

It was not until 1874 that Van't Hoff [7] proposed a precise theory for molecular asymmetry. Van't Hoff recognised that a sp^3 hybridised carbon atom, with all of its four linking bonds pointing towards the corners of a regular tetrahedron could generate two non-superimposable molecules (enantiomers), if each of the substituents attached to the central carbon atom were different.

LeBel [8] was to take the concept of chirality one step further when he considered the asymmetry of the whole molecule. LeBel realised that a molecule can be chiral even if there was no asymmetric carbon atom present. LeBel attributed the chirality to the lack of symmetry found in molecules where rotation about a carbon-carbon bond is hindered.

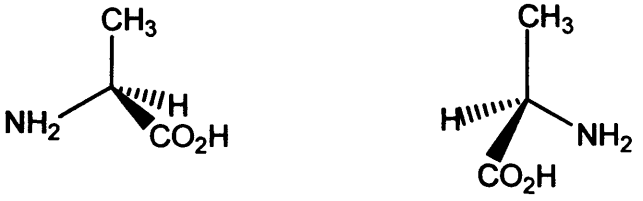

Figure 1.4 The two enantiomers of alanine.

1.3.2 Relevance of chirality

Chirality is important in the context of biological activity, because at a molecular level asymmetry dominates biological processes. In bioactive compounds in which a stereogenic centre is present, great differences are usually observed in the activities of each of the different enantiomers. This phenomenon is observed for almost all bioactive substances; such as drugs, insecticides, herbicides, flavours and fragrances [9]. The most infamous example in this respect is the 'thalidomide tragedy'. Thalidomide, commercially

sold under the name Softenon™, was prescribed in racemic form (Figure 1.5). The (*R*)-enantiomer of the drug was effective in alleviating the symptoms of morning sickness in pregnant women. The mirror image, however, had devastating effects on the development of the unborn foetus [10].

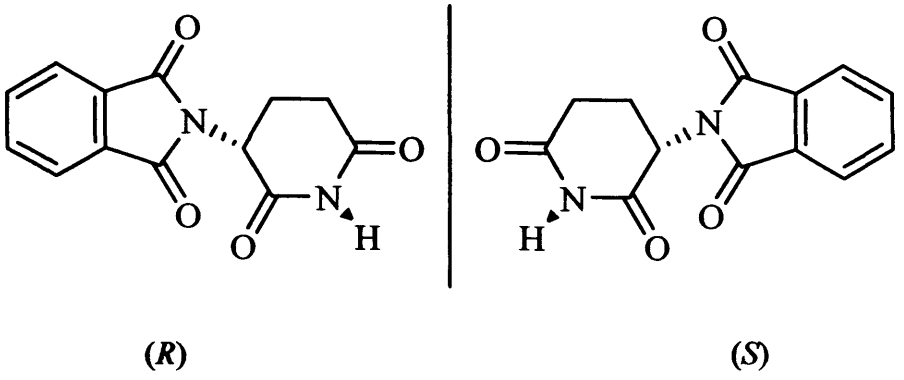

(*R*) (*S*)

Figure 1.5 The two enantiomers of thalidomide.

Thus, for the many applications of chiral compounds the racemic form has become totally unacceptable. As a consequence, the demands for effective methodologies for the production of enantiomerically pure (e.e. >99%) and enantiomerically enriched compounds has increased and will undoubtedly continue to increase in the foreseeable future [11].

1.4 Preparation of Enantiopure Chiral Compounds

There are a number of methods which have been developed for the production of enantiopure (e.e. >99%) and enantioenriched compounds. These are summarised below:

1.4.1 The chiral pool

The chiral pool refers to the readily available assortment of chiral compounds originating from natural sources such as plants, trees and sea creatures etc. These enantiomerically

pure compounds can be isolated and synthetically incorporated in the production of compounds. For example, in the early stages of drug development [12].

1.4.2 Chiral resolution

The separation of enantiomers by resolution is the most widely used industrial technique in the production of enantiomerically pure products [13]. Methods for the resolution of enantiomers include kinetic resolution: either chemical [14] or enzymatic [15] or classical resolution: *via* the preferential crystallization of diastereomeric adducts formed between enantiomers and chiral auxiliaries. These diastereoisomers possess different physical and chemical properties, which allow separation using conventional chromatography techniques such as high performance liquid chromatography (HPLC).

1.4.3 The use of pro-chiral substrates

1.4.3.1 Stoichiometric asymmetric synthesis

Stoichiometric asymmetric organic synthesis [16] is a common method for the introduction of chirality into a molecule. It involves the reaction between a pro-chiral substrate and a chiral auxiliary, where the chiral entity is used to direct the reaction onto a pro-chiral centre. The reaction is diastereoselective in that one of two possible diastereoisomers is preferentially formed. The removal of the chiral auxiliary from the diastereoisomers gives a mixture of enantiomers with one predominating.

1.4.3.2 Biocatalysis

Originally it was believed that the synthesis of enantiomerically pure compounds from pro-chiral substrates was only possible using biocatalytic processes. Indeed, some of the

highest enantioselectivities and rates of reaction have been achieved using biocatalytic systems [17]. However, there are drawbacks, biocatalysts can be highly substrate specific and have been known to selectively catalyse the reaction of only one particular substrate (Figure 1.6).

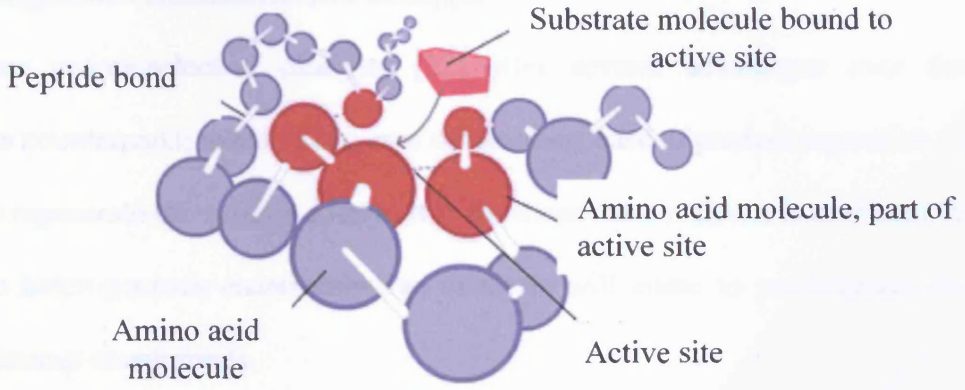

Figure 1.6 Diagramatic representation of a substrate molecule interacting with the active site of an enzyme.

1.4.3.3 Homogeneous enantioselective catalysis

Homogeneous enantioselective catalysts [18] consisting of transition metal complexes having chiral ligands are to date, the most effective enantioselective catalysts. The use of homogeneous catalysts in enantioselective synthesis came to the scientific forefront in the late 1960's as a result of two independent discoveries. Firstly, there was the observation by Wilkinson and co-workers on the extraordinary catalytic properties of chiral rhodium phosphine complexes in the hydrogenation and hydroformylation of pro-chiral olefins [19], secondly, was the development of synthetic methodologies by Knowles and Sabacky for the production of chiral phosphine ligands [20]. These discoveries were to mark the start of modern day enantioselective synthesis using homogeneous catalytic systems. A highly selective example of a homogeneous catalyst used in enantioselective hydrogenation is Rh (DIPAMP). The catalyst is used in the

production of (*L*)-3,4-dihydroxyphenylanaline (L-DOPA), a drug used in the treatment of Parkinson's disease and was the first large-scale industrial application of an asymmetric homogeneous hydrogenation catalyst [21].

1.4.3.4 Heterogeneous enantioselective catalysis

Heterogeneous enantioselective catalysts [22] offer several advantages over their homogeneous counterparts; namely cost, ease of handling, ease of product separation and the ability to regenerate the catalyst *in-situ*. It is for these reasons that it is predicted that in the future heterogeneous enantioselective catalysts will come to predominate over their homogeneous counterparts.

One of the earliest examples of enantioselective heterogeneous catalysis was observed by Schwab [23] in 1932. Schwab reported that metals such as Cu, Ni and Pt supported on a chiral quartz surface were able to catalyse the dehydrogenation resolution of butan-2-ol to butan-2-one (e.e. 10%); he attributed the observed kinetic resolution to the chiral arrangement of the quartz crystals. Akabori *et al* [24] observed that a Pd catalyst supported on silk fibre was active in the hydrogenative production of D-(+)-phenylalanine with an enantiomeric excess of 60%.

A more direct approach to the enantioselective hydrogenation of pro-chiral substrates is through the adsorption of chiral organic ligands (a chiral modifier) on to an achiral catalytic surface, typically a metal. Chirality can be imposed on to the surface in one of two ways; the inherent chirality of the modifier induces a chiral environment on the surface in the immediate vicinity of the adsorption site. Alternatively these modifiers can take up an ordered array on the surface generating a chiral template.

It was Lipkin and Stewart [25] who in 1939, first reported the use of chiral modifiers in enantioselective hydrogenation, achieving the enantioselective hydrogenation of C=C

functionalities over PdO_2 catalysts modified with the cinchona alkaloid cinchonine (e.e. 8%) and a glucose modified Raney Ni catalyst (e.e. 10%).

Despite the pioneering work of Lipkin and Stewart research in the field lay idle for over twenty years before the Japanese researcher Izumi recognised the true potential of chiral surface modification in heterogeneous catalysis. Izumi [26] investigated the modification of Ni and Pt surfaces with chiral organic acids such as tartaric acid, which was to lead to the development of the Ni/tartrate/NaBr catalytic system. This system has been hugely successful in the enantioselective hydrogenation of β-ketoesters giving chiral β-hydroxy esters with e.e. values as high as 95% [27] (Scheme 1.1). It has also been applied to the enantioselective hydrogenation of 1,3-β-diketones [28] and methyl ketones [26] with equal success.

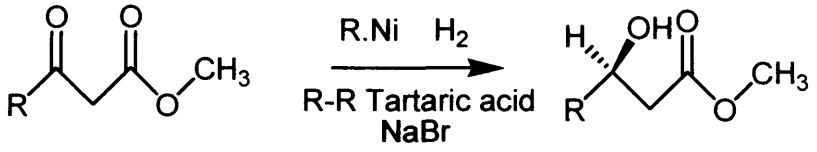

Scheme 1.1 The enantioselective hydrogenation of a 1,3-β-ketoester.

1.5 Enantioselective hydrogenation of α-ketoesters over cinchona modified platinum

The use of Pt modified with cinchona alkaloids in the enantioselective hydrogenation of α-ketoesters to give chiral α-hydroxyesters was first reported by Orito [29]. The research groups of Baiker [30], Wells [31] and Blaser [32] have conducted extensive studies into the cinchona modified platinum achieving enantioselectivity in excess of 95% [33]. It is

this fascinating reaction, which forms the basis of this thesis and shall be discussed in greater detail in the remainder of this introduction chapter.

1.5.1 The Orito reaction

The Orito reaction (Scheme 1.2) takes its name from the Japanese scientist Yoshio Orito who in 1979 reported that adsorbing a solution of the cinchona alkaloid cinchonidine onto the surface of a carbon supported platinum catalyst resulted in the enantioselective hydrogenation of the pyruvate esters, methyl and ethyl pyruvate to their corresponding lactates with high enantiomeric excess [34-36].

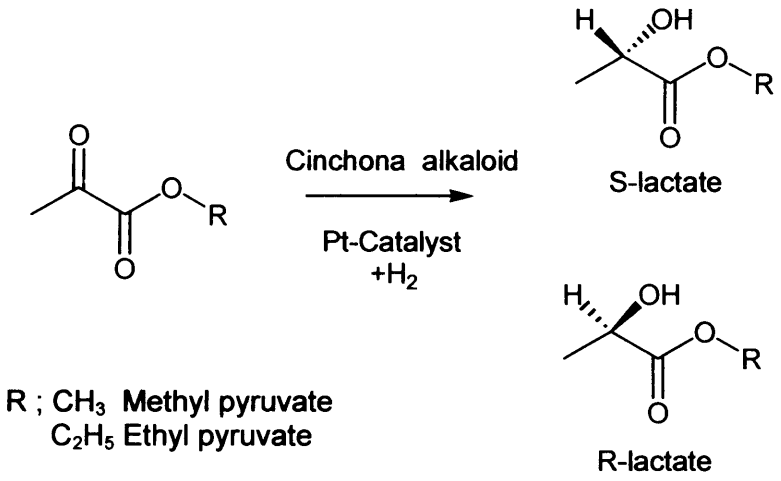

Scheme 1.2 The Orito reaction.

The reaction is typically carried out in a solvent medium; with the best optical yields being achieved in solvents with dielectric constants ranging between 2 and 10. The best results have been reported when acetic acid is used as reaction solvent [33] (e.e. 95%, ethyl pyruvate). The reaction is usually conducted at temperatures between 20 – 50 °C. Platinum metal can be held on supports such as alumina [37], silica [38] or within the pores of zeolites [39]. The structure and concentration of cinchona alkaloid employed in

the reaction has a large influence on enantioselectivity and activity. The reaction provides (*R*)-lactate when cinchonidine or quinine is used as the chiral modifier, where as (*S*)-lactate is preferentially produced when the chiral modifier employed is cinchonine or quinidine. This is also the case for the partially hydrogenated derivatives 10,11-dihydroquinidine and 10,11-dihydroquinine. No enantiodifferentiation is observed in the unmodified reaction. The presence of the cinchona alkaloid not only induces enantioselectivity but also results in a substantial enhancement of the rate of reaction. Typically a 10 to 100-fold increase in rate is observed compared to when the reaction is carried out in the absence of the modifier.

1.6 Cinchona Alkaloids

1.6.1 Variation of enantioselectivity with cinchona alkaloid structure

There exist three main structural features (Figure 1.7) of the cinchona alkaloids that are thought to be of importance in its role as a chiral modifier in the enantioselective hydrogenation of α-ketoesters; (i) the aromatic quinoline ring, which is proposed to anchor the modifier on the metal surface via its π bond electron system. (ii) The absolute configuration at the *C8* and *C9* carbon atoms which controls the observed sense of enantioselectivity. (iii) The basic quinuclidine nitrogen atom which is widely believed to interact directly with the substrate during hydrogenation and is thought to be the origin of the rate enhancement observed. The effect of cinchona alkaloid structure on enantioselectivity and rate in the Orito reaction is illustrated in Table 1.2.

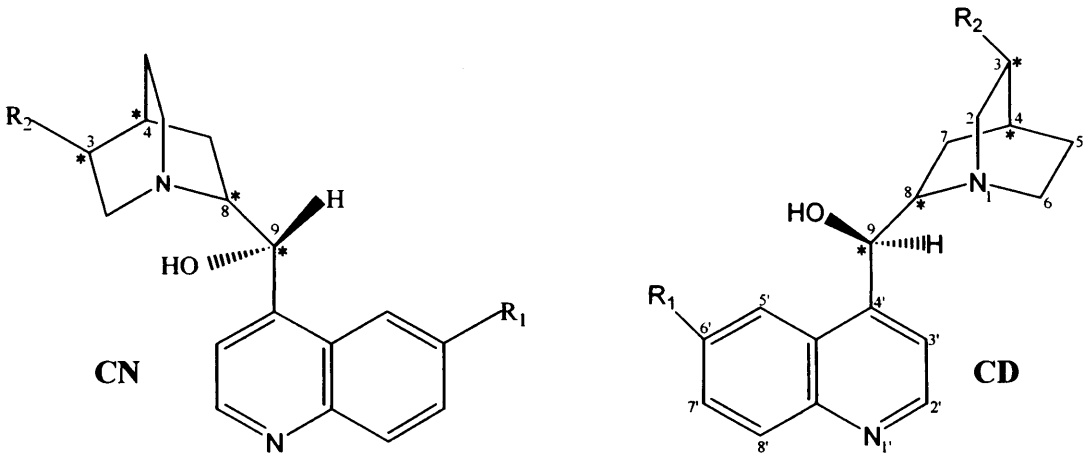

*donates chiral centre.

$\mathbf{R_1}$ = H, $\mathbf{R_2}$ = C_2H_3	Cinchonine **CN**	Cinchonidine **CD**
$\mathbf{R_1}$ = OMe, $\mathbf{R_2}$ = C_2H_3	Quinidine **QD**	Quinine **QN**
$\mathbf{R_1}$ = H, $\mathbf{R_2}$ = C_2H_5	10,11-Dihydrocinchonine **DHCN**	10,11-Dihydrocinchonidine **DHCD**

Carbon atom	3	4	8	9	3	4	8	9
Configuration	R	S	S	R	R	S	R	S

Figure 1.7 Structures and stereogenic centre configurations of some cinchona alkaloids.

As described in the earlier work of Orito, the results shown in Table 1.2 confirm that cinchonidine (entry **1**) and quinine (entry **3**) always preferentially give (*R*)-ethyl lactate while the pseudo enantiomers cinchonine (entry **2**) and quinidine (entry **4**) generate an excess of (*S*)-product. The same sense of enantioinduction is retained for the partially hydrogenated derivatives 10,11-dihydrocinchonidine (entry **5**) and 10,11-dihydrocinchonine (entry **6**). These entries clearly indicate that the sense of enantioinduction is dependent upon the absolute configuration at the *C8* and *C9* carbon

atoms within the cinchona molecules. Cinchonidine and its derivatives yield higher enantioselectivities and rates compared to the cinchonine equivalents. The introduction of a methoxy group into the quinoline ring (position R^1) is detrimental to rate and enantioselectivity for both parent alkaloids. The replacement of the hydroxyl function at *C9* in 10,11-dihydrocinchonidine with a methoxy group (entry **7**) has little effect on the enantioselective outcome of the reaction. Partial hydrogenation of the quinoline ring in cinchonidine (Hexahydro (CD), entry **8**) results in a 70% drop in enantioselectivity and a 12-fold reduction in reaction rate, which exemplifies the need for the modifier to possess an efficient pi bond system to achieve adsorption on to the metal surface. The quaterization of the quinuclidine nitrogen atom of cinchonidine, by conversion to benzyl cinchonidinium chloride (Benzyl (CD) Cl entry **9**) results in a complete loss in enantioselectivity and a substantial decrease in rate of reaction, highlighting the important role the quninuclidine nitrogen atom plays in this enantioselective reaction.

Table 1.2 The effect of cinchona alkaloid structure on enantioselectivity in the Orito reaction. Reproduced from reference [37]

Catalyst	Conversion (%)	Rate (mmol $h^{-1}g_{cat}^{-1}$)	Enantiomeric excess (%)
1	CD	110	88 (*R*)
2	CN	40	81 (*S*)
3	QN	7	81 (R)
4	QD	3	56 (*S*)
5	DHCD	120	90 (*R*)
6	DHCN	70	63 (*S*)
7	O-MeDHCD	190	93 (*R*)
8	Hexahydro (CD)	10	20 (*R*)
9*	Benzyl (CD) Cl	N/A	1 (*R*)

* reaction in ethanol.

1.6.2 Cinchona alkaloid conformation

The conformation that the cinchona alkaloid adopts under the reaction conditions has been recognised as being crucial to the enantioselectivity observed in α-ketoester hydrogenation. The structural complexity of the cinchonidine molecule means that there are four locations where rotation about a single bond is possible.

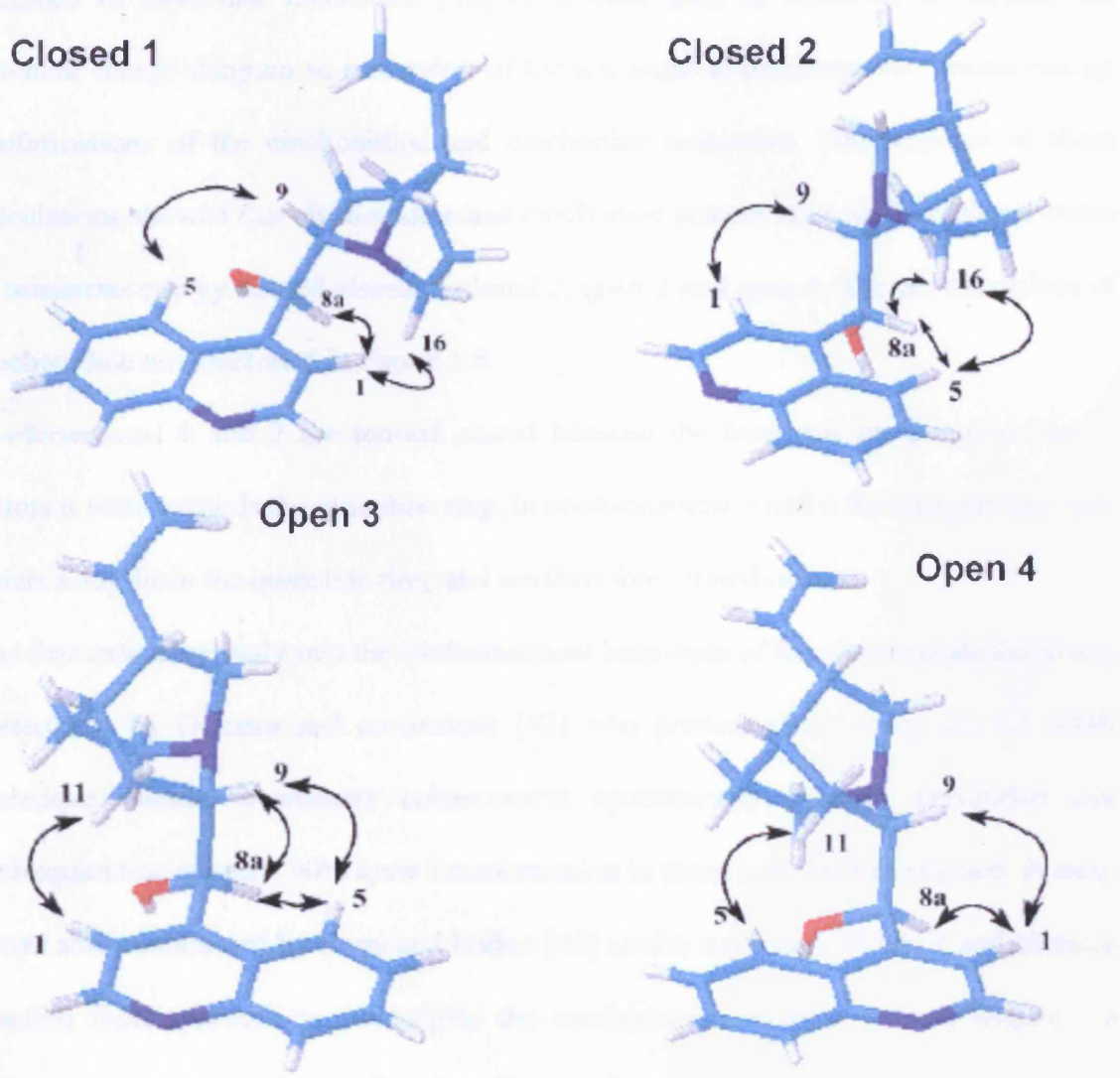

Figure 1.8 The four lowest energy conformations of cinchonidine and their associated noe interactions. Reproduced from reference [40]

The most important of these rotational degrees of freedom are controlled by the torsion angles $_{\tau 1}$: *C3–C4–C9–C8* and $_{\tau 2}$: *C4–C9–C8–N* which determine the spatial arrangement of the quinoline and quinuclidine ring systems with respect to each other.

Methods in molecular mechanics [41] have been used to construct conformational potential energy diagram as a function of torsion angle to determine the lowest energy conformations of the cinchonidine and cinchonine molecules. The outcome of these calculations showed that cinchonidine and cinchonine possess four conformational states of minimum energy termed *closed 1*, *closed 2*, *open 3* and *open 4*. The conformations of cinchonidine are illustrated in Figure 1.8.

Conformations 1 and 2 are termed closed because the lone pair on the quinuclidine nitrogen point towards the quinoline ring. In conformations 3 and 4 the nitrogen lone pair points away from the quinoline ring, and are therefore termed open.

The first extensive study into the conformational behaviour of the cinchona alkaloids was undertaken by Dijkstra and co-workers [42] who predominately using the ^{1}H NMR technique nuclear overhauser enhancement spectroscopy (noesy), concluded that hydroquinidine adopts a 90% *open 3* conformation in those solvents investigated. A more recent study conducted by Burgi and Baiker [40] used a combined ^{1}H NMR and *ab initio* reaction field approach to investigate the conformation adopted by cinchonidine in different solvents and also studied the effect conformation had on the catalytic outcome of the platinum catalysed enantioselective hydrogenation of α-ketopantolactone.

Baiker found there were three conformational states of cinchonidine present at room temperature, *closed 1*, *closed 2* and *open 3*. Both ^{1}H NMR experiments and *ab initio* calculations indicated that the most populated conformer in apolar solvents was *open 3* (toluene, 70% *open 3*). A shift to a more polar solvent system saw a dramatic change in the cinchonidine conformational distribution. The closed conformers, with their larger dipole moment, were more strongly stabilised relative to the *open 3* conformation with the fraction of cinchonidine adopting a closed conformation in excess of 70% in dimethyl sulphoxide.

1.6.3 Mode of cinchona alkaloid adsorption

Extensive studies have been conducted into the mode of cinchonidine adsorption on platinum supported catalysts. Blaser [43] postulated that cinchonidine adsorbs onto the platinum active phase via the interaction of the π electrons of the quinoline ring. Wells [44] conducted deuterium tracer studies to illustrate the cinchonidine mode of adsorption. Hydrogen-deuterium exchange occurred at all positions on the quinoline ring system, while the protons of the quinuclidine ring system remained intact. These observations, accompanied by the poor enantioselectivity observed for the partially hydrogenated modifier 5',6',7,8',10,11-hexahydrocinchonidine suggest that the alkaloid is preferentially chemisorbed via the quinoline ring. Reports that the vinyl group of cinchonidine can be hydrogenated under the reaction conditions indicate that this mode of adsorption is also possible [45].

Temperature has been reported to influence the mode of cinchonidine adsorption; N K-edge spectra recorded in the near-edge region confirmed that the quinoline ring was parallel to the platinum surface at 293 K. When the temperature was increased to 323 K the quinoline ring became inclined at an angle approximately 60° to the platinum surface. Baiker conducted an *in-situ* ATR-IR investigation into the mode of cinchonidine adsorption using a model $Pt/\gamma\text{-}Al_2O_3$ catalyst [46]. Three modes of cinchonidine adsorption were identified, the populations of which were dependent upon the level of surface modifier coverage; At low coverage a strongly adsorbed species was identified where the quinoline ring was orientated parallel to the platinum surface, at higher cinchonidine surface coverage two weakly adsorbed moieties were observed, in both cases, the quinoline ring was tilted away from the catalyst surface.

1.7 The effect of experimental variables on activity and enantioselectivity in the Orito reaction

1.7.1 Catalyst

Variations in catalyst support, preparation procedure and reductive pre-treatment have a huge bearing on the enantioselectivity observed in the hydrogenation of α-ketoesters.

To date, the majority of studies of the cinchona platinum system have been conducted over commercially available catalysts such as the 5% Pt/γ-Al_2O_3 catalyst (JMC 5R 94) or over the 6.3 wt/% Pt/SiO_2 catalyst (EUROPT-1).

Other platinum supported materials have been investigated as potential enantioselective catalysts. Zuo *et al* [47] prepared a PVP–stabilized platinum colloidal catalyst with a mean particle size of 1.4 nm which afforded an e.e. of 97.5%, the highest recorded for pyruvate ester hydrogenation. Platinum supported AlMCM-41 [48] modified with cinchonidine gave an enantiomeric excess of 64% in the hydrogenation of ethyl pyruvate, yet conversion was low. Pt/NaY [49] and Pt/clay [50] have also been employed as catalysts in the enantioselective hydrogenation of α-ketoesters but resulted in only moderate enantioselectivity being observed.

Platinum particle size and dispersion has been found to strongly influence both enantioselectivity and activity in α–ketoester hydrogenation. Pt particle size can control the distribution of exposed face, edge or corner atoms and thus influence the adsorption of substrates [51].

Baiker [52] reported that lowering platinum dispersion on an alumina support was favourable in terms of activity and enantioselectivity. It was postulated that the average platinum particle size of an alumina catalyst can be increased and dispersion lowered by subjecting the material to reductive heat treatment in flowing hydrogen. Catalysts

reduced at moderate temperatures had a mean platinum particle size below 2 nm and performed badly in terms of enantioselectivity and activity. This corroborates Well's [53] observation that small Platinum particles (< 0.8 nm) were detrimental to enantioinduction. Wells attributed the poor enantioselectivity to the inability of particles of this size to effectively co-adsorb the cinchona modifier and the pro-chiral substrate.

The most striking example of the benefits of thermal pre-treatment was observed when a $Pt/\gamma\text{-}Al_2O_3$ catalyst was pre-reduced in hydrogen at 673 K. An increase in the enantioselectivity was observed from 34 to 84% to (*R*)-ethyl mandelate [35].

The morphology of the platinum particle is considered to make a vital contribution to the enantioselective outcome of the Orito reaction [31]. An electrochemical investigation by Attard *et al* [54] on a number of different annealed platinum-graphite catalysts revealed a restructuring of the platinum crystallite establishing a link between enantioselectivity and platinum surface morphology, particle size and particle edge crystallography.

Heat treatment has been found to influence the morphology of the metal particle. Heating a $Pt/\gamma\text{-}Al_2O_3$ catalyst to between 450-625 °C in a hydrogen atmosphere resulted in the platinum particle morphology being cube like with facets, compared to spherical particles when heated under air or N_2 [55].

The choice of support plays an important role in influencing the platinum particle morphology and the enantioselective outcome of pyruvate ester hydrogenation. Mallat *et al* [56] used HRTEM to probe platinum particle morphology of a number of different alumina catalysts that had been previously heated in hydrogen. Areas of the alumina, which were highly crystalline and contained only faceted platinum particles, whilst areas of less crystalline alumina were found to contain particles more spherical in shape.

1.7.2 Solvent effects

The nature of the solvent used in the enantioselective hydrogenation of α-ketoesters has a pronounced effect on the observed enantioselectivity and activity in the platinum cinchona alkaloid system. Despite this, there are a large number of solvents which are compatible with this reaction. Blaser [57] carried out the first systematic study into the effect of solvent on enantioselectivity, and reported a linear relationship between enantioselectivity and solvent polarity in the hydrogenation of ethyl pyruvate over cinchonidine-modified platinum. The observation was also made that the optimum selectivity was obtained in apolar solvents with dielectric constants in the range 2–10 (cyclohexane, $\varepsilon = 2.02$; e.e. = 80%; dichloromethane, $\varepsilon = 9.08$; e.e. = 81%). Inferior enantioselectivity was observed when the reaction was conducted in strongly polar solvent systems (water, $\varepsilon = 80$; e.e. = 54%; formamide, $\varepsilon = 109$; e.e. = 48%) as these solvents serve to stabilise the closed conformations of cinchonidine, which are detrimental to high enantioselectivities . Reactions carried out in acetic acid, however, go against this trend, with the enantioselectivities achieved being markedly higher than examination of polarity would suggest. As reported earlier (section 1.6.2) solvent polarity is known to influence the alkaloid conformational distribution and alkaloid conformation has considerable bearing on the enantioselectivity observed. Baiker [58] reported that apolar solvents serve to stabilise the preferred *open 3* conformation of cinchonidine; whilst in acetic acid, *open 3* is the sole conformer present due to protonation of the quinuclidine nitrogen. Rates of reaction show no significant variation with changes in reaction solvent and no clear correlation between polarity and rate is apparent.

Solvent impurities have been also shown to influence the enantioselective outcome of the Orito reaction. Wells [59] and co-workers made the observation that solutions of

cinchonidine containing trace amounts of water catalyse the base hydrolysis of ethyl pyruvate to pyruvic acid. The pyruvic acid serves to stabilise the *open 3* conformation of cinchonidine leading to higher observed enantioselectivity in favour of the (*R*)-enantiomer.

Baiker [60] has made use of supercritical ethane in the continuous enantioselective hydrogenation of ethyl pyruvate over cinchonidine modified Pt/γ-Al_2O_3. The use of supercritical ethane as a solvent resulted in good enantioselectivity and high turnover frequencies.

Hutchings *et al* [61] recently showed that it is possible to effectively hydrogenate pyruvate esters in the absence of solvent, in the gaseous phase, over cinchonidine modified platinum with enantiomeric excess values close to 50%.

1.7.3 Hydrogen pressure and temperature.

Hydrogen pressure and reaction temperature have been shown to influence the enantioselective outcome of the Orito reaction. Wells [62] reported a first order rate dependence in hydrogen and only slight variations in enantiomeric excess for a series of pyruvate ester hydrogenations at pressures in the range 10 to 100 bar with a cinchonidine modified EUROPT-1 catalyst.

Augustine *et al* [63] observed an increase in enantiomeric excess from 1% to 15% over the pressure range 200 - 400 torr which remained constant until the pressure reached 800 torr for a 10,11-hydroquinidine modified platinum system. Blackmond [64] reported a continuous increase in enantiomeric excess from 15% to 55% for a 10,11-dihydroquinidine modified Pt/γ-Al_2O_3 catalyst. The increase was achieved by raising the dissolved hydrogen concentration from 0.01 to 10 mmol.

The effect of reaction temperature has been investigated for both cinchona modified and un-modified systems. In the un-modified system Wells [62] reported a linear Arrhenius plot at temperatures between room temperature and 70 °C.

Conversely, in the cinchonidine modified platinum catalysed hydrogenation of ethyl pyruvate the rate and e.e. was found to decrease in the production of the (R)-enantiomer at reaction temperatures above 50 °C. Augustine [63] accredited the loss of selectivity to desorption of the modifier from the catalyst surface at such elevated temperatures.

1.8 The proposed enantioselective site

The origin of enantioselectivity in the Orito reaction has been the main focus of research for a number of world-renowned catalysis groups over the last quarter of a century. Kinetic models for the observed rate enhancement, and enantio-differentiation have been proposed by Blaser [66] and Blackmond [xx]. Several other models have been proposed to explain the mechanism of enantioinduction, the most eminent of which are outlined below.

1.8.1 The Wells Models

One of the earliest models to explain the enantiodiscrimination observed in the hydrogenation of α-ketoesters over cinchona modified platinum was provided by Wells in 1990 and became known as the template model [65].

Wells proposed, (later confirmed by deuterium tracer studies) that cinchonidine adsorbs onto the platinum surface *via* the interaction of the π-bond electron system of the quinoline ring (naphthalene is known to form ordered structures on a platinum (111) single crystal surface). Wells believed the L-shaped cinchonidine molecules adsorb onto the platinum surface in an ordered array leaving a templated exposed area of platinum

ensembles that would only allow adsorption of the methyl pyruvate molecule in the favoured geometry to yield (*R*)-methyl lactate on hydrogenation.

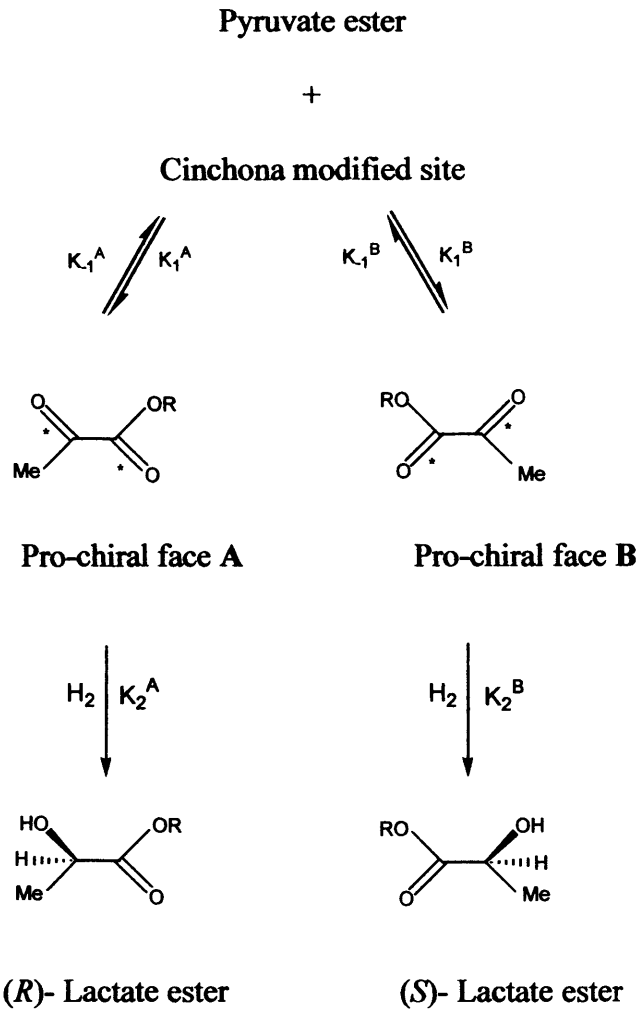

Figure 1.9 Reaction scheme showing pyruvate esters absorbed by their two different pro-chiral faces at a modified catalyst surface.

Wells [66] was later forced to retract the template model in light of XPS, NEXFAS and LEED studies of 10,11-dihydrocinchonidine adsorption on a platinum (111) surface, as no ordered adsorption of the modifier was seen.

Computational studies based on docking interactions between cinchonidine in its most stable conformation, *open 3*, and methyl pyruvate by its two pro-chiral faces (Figure 1.9) prompted Wells to propose a revised model based on a 1:1 interaction between modifier and substrate.

Wells calculated that adsorption of methyl pyruvate by pro-chiral face **A** in the vicinity of the quninuclidine nitrogen of cinchonidine was more energetically stable than adsorption by pro-chiral face, **B**. The catalytic site is observed to exhibit selective adsorption in favour of **A**, resulting in the preferential formation of the (*R*)-enantiomer. Adsorption of the pyruvate molecule by the opposite face resulted in the (*S*)-enantiomer being preferentially formed; both hypotheses concur with experimental results.

Wells accredited the rate enhancement observed in the Orito reaction to hydrogen bond formation between the quinuclidine nitrogen of the alkaloid and a partially hydrogenated α-ketoester. This bonding served to increase the steady state concentration of the pyruvate intermediate resulting in rapid addition of the second hydrogen atom which is believed to be the rate determining step.

1.8.2 Baiker model

Baiker [67] proposed that the enantiofacial differentiation observed in the Orito reaction was due to a 1:1 complex between cinchonidine and the α-ketoester which adsorbs planar to the platinum surface *via* the conjugated π-bond system. In acidic media Baiker proposed the two molecules interact through a hydrogen bond between the α-keto group of the pyruvate ester and the protonated quninuclidine nitrogen of the alkaloid. In non-protic solvents the interaction was believed to take place between a partially hydrogenated α-ketoester species and the unprotonated quninuclidine nitrogen. Using *ab initio* calculations Baiker determined the most energetically stable complexes between

cinchonidine in its *open 3* conformation and the two conformations of the *cis-* and *trans-* forms of methyl pyruvate. Gas phase calculations showed the *S-cis* methyl pyruvate complex to be considerably more stable than the corresponding *S-trans* methyl pyruvate complex. Conversely, when solvents effects are included and a reaction field model is applied, the energy differences between the two sets of complexes were dramatically reduced.

For *S-trans* methyl pyruvate the complex leading to (*R*)-methyl lactate upon hydrogenation was found to be more stable than the pro-(*S*) complex by 1.8 Kcal/mol that corresponds to an e.e. of 92% in favour of the (*R*)-enantiomer, in good agreement with experimental observations. For the analogous *S-cis* complex the calculated energy difference was 0.2 Kcal/mol, which would generate an enantiomeric excess of 17% in favour of the (*R*)-enantiomer, far below that determined by experiment.

1.8.3 Margitfalvi Model

Margitfalvi *et al* [68] have proposed a quite different model to that previously described to explain the origin of enantiofacial differentiation in α-ketoester hydrogenation in the presence of cinchonidine modified platinum.

Margitfalvi suggested that the key interaction between substrate and modifier takes place in the liquid phase with the pyruvate molecule forming a 1:1 complex with the cinchonidine molecule via a π-π stacking interaction between the quinoline ring of cinchonidine and the ketone carbonyl of the α-ketoester. Using kinetic measurements, ^{1}H NMR and molecular modelling techniques Margitfalvi deduced that within the complex cinchonidine adopted a closed conformation with the quinoline ring acting as an umbrella, shielding one enantio-face of the carbonyl group leaving the unhindered face open to hydrogenation. The role of the Pt surface was to simply supply activated

hydrogen to the inward bound complex. A major flaw within this model lies in the fact that hydrogen activation can occur on all metals in groups 8-10, thus, the reaction should proceed enantioselectively over all such metal catalysts, Wells [69] has shown this not to be the case. A diagrammatic representation of the Margitfalvi model is shown in Figure 1.10

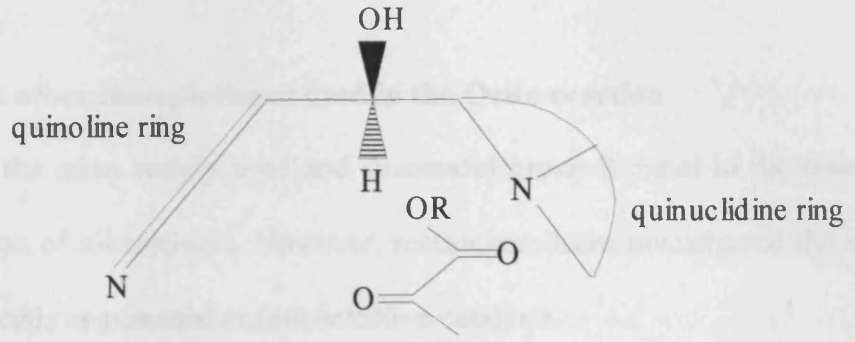

Figure 1.10 Diagrammatic representation of Margitfalvi 'shielded' model

1.8.4 The Augustine Model.

In contrast to the Wells and Baiker models, which assume adsorption of the modifier parallel to a flat Pt-surface via the quinoline ring, Augustine first proposed a different interaction involving edge-on adsorption of cinchonidine via the quinoline-N atom [63]. Augustine's view of the surface modifier interaction was subsequently modified however, the common feature of both models was the bidentate complex formed between modifier and the pyruvate ester. Here the interaction of modifier and pyruvate ester is via both the quinuclidine-N and the O-atom of the hydroxyl group at C9. This proposal was based on the observation that alcohols and amines predominantly attack activated ketones via a nucleophilic process at electrophilic carbonyl functionalities. However the model lacks support for a number of reasons: (1) the model does not predict the sense of the chiral outcome of the reaction when either of the proposed interacting functions (quinuclidine-N: or C9 hydroxy group) is not present in the modifier. (2) The enhanced

enantioselectivity observed in protic solvents (where the quinuclidine-N is protonated and its lone pair is not available to interact with the reactant) cannot be explained nor can the retention of enantioselectivity on the methylation of the C9-OH group [37].

1.9 Diversification from the Orito reaction

1.9.1 Metals other than platinum used in the Orito reaction

Platinum is the most widely used and successful group 8 metal in the enantioselective hydrogenation of α-ketoesters. However, researchers have investigated the role of other transition metals as potential enantioselective catalysts.

Blaser and co-workers [70] reported optical yields of between 20 and 30% in favour of the (*R*)-enantiomer in the hydrogenation of ethyl pyruvate over cinchonidine modified $Rh/\gamma\text{-}Al_2O_3$.

The use of polyvinylpyrrolidone stabilised rhodium nanoclusters with a mean particle size of 1.8 nm, gave an enhanced e.e. of 42% and a 50 fold rate increase over the unmodified reaction [71].

Wells [72] investigated the Orito reaction over a number of different supported iridium catalysts and found that their catalytic behaviour followed that previously observed for platinum. Cinchonidine modified iridium gave enantiomeric excess of up to 39% in favour of the (*R*)-lactate in the hydrogenation of methyl pyruvate. Wells reported enantioselectivity to be highly dependent upon the calcination and reduction temperature employed during catalyst preparation, indicating a high dependency of enantiomeric excess observed on the metal particle morphology. Surprisingly, there was little or no rate enhancement observed for the iridium catalyst in comparison to the un-modified reaction.

Blaser [70] was the first to report the use of a palladium catalyst in the enantioselective hydrogenation of ethyl pyruvate in the presence of cinchonidine. Blaser observed that a cinchonidine Pd/C system was mildly enantioselective for the hydrogenation of ethyl pyruvate giving an enantiomeric excess of 4% in favour of the (*S*)-enantiomer. This result indicated the sense of enantioselectivity was the reverse to that observed with the corresponding platinum system.

Wells conducted a closer examination of the palladium catalysed hydrogenation of ethyl pyruvate, confirming the reversal in enantioselectivity and illustrated that the reaction over palladium differed significantly to that observed for platinum. The rate enhancement observed over cinchonidine modified platinum was absent over palladium. This explained the low enantioselectivity observed in the palladium system. Palladium catalysts are sensitive to reduction temperature and are only enantioselective if reduced at low temperatures, suggesting that some degree of positive character may be required at the palladium surface. Platinum catalysts showed no comparable reduction temperature dependence. Over palladium, the enantioselective hydrogenation of α-ketoesters is half-order with respect to hydrogen and self poisoning. Over platinum there is no self-poisoning and the rate is first order with respect to hydrogen.

Deuterium and methyl pyruvate ester tracer studies conducted over cinchonidine modified palladium conducted by Wells [73] exemplified that the primary product forming route involved the rate determining conversion of the α-ketoester to the analogous enol tautomer, the resultant carbon-carbon double bond being rapidly hydrogenated to the (*S*)-lactate product.

1.9.2 Enantioselective hydrogenation of other pro-chiral substrates over cinchona modified metals

There are numerous other carbonyl containing pro-chiral substrates that have been successfully hydrogenated enantioselectively over cinchona modified metal catalysts. Baiker [74] has used platinum-cinchonidine catalysts for the hydrogenation of α-ketolactone to (*R*)-pantolactone, (Scheme 1.3) an intermediate in the synthesis of vitamin B5, with an enantiomeric excess of 92%.

Nitta [75] has been successful in the enantioselective hydrogenation of the bulky *E*-α-phenylcinnamic acid over a cinchonidine modified Pd/TiO_2 catalyst with an enantiomeric excess of 72%, the highest recorded value for an α, β-unsaturated acid.

Wells *et al* [76] have reported the enantioselective hydrogenation of butane-2,3-dione to 3-hydroxy-butan-2-one with an enantiomeric excess of up to 38% in favour of the (*R*)-enantiomer over cinchonidine modified Pt/silica. Blaser [77] has successfully hydrogenated a series of α-keto acetals to the corresponding α-hydroxy acetals with enantiomeric excess values of up to 97% using cinchona modified platinum catalysts.

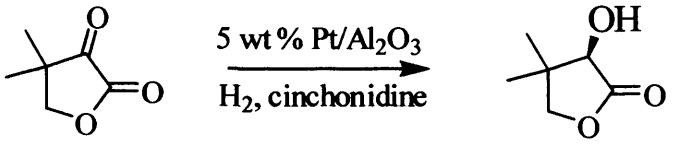

Scheme 1.3 The enantioselective hydrogenation of α-ketopantalactone to (*R*)-pantolactone.

1.9.3 Other families of Modifiers

To date, compounds originating from the cinchona family of alkaloids are the most efficient naturally occurring modifiers in the enantioselective hydrogenation of α-ketoesters. Baiker and co-workers [78] has demonstrated has that synthetic cinchona

alkaloid mimics are effective modifiers in the enantioselective hydrogenation of pyruvate esters.

Compounds originating from other classes of alkaloids including morphine, vinca and stychnos systems (Figure 1.11) have been screened as potential chiral modifiers. These compounds possess all the essential physical attributes to be efficient chiral modifiers, in that they possess an aromatic moiety to enable adsorption at a metal surface and a tertiary nitrogen atom that can interact directly with the substrate *via* a hydrogen bond. However, the enantiomeric excess obtained with these types of alkaloids fall far below that obtained with the cinchona alkaloids.

Table 1.3 Enantiomeric excess values obtained in the methyl pyruvate hydrogenation over alkaloid modified platinum-silica catalysts.

Alkaloid family	**Modifier**	**Enantiomeric excess (%)**	**Reference**
Strychnos	Brucine	20 (*S*)	79
Morphine	Codeine	5 (*S*)	79
Vinca	Nalaxone	5 (*R*)	69
Morphine	Oxycodone	15 (*R*)	69

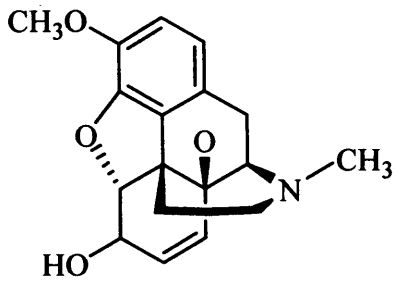

codeine

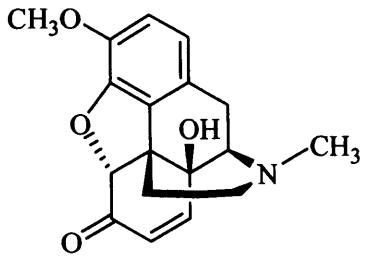

oxycodone

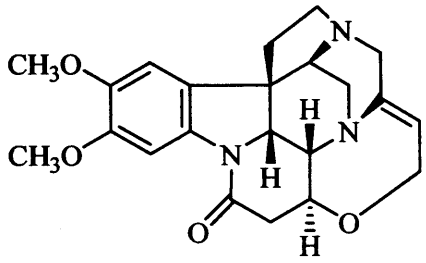

brucine

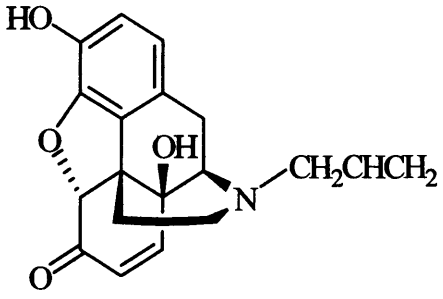

naloxone

Figure 1.11 Structures of other alkaloid types used in the Orito reaction.

1.10 Objectives

The objectives of this investigation were to advance our understanding of pyruvate ester hydrogenation over cinchona alkaloid modified platinum. The areas of novel study have been:

1 An investigation into whether a mesoporous material can provide a suitable environment to conduct an enantioselective reaction and the potential influence the pore structure has on the enantioselective outcome of the reaction.

2 A detailed investigation into the feasibility of a continuous flow reactor, operating under mild conditions, to enantioselectively hydrogenate pyruvate esters over cinchonidine modified platinum.

3 An investigation into the modifier concentration dependence on enantioselectivity exhibited by 4-chlorobenzoate derivatives of hydroquinidine and hydroquinine.

1.11 References

1 J.J. Berzelius, *Edinburgh New Philosophical Journal.*, **XXI** (1836) 223.

2 V.N. Ipatieff and B. Corson, *J. Ind. Engin Chem.*, **27** (1935) 1069.

3 H. Cota, T. Katan, M. Chin and F. J. Schoenweis, *Nature*, **203** (1962) 1281.

4 A. Baiker, H. Baris and R. Schloegl, *J. Catal.*, **108** (1987) 467.

5 J.B. Biot, *Bull. Soc. Philomath.* Paris, 190 (1815).

6 L. Pasteur, *C.R. Acad. Sci.*, **26** (1848) 535.

7 J.H. van't Hoff, *Sci. Exacts Nat.*, **9** (1874) 445.

8 J.A. LeBel, *Bull. Soc. Chim. Fr.*, **22** (1874) 337.

9 R.A Sheldon, *Chirotechnology,* (1993) 39.

10 T. Ericksson, S. Björkman, B. Roth, Å. Fyge and P. Höglund, *Chirality,* **7** (1995) 44 and references therein.

11 M. Burke, *Chem. Ind.*, **1994** 10.

12 D. Lednicer, *Chronicals of Drug discovery,* **1-3**, (1982-1983).

13 A.N. Collins, G.N. Sheldrake and J. Crosby, *Chirality in Industry II*, 1997.

14 W.S. Faber, J. Kok, B. de Lange and B.L. Feringa, *Tetrahedron*, **50** (1994) 4775.

15 H. van der Deen, A.D. Cuiper, R.P. Hof, A. van Oeveren, B.L. Feringa and R.M. Kellogg, *J. Am.Chem. Soc.*, **118** (1996) 3801.

16 P. Vogel, *Recent developments in asymmetric organic synthesis: principles and examples.*

17 C.J. Sih, R.L. Gu, J.Z. Crich and R. Brieva, *Steriocontrolled Organic Synthesis,* (1994) 399.

18 J.P. Genet *Advanced Asymmetric Synthesis*, (1996), 146.

19 J.A. Osborn, F.H. Jardine, J.F. Young and G. Wilkinson, *J. Chem. Soc.*, (A) (1966) 1711.

20 W.S. Knowles and M.J. Sabacky, *J.Chem., Chem Commun.*, (1968) 1445.

21 W.S. Knowles, *J. Chem. Ed.*, **63** (1986) 222.

22 A.Tungler, T.tarnai, T. Mathe, J. Petro and R.A. Sheldon, *'Chiral Reactions in Heterogeneous Catalysis,* (1995) 121.

23 G.M. Schwab and L. Rudolph, *Naturwiss*, **20** (1932) 363.

24 S. Akabori, S. Sakurai, Y. Izumi and Y. Fujii, *Nature,* **178** (1956) 323.

25 D. Lipkin and T.D. Stewart, *J. Am. Chem. Soc.*, **61** (1939) 3295.

26 Y. Izumi, *Adv. Catal.*, **32** (1983) 215.

27 W.M.H. Sachtler, *Chem. Ind.*, **22** (1995) 189

28 J. Bakos, I. Tóth and L. Markó, *J. Org. Chem.*, **46** (1981) 5427.

29 Y. Orito, S. Imai and S. Niwa, *J. Chem. Soc. Jpn.*, (1979) 1257.

30 A. Baiker. *J. Mol. Catal. A: Chem.*, **115** (1997) 473.

31 P.B. Wells and A.G. Wilkinson, *Topics in Catal.*, **5** (1998) 39.

32 H.U. Blaser, H.P. Jalett, M. Müller and M. Struder, *Catal. Today,* **37** (1997) 441.

33 H.U. Blaser, H.P. Jalett and J.Wiehl *J. Mol. Catal.*, **68** (1991) 215.

34 Y. Orito, S. Imai and S. Niwa, *J. Chem. Soc. Jpn.*, (1979) 1257.

35 Y. Orito, S. Imai and S. Niwa, *J. Chem. Soc. Jpn.*, (1980) 670.

36 Y. Orito, S. Imai and S. Niwa, *J. Chem. Soc. Jpn.*, (1982) 137.

37 H.U. Blaser, H.P. Jalett, W. Lottenbach and M. Struda *J. Am. Chem. Soc.*, **122** (2000) 12675.

38 P. Griffiths, P. Johnston and P.B. Wells, *Appl. Catal. A: Gen.*, **191** (2000) 1993.

39 U. Boehmer, K. Morgenschweiss and W. Reschetilowski, *Catal. Today*, **24** (1995) 195.

40 T. Burgi and A. Baiker, *J. Am. Chem. Soc.*, **120** (1998) 1290.

41 K.E. Simons, Ph.D. Thesis, University of Hull, 1994.

42 G.D.H. Dijkstra, R.M. Kellogg, H. Wynberg, J.S. Svendsen, I. Marko and B.K. Sharpless, *J. Am. Chem. Soc.,* **111** (1989) 8069.

43 H.U. Blaser, M. Garland and H.P. Jalett, *J. Catal.*, **144** (1993) 569.

44 G. Bond and P.B. Wells, *J. Catal.*, **150** (1994) 329.

45 H.U. Blaser, H.P. Jalett, D.M. Monti, A. Baiker and J.T. Wehrli, '*Symposium on Structure-Activity Relationships in Heterogeneous Catalysis*', American Chemical Society, Boston (1990) p.79.

46 D. Ferri, T. Bürgi and A. Baiker, *J. Chem. Soc. Chem. Commun.*, (2001) 1172.

47 X. Zuo, H. Liu and M. Liu, *Tetrahedron, Lett.*, **39** (1998) 1941.

48 T.J. Hall, J.E. Halder, G.J. Hutchings, R.L. Jenkins, P. Johnston, P. McMorn, P.B. Wells and R.P.K. Wells, *Topics in Catalysis,* **11-12** (2000) 351.

49 K. Balázsik, B. Török, G. Szakonyi and M.Bartók, Appl. *Catal. A: Gen.*, 182 (1999) 53.

50 U .Böhmer, F. Franke, K. Morgenschweis, T. Bieber and W. Reschetilowski, *Catal. Today,* **60** (2000) 167.

51 R.Van Hardeveld and F Hartog, *Surf. Sci.,* **15** (1969) 189.

52 J.T. Wehrli, A. Baiker, D.M. Monti and H.U. Blaser, *J. Mol. Catal.,* **61** (1990) 207.

53 S.D. Jackson, M.B.T. Keegan, G.D. McLellan, P.A. Meheux, R.B. Moyes, G. Webb, P.B. Wells, R. Whyman and J. Willis, *Preparation and Characterisation of Catalysts,* (1991) 135.

54 G.A. Attard, J.E. Gillies, C.A. Harris, D.J. Jenkins, P. Johnston, M.A. Price, D.J. Watson and P.B. Wells, *Appl. Catal. A.,* **222** (2001) 393.

55 T. Wang, C. Lee and L.D. Schmidt, *Surf. Sci.*, **163** (1985) 181.

56 T. Mallat, S. Frauchiger, P.J. Kooymen, M. Schürch and A. Baiker, *Catal. Lett.*, **63**

(1999) 121.

57 J.T. Wehrli, A. Baiker, D.M. Monti, H-U. Blaser and H.P. Jalett, *J. Mol. Catal.*, **57** (1989) 245.

58 T. Burgi and A. Baiker, *J. Am. Chem. Soc.*, **120**, (1998), 12920.

59 R.P.K. Wells, N.R McGuire, X. Li, R.L. Jenkins, P.J. Collier, R. Whyman and G.J. Hutchings, *Phys. Chem. Chem. Phys.*, **4** (2002) 2839.

60 R. Wandeler, N. Kunzle, M. S. Schneider, T. Mallat and A. Baiker *J. Catal.*, **200** (2000) 377.

61 M. von Arx, N.F. Dummer, D.J. Willock, S.H. Taylor, R.P.K.Wells, P.B. Wells and G.J.Hutchings, *J. Chem. Soc. Chem. Commun.*, (2003) 1926.

62 P.A. Meheux, and P.B. Wells, *J. Catal.*, **128** (1991) 387.

63 R.L. Augustine, S.K. Tanielyan and L.K. Doyle, *Tetrahedron: Asymmetry,* **4** (1993) 1803.

64 Y. Sun, J. Wang, C. LeBlond, R.N. Landau and D.G. Blackmond, *J. Catal.*, **161** (1996) 759.

65 I.M. Sutherland, A. Ibboston, R.B. Moyes and P.B. Wells, *J. Catal.*, **23** (1994) 271.

66 A.F. Carley, M.K. Rajumon, M.W. Roberts and P.B. Wells, *J. Chem. Soc., Faraday Trans.*, **91** (1995) 2167.

67 O. Schwalm, B. Minder, J. Weber and A. Baiker, *Catal. Lett.*, **63** (1999) 121.

68 J. Margitfalvi, M. Hegedűs and E. Tfirst, *Tetrahedron: Asymmetry*, **7** (1994) 571.

69 P.B. Wells and R.P.K. Wells, *Chiral Catalyst Immobilisation and Recycling* P.123-154 and references there within.

70 H.U. Blaser, H.P. Jalett, D.M. Monti, J.F. Reber and J.T. Wehrli, *Stud. Surf. Sci ,Catal.*, **41** (1988) 153.

71 Y. Huang, J. Chen, H. Chen, R. Li, Y. Li, L. Min and X. Li, *J. Mol. Catal. A: Chem.*,

170 (2001) 143.

72 K.E. Simons, A. Ibbotson, P. Johnston, H. Plum and P.B. Wells, *J. Catal.*, **150** (1994) 321.

73 T.J. Hall, P. Johnston, W.A.H. Vermeer, S.R. Watson and P.B. Wells, *Stud. Surf. Sci. Catal.*, **101** (1996) 221.

74 M. Schürch, N. Künzle, T. Mallat and A. Baiker, *J. Catal.*, **176** (1998) 569.

75 Y. Nitta, T. Kobota and Y. Okamoto, *Bull. Chem. Soc. Jpn.*, **73** (2000) 2635.

76 W.A.H Vermeer, A. Fulford, P. Johnston and P.B. Wells, *J. Chem. Soc. Chem., Commun.*, (1993) 1053.

77 M. Struder, S. Burkhardt and H.U. Blaser, *J. Chem. Soc. Chem., Commun.*, (1999) 1725.

78. K.E. Simons, G. Wang, T. Heins, T. Giger, T. Mallat, A. Pfaltz and A. Baiker, *Tetrahedron: Asymmetry*, **6** (1995) 505.

79 S. P. Griffiths, P. Johnston, W.A.H Vermeer and P.B. Wells, *J. Chem. Soc. Chem., Commun.*, (1994) 2431.

Chapter Two

Chapter Two Experimental

2.1 Materials

2.1.1 Catalysts

During the course of this study only supported platinum catalysts were used, these catalysts were mainly a 5% Pt/γ-Al_2O_3 (5R94) supplied by Johnson Matthey or a series of platinum supported AlMCM-41 catalysts prepared in this laboratory which differed in pore size and platinum loading. Other supported platinum catalysts were occasionally used to investigate support effects namely 2.5% Pt/SiO2 and a 5% Pt/C catalyst both of which were supplied by Johnson Matthey.

2.1.2 Reactants and reagents

Ethyl pyruvate (Fluka, $\geq$ 97%) and methyl pyruvate (Fluka, 98%) were used as received, as were ethyl lactate (Fluka, 98%), (*R*)-ethyl lactate (Fluka, 98%) and (*S*)-ethyl lactate (Fluka, $\geq$ 99%) and methyl lactate (Fluka, $\geq$ 97%), their purity was confirmed using gas chromatography. The cinchona alkaloids cinchonidine (Fluka, $\geq$ 98%) hydroquinidine-4-chlorobenzoate (Aldrich 98%) and hydroquinine-4-chlorobenzoate (Aldrich 98%) employed during the course of the study were used as received, requiring no further purification.

Other materials used during the course of this study along with their suppliers and purity specification are listed on the following page (Table 2.1).

Table 2.1 Materials, suppliers and purity specification.

Material	Supplier	Specification
Aluminium isopropoxide	Aldrich	≥ 98%
Tetraethyl orthosilicate	Aldrich	≥ 98%
Cetyltrimethylammonium bromide	BDH	≥ 99%
Octadecyltrimethylammonium bromide	Aldrich	≥ 98%
tetramineplatinum (II) nitrate	Strem	99%
Dichloromethane	Fisher	≥ 99.8%
Ethanol	Fisher	≥ 95%
Silicon carbide 250μm	Washington Mills	99%

2.2 Synthesis of Pt-AlMCM-41 catalysts

2.2.1 Hydrothermal synthesis of *C16* AlMCM-41

AlMCM-41 with a Si/Al ratio of 9:1 was prepared following a procedure similar to that described by Kim *et al* [1], with the following gel composition:

$$1\ SiO_2 : 0.04\ Al_2O_3 : 0.24\ CTMABr : 0.3\ Na_2O : 150\ H_2O$$

Sodium hydroxide (1.60 g) was added under constant stirring to a solution of cetyltrimethylammonium bromide (5.8 g, CTMABr) in distilled water (180 g) contained within a teflon liner. This was followed by the addition of aluminium isopropoxide (1.08 g) and the dropwise addition of tetraethylorthosilicate (13.88 g). The mixture was stirred at room temperature for 1 h prior to its transferral to an autoclave where it was heated at

343 K for 96 h. After cooling to room temperature, the resultant solid product was recovered by vacuum filtration, washed thoroughly with deionised water and air dried at room temperature.

2.2.2 Hydrothermal synthesis of *C18* AlMCM-41

The synthesis procedure followed was identical to that described in section 2.2.1 the only exception was the replacement of CTMABr for octadecyltrimethylammonium bromide (6.28 g, OTMABr).

2.2.3 Calcination of AlMCM-41 materials

Removal of the surfactant template within the pores of AlMCM-41 was achieved by heating the material in a flow of dry nitrogen, the temperature was linearly increased from 293 K to 813 K over 12 h and maintained at 813 K for a further 2 h, calcination was completed with an additional 2 h heating at 813 K in static air.

2.2.4 Ion exchange

Calcined or uncalcined AlMCM-41 (1.0 g) was slurried with 100 cm^3 of an aqueous $Pt(NH_3)_4(NO_2)_2$ solution ($1.05x10^{-3}$ M) for 1 h at 293 K. The sample was vacuum filtered, washed with de-ionised water and air dried at room temperature.

2.2.5 Catalyst activation

2.2.5.1 Oxidation

Oxidation of the platinum precursor within the pores of AlMCM-41 was achieved by heating the catalyst in a flow of oxygen dried over molecular sieves. The temperature

was increased linearly from 293 to 593 K over 12 h and maintained at 593 K for a further 2 h.

2.2.5.2 Reduction

Reduction of the platinum precursor was facilitated by heating the catalyst in a flow of 5% H_2/Ar or 100% H_2 (Figure 2.1); the temperature was ramped from 293 to 593 K over 4 h and maintained at 593 K for a further 2 h.

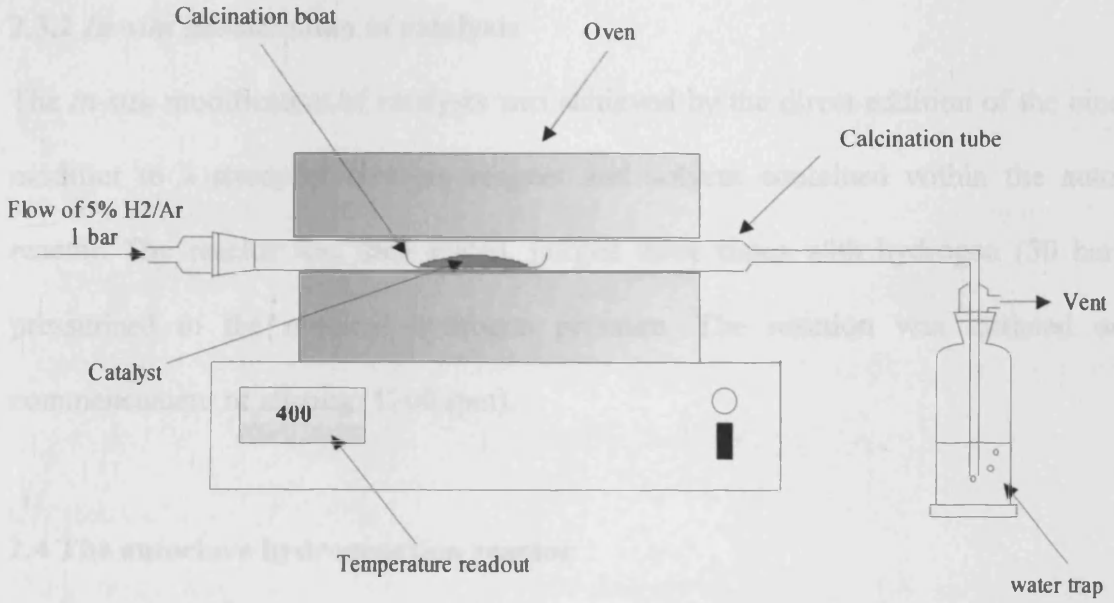

Figure 2.1 Schematic representation of the apparatus used in catalyst activation.

2.3 Catalyst modification

Modification is the process to adsorb chiral modifier on to a catalyst surface thus creating an enantioselective catalyst. Two modification procedures were used and are outlined below.

2.3.1 The Orito method

The pre-adsorption modification of the catalyst was carried out prior to the introduction of the catalyst to the reactor. The procedure for catalyst pre-modification was as follows. 0.5 g of freshly reduced catalyst was suspended in 20 cm^3 of dichloromethane and the relevant amount of modifier added; the mixture was vigorously stirred in air for 1 h at room temperature. The solvent was removed by vacuum filtration and the pre-modified catalyst was dried in air and stored in a desiccator prior to use, typically within 5 days.

2.3.2 *In-situ* modification of catalysts

The *in-situ* modification of catalysts was achieved by the direct addition of the cinchona modifier to a slurry of catalyst, reagent and solvent contained within the autoclave reactor. The reactor was then sealed, purged three times with hydrogen (30 bar) and pressurised to the required hydrogen pressure. The reaction was initiated on the commencement of stirring (1200 rpm).

2.4 The autoclave hydrogenation reactor

All enantioselective batch reactions were carried out using a stainless steel Parr micro reactor system (Figure 2.2). The reactor was equipped with a stainless steel vessel (50 cm^3), a pressure gauge, a thermocouple connected to a digital temperature display and a mechanical stirrer driven by an integrated motor and magnetic drive unit. Prior to every reaction the autoclave and stirrer mechanism was thoroughly cleaned with acetone and if a new modifier or reagent was used the autoclave was cleaned with refluxing methanol to ensure an impurity free system. An ice water bath was used to regulate temperature during the course of the reaction to 20 °C ± 2 °C.

The system was pressure and leak tested on a regular basis to ensure system integrity.

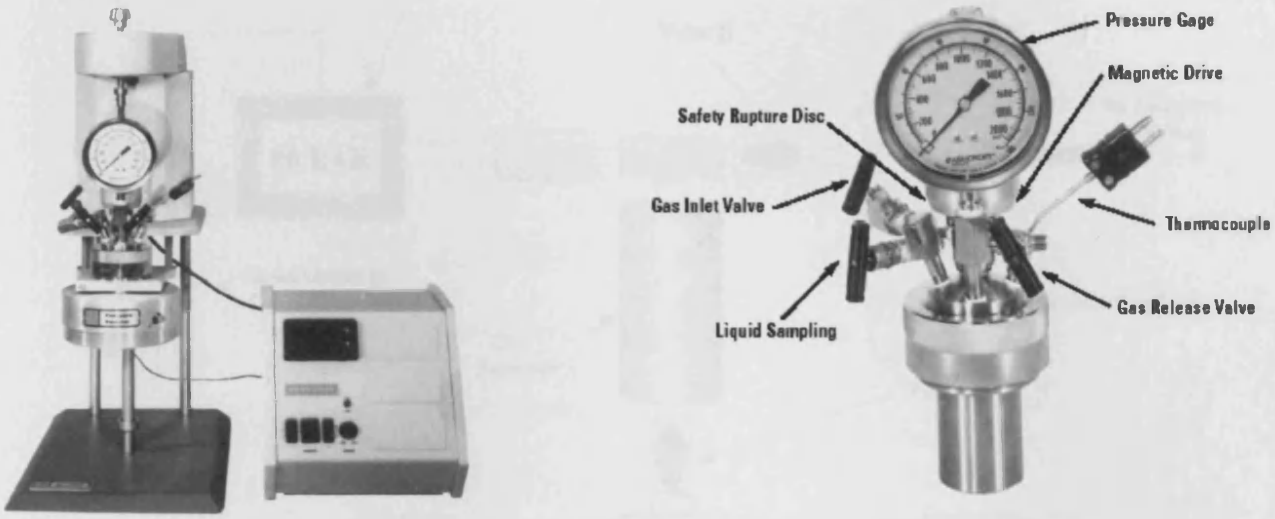

Figure 2.2 Parr 4590 micro reactor and controller.

2.5 Enantioselective hydrogenation of ethyl pyruvate over cinchonidine modified Pt-AlMCM-41 catalysts

Cinchonidine (0.05 g, 0.170 mmol) and ethyl pyruvate (7.66 g, 66 mmol) were charged to the reactor, which contained the platinum MCM-41 catalyst (0.1 g) suspended in dichloromethane (12.5 cm^3).

The autoclave was sealed and purged three times with hydrogen (30 bar) to remove any residual air from the reactor, then pressurised to the experimental operating pressure (70 bar). The contents of the autoclave were cooled to 20 °C using an ice bath prior to the start of the reaction.

The reaction was initiated on commencement of stirring (1200 rpm); the temperature, H_2 pressure and stirring rate were maintained throughout the course of the reaction (1 h).

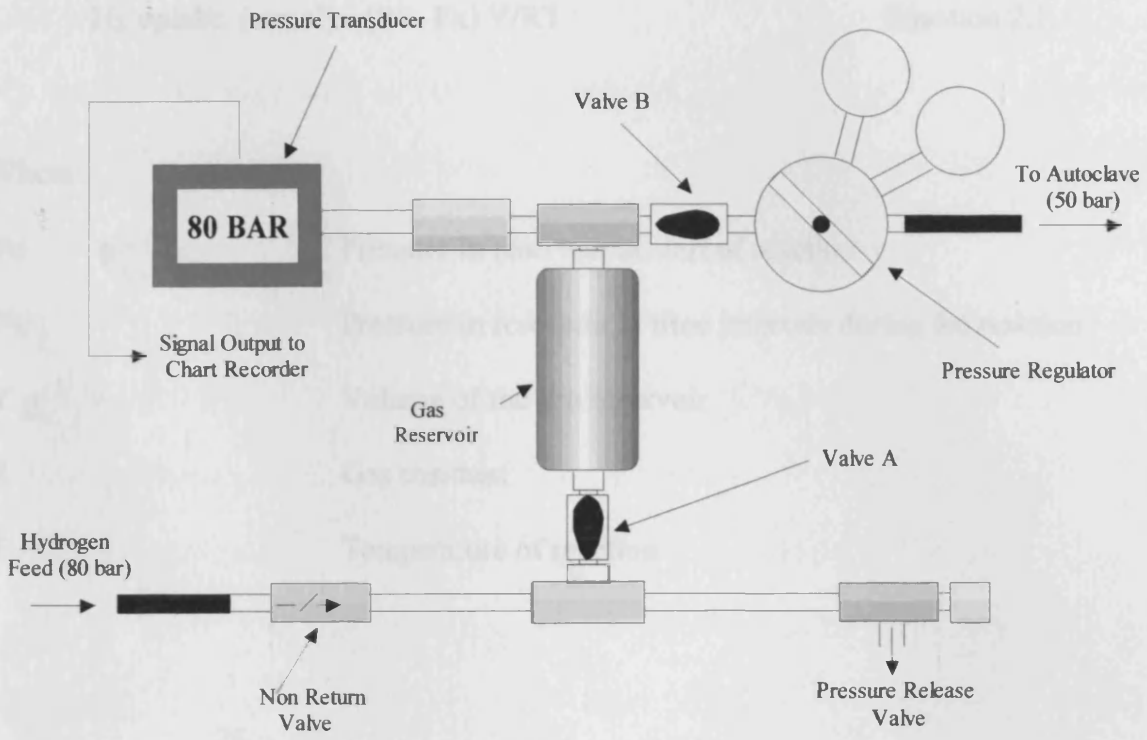

Figure 2.3 Schematic representation of the hydrogenation apparatus used in the enantioselective catalytic reactions.

The progress of reaction was monitored using a digital pressure display and a pressure transducer coupled to a chart recorder that measured the pressure variation in a fixed volume gas reservoir (100 cm^3). The reservoir was connected to the gas inlet of the autoclave, via a pressure regulator, which maintained a constant hydrogen pressure inside the autoclave (Figure 2.3).

During the catalytic reaction, the pressure inside the reservoir was measured at regular time intervals as to ascertain the amount of hydrogen consumed during the course of the catalytic reaction. A typical hydrogen uptake curve generated during the course of a catalytic enantioselective reaction is shown in Figure 2.4. The number of moles of hydrogen consumed at each point of the curve was calculated from the ideal gas law equation (Equation 2.1):

H_2 uptake (mmol) = (Po - Px) V/RT Equation 2.1.

Where:

Po	Pressure in reservoir at start of reaction
Px	Pressure in reservoir at time intervals during the reaction
V	Volume of the gas reservoir
R	Gas constant
T	Temperature of reaction

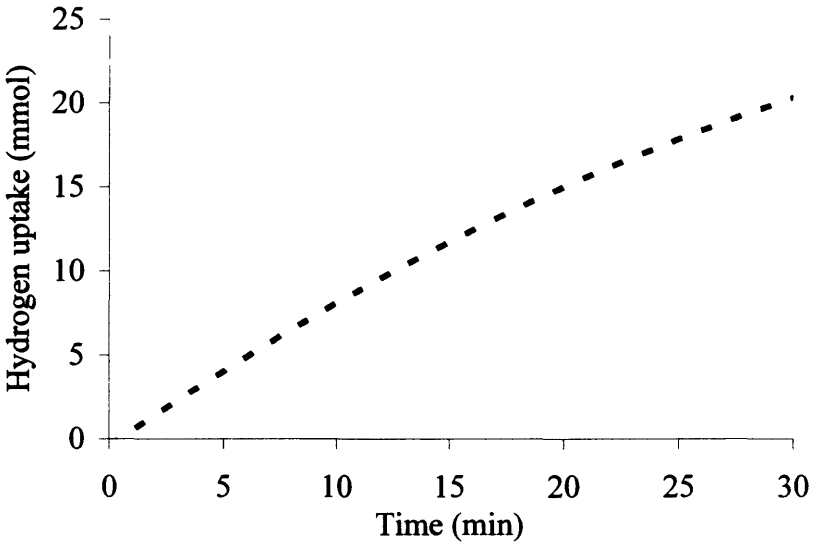

Figure 2.4 A typical hydrogen uptake curve for the enantioselective hydrogenation of ethyl pyruvate over Pt-AlMCM-41.

2.5.1 Product recovery

The reaction mixture was separated from the catalyst by vacuum filtration using a por 3 sintered glass funnel. The filtrate was diluted with dichloromethane in a 1:10 ratio and stored at 5 °C prior to its analysis.

2.5.2 Product analysis

The enantiomeric excess and conversion of reactants to products was achieved by the use of chiral gas chromatography. The instrument used was a Perkin Elmer 8700 series gas chromatograph equipped with a split/splitless injection system and flame ionisation detector (FID). Separation of various mixtures of ethyl and methyl pyruvate, [R] and [S] ethyl and methyl lactate enantiomers was achieved using a β- DexTM fused silica capillary column, (30 M x 0.25 mm x 0.25 μm) using a 0.1 μl injection volume, an isothermal temperature programme (80 °C), and a helium carrier gas flow rate of 1 ml. min^{-1}. The injector and detector temperatures were both set at 250 °C. A typical GC trace is shown in Figure 2.5.

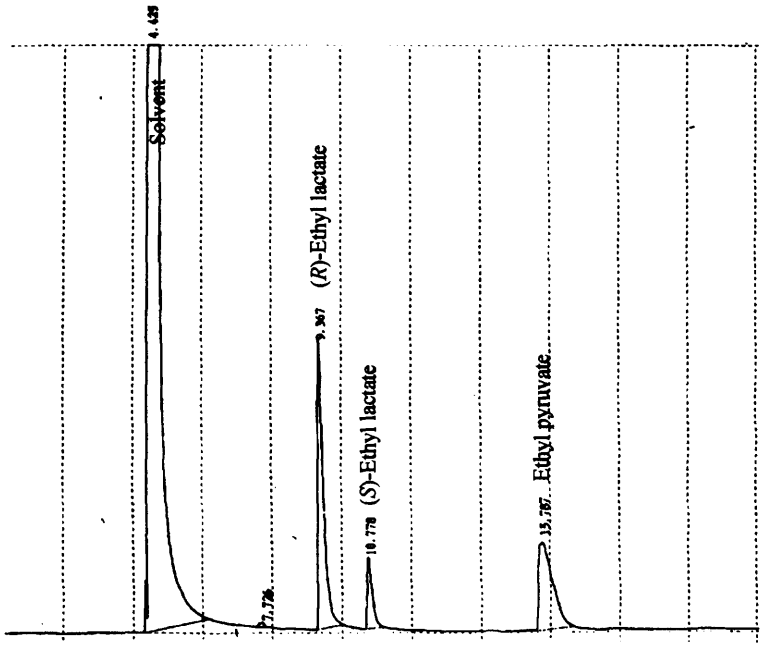

Figure 2.5 A typical chiral GC trace of the products catalysis.

2.5.3 Determination of enantiomeric excess

The enantiomeric excess (e.e. %) is defined by the equation:

$$\text{e.e. (\%)} = \frac{A_{[R]} - A_{[S]}}{A_{[R]} + A_{[S]}} \times 100 \qquad \text{Equation. 2.2}$$

Where [*R*] and [*S*] represent the relative concentration of enantiomeric products in solution as calculated from the integrated peak areas of the [*R*] and [*S*] enantiomers generated using chiral gas chromatography. To ensure the accuracy of the enantiomeric excess results a calibration graph (Figure 2.6) was constructed using a range of standard solutions prepared using commercially available [*R*] and [*S*] ethyl lactate, the solutions represented enantiomeric excess values in the range 40% [*S*] and 80% [*R*], which exceed the e.e. values achieved in this thesis.

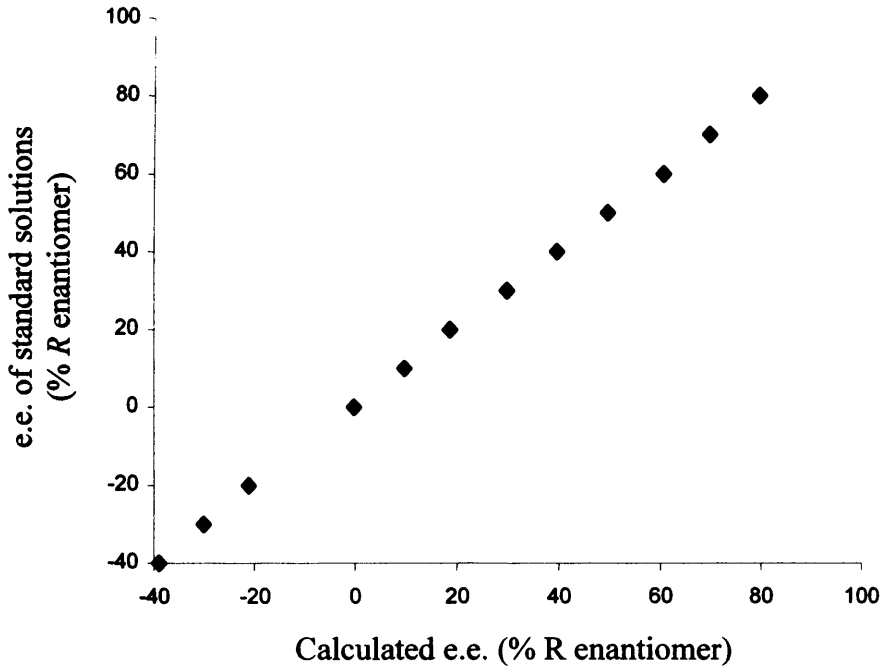

Figure 2.6 Calibration plot for chiral gas chromatography

2.5.4 Determination of conversion

Conversion is defined by the equation:

$$\text{Conversion (\%)} = \frac{\alpha_1 A_{[R]} + \alpha_2 A_{[S]}}{\alpha_1 A_{[R]} + \alpha_2 A_{[S]} + A_{[EtPy]}} \times 100 \qquad \text{Equation. 2.3}$$

Where $A_{[R]}$, $A_{[S]}$, and $A_{[EtPy]}$ are the respective GC integrated peak areas for [*R*] and [*S*] ethyl lactate and ethyl pyruvate. The coefficients α_1 and α_2 are the correction factors which normalize the peak areas of the [*R*] and [*S*] lactate enantiomers to that of ethyl pyruvate; these were individually measured by the GC analysis of differing mole ratio standard solutions of ethyl lactate enantiomers to that of ethyl pyruvate. The coefficients for the hydrogenation of ethyl lactate were calculated as being $\alpha_1 = 0.61$ and $\alpha_2 = 0.63$.

2.6 Techniques used in the characterisation of Pt-AlMCM41 catalysts

Pt-AlMCM-41 catalysts and their precursors were characterised by use of several routine analytical methods including X-ray diffraction (XRD), Brunauer, Emmett and Teller (BET) surface area analysis, magic angle spinning nuclear magnetic resonance (MAS-NMR), inductively coupled plasma mass spectrometry (ICP-MS), and high resolution transmission electron microscopy (HRTEM). A brief description of the apparatus used in characterisation is given in the following sections.

2.6.1 BET surface area

When a quantity of nitrogen gas (77 K) is exposed to an out-gassed solid in a vacuum, part of the gas is adsorbed on to the surface of the solid whilst part remains unabsorbed. The relationship between the amount of nitrogen adsorbed (at constant temperature) and

the nitrogen pressure is termed an adsorption isotherm. The surface area of a material can be determined using the BET (Brunauer, Emmet and Teller) model, which is used to determine the monolayer volume of the adsorbate from which the surface area of the solid material can be calculated using the following equation:

$$\frac{P}{V(P_0-P)} = \frac{1}{V_m \cdot C} + \frac{(C-1)}{V_m \cdot C} \cdot \frac{P}{P_0} \qquad \text{Equation 2.4}$$

Where:

P	Pressure
C	Constant
V	Volume
V_m	Volume of gas required to form monolayer

A plot of $P / V(P_O - P)$ against P / P_O should generate a straight line, whose intercept is $1 / V_m C$ and where the slope is $(C-1) / V_m C$. From the slope Vm, the volume of nitrogen required to form a complete unimolecular adsorbed layer can be determined. The surface area of a material can then be calculated by multiplying V_m by the area per molecule.

The pore volume and the pore-sized distribution of a material can be determined using the BJH (Barret, Joyner and Halenda) logarithm, which is dependent upon the relationship of nitrogen pressure and the increasing thickness of the layer of adsorbed nitrogen on the pore walls.

The surface area and pore characteristics of the mesoporous MCM-41 materials were determined using a Micromeretics ASAP 2000 analyser. The pre-weighed samples were

degassed under vacuum for 4 h at 373 K, nitrogen adsorption isotherms were then collected at 77 K and analysed using the BET and BJH isotherm models [2].

2.6.2 MAS-NMR magic angle spinning nuclear magnetic resonance

Magic angle spinning (MAS) is a procedure, which enables high resolution NMR spectra of solids to be obtained [3]. The procedure consists of rotation of the powdered solid sample about a fixed axis at an angle of 54° 44' to the direction of the external magnetic field B_o (Figure 2.7). It has been shown that rapid rotation about this macroscopic axis averages most of the detrimental solid state interactions such as quadrupole, dipolar and chemical shift anisotropy and lead to NMR spectra with fine structure similar to that observed in the NMR spectra of liquids.

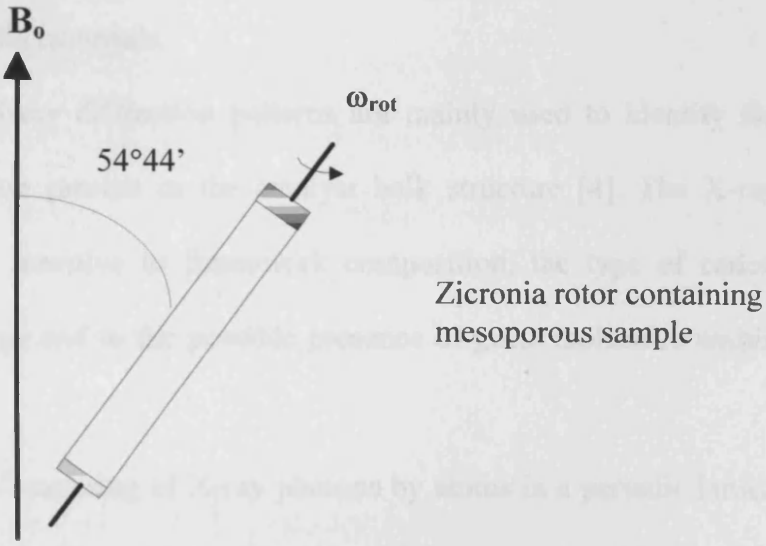

Figure 2.7 Magic angle spinning

MAS-NMR spectroscopy was carried out using a 400 MHz Chemagnetics CMX infinity spectrometer controlled by spinsight software. All samples were analysed using zicronia pencil rotors spun a on a bearing of dry air.

^{29}Si spectra were recorded using a 7.5 mm chemagnetics probe at a resonance frequency of 79.472 MHz; the samples were spun at a speed of 3 KHz and externally referenced to tetramethylsilane. ^{27}Al spectra were recorded using a 7.5 mm chemagnetics probe at a resonance frequency of 104.2439 MHz; the samples were spun at a speed of 3 KHz and externally referenced to kaolin.

2.6.3 Powder X-ray diffraction

X-Rays have wavelengths in the in the Angstrom range, which are sufficiently energetic to penetrate solids, therefore well suited to probe their internal structure. XRD has been used to identify bulk phases, to monitor the kinetics of bulk transformations and to estimate the particle size of solid materials.

In catalyst characterisation, X-ray diffraction patterns are mainly used to identify the crystallographic phases that are present in the catalyst bulk structure [4]. The X-ray powder diffraction pattern is sensitive to framework composition, the type of cation balancing the framework charge and to the possible presence of guest molecules within the pores of the structure.

X-ray diffraction is the elastic scattering of X-ray photons by atoms in a periodic lattice [5]. The scattered monochromatic X-rays that are in phase give constructive interference, thus if the angles are measured at which constructively interfering X-rays leave the crystal; the Bragg relation (Equation 2.5) gives the corresponding lattice spacings, which are characteristic for a certain compound.

$$n\lambda = 2d\sin\theta \qquad \text{Equation 2.5}$$

Where:

n	the order of reflection
λ	the wavelength of the X-rays
d	the distance between two lattice planes
θ	the angle between the incoming X-rays and the reflecting lattice plane

The angles of maximum intensity (θ) enable the spacings between the lattice planes (d) to be calculated, and hence the phase identified. X-ray diffractograms are a measure of X-ray intensity against 2θ. When the sample of interest is a polycrystalline powder only a small fraction of particles actually contributes towards the diffraction pattern, thus to increase this contribution the sample is rotated during measurement.

X-ray diffraction patterns were generated by use of a siemens D5000 spectrometer at the University of Hull. The diffractometer was operated at 40 KeV and 40 mA using Cu Kα radiation (λ = 1.542 Å). Values of 2θ over the range 1° to 65° were scanned at a rate of 1° per minute.

2.6.4 ICP-MS inductively coupled plasma mass spectrometry

Inductively coupled plasma mass spectroscopy (ICP-MS) was developed in the late 1980's [6] to combine the easy sample introduction and quick analysis of ICP technology with the accurate and low detection limits of a mass spectrometer. The resulting

instrument is capable of quantitative multi-element analysis, often at the part per trillion level.

ICP technology was built upon the same principles used in atomic emission spectrometry. Samples are decomposed to neutral elements in high temperature argon plasma and analysed according to their mass to charge ratios. ICP-MS can be thought of as four main processes, sample introduction and aerosol generation, ionisation, mass filtration and detection system.

The catalyst samples of interest were digested with hydrofluoric acid and subsequently diluted with deionised water prior to their introduction into the instrument by way of a nebulizer, which aspirates the sample using high velocity flowing argon to form a fine mist. The nebulised sample then moves into the torch body where it is mixed with additional heated argon gas. This heated matrix is then subjected to radio frequency transmitted from a coupling coil, producing an argon plasma "flame" located at the top of the torch. This hot plasma removes any remaining solvent molecules and induces sample atomisation followed by ionisation. The ionised sample is subsequently introduced into the mass spectrometer, which is under vacuum, as a supersonic jet.

The first stage of the spectrometer focuses the ions into a narrow beam, prior to their entrance into a quadrupole mass analyser, which is able to separate ions according to their different mass to charge (m/z) ratios. These mass filtered ions then go on to strike a photomultiplier detector generating a digital output signal.

ICP-MS was carried out by S. Goldsmith at Cardiff University using a Perkin Elmer Elan 5000, a Perkin Elmer HGA 600 ETV, a Perkin Elmer FIAS 200 flow injection system and a CETAC 200 laser ablation unit.

2.6.5 HRTEM high resolution transmission electron microscopy

Bright field (BF) and high resolution transmission electron microscopy (HRTEM) was performed at 200 kV using a JEOL 2200FS transmission electron microscope having a point-to-point resolution of 0.19 nm. Samples were prepared for TEM analysis by dispersing the catalyst powder in high purity ethanol, then allowing a drop of the suspension to evaporate on a holey carbon film supported by a 300 mesh copper TEM grid.

2.7 Continuous flow reactor (CFR) studies

2.7.1 CFR reactor construction

The CFR reactor (Figure 2.8) was composed of three main components: A glass reactor vessel, a reactor head assembly and an aluminium clamping system. The glass reactor was 250 mm in length had an internal diameter of 28 mm and constructed from heavy wall glass tubing. Sealed into the inside of the reactor was a glass frit (por 3) on which the catalyst bed rests.

The reactor head consisted of a pressure gauge (0 – 3 bar) which was used to monitor the pressure of the reaction, a five port distributor head which delivered the liquid and gaseous reagents to the catalyst bed, a vent valve and a needle valve located on the incoming gas line which was used to control the flow of gas and pressure inside the reactor.

The glass reactor vessel and reactor head assembly were interfaced by means of an aluminium clamp, rubber and PTFE o-ring. The system was leak tested prior to the start of each reaction.

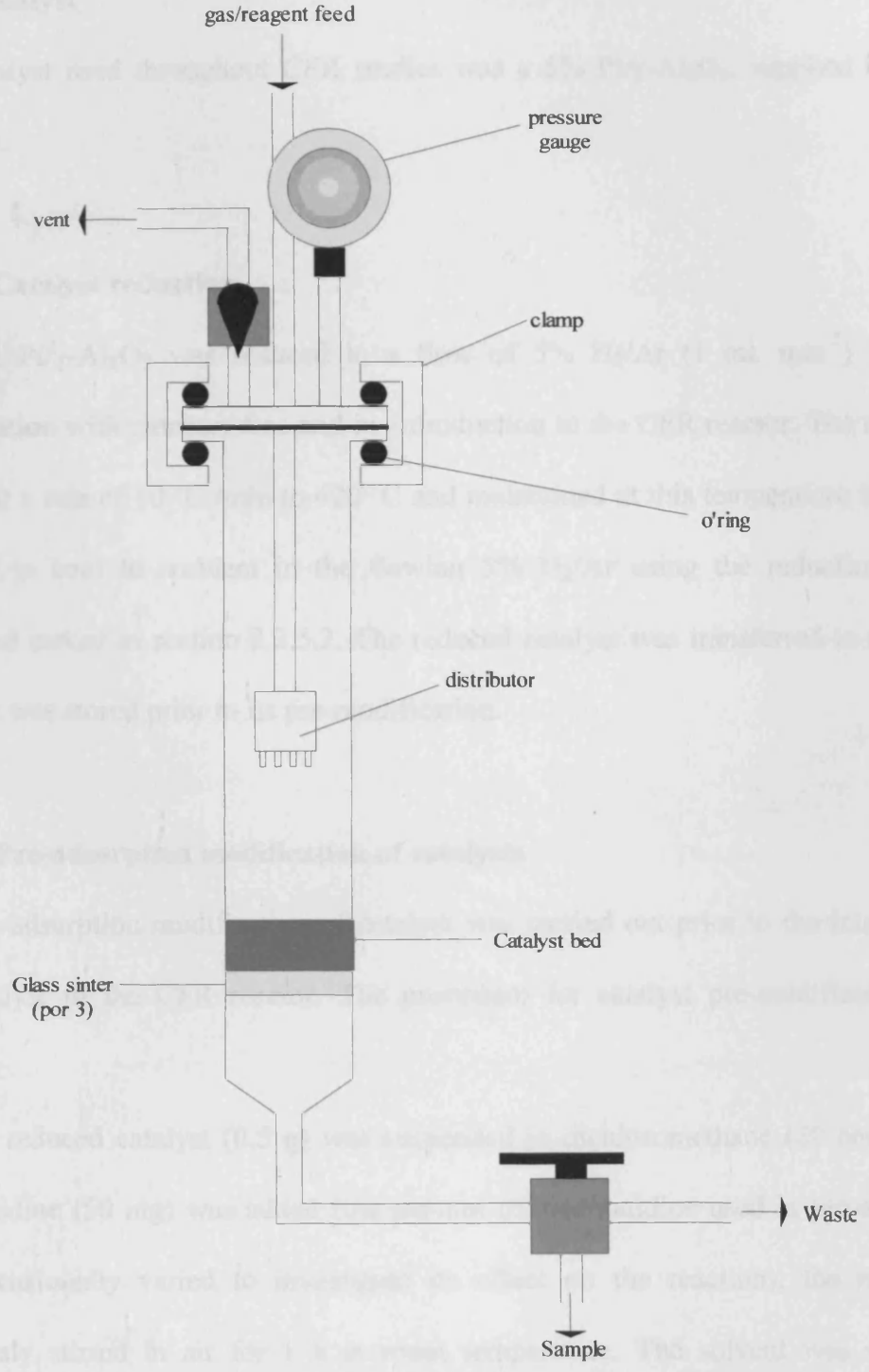

Figure 2.8 Diagrammatic representation of the CFR apparatus used in the enantioselective hydrogenation of pyruvate esters.

2.7.2 Catalyst

The catalyst used throughout CFR studies was a 5% $Pt/\gamma\text{-}Al_2O_3$, supplied by Johnson Matthey.

2.7.2.1 Catalyst reduction

The 5% $Pt/\gamma\text{-}Al_2O_3$ was reduced in a flow of 5% H_2/Ar (1 ml. min^{-1}) prior to its modification with cinchonidine and its introduction to the CFR reactor. The catalyst was heated at a rate of 10 °C /min to 420 °C and maintained at this temperature before being allowed to cool to ambient in the flowing 5% H_2/Ar using the reduction apparatus described earlier in section 2.2.5.2. The reduced catalyst was transferred to a desiccator where it was stored prior to its pre-modification.

2.7.2.2 Pre-adsorption modification of catalysts

The pre-adsorption modification of catalyst was carried out prior to the introduction of the catalyst to the CFR reactor. The procedure for catalyst pre-modification was as follows:

Freshly reduced catalyst (0.5 g) was suspended in dichloromethane (20 cm^3) to which cinchonidine (50 mg) was added (the amount of cinchonidine used in pre-modification was occasionally varied to investigate its effect on the reaction); the mixture was vigorously stirred in air for 1 h at room temperature. The solvent was removed by vacuum filtration and the pre-modified catalyst was air dried and stored in a desiccator prior to use, typically within 2 days.

2.7.3 The hydrogenation of pyruvate esters in the CFR reactor

A 0.4 g portion of cinchona catalyst doped catalyst (particle size 50 μm) was thoroughly mixed with 8.0 g of silicon carbide (25 gauge) and transferred to the reactor to give a bed depth of 12-13 mm.

Prior to the start of the reaction the reactor was thoroughly purged with helium gas (300 ml. min^{-1}, 0.25 bar/g) to remove any residual air. The helium was switched for hydrogen (300 ml. min^{-1}, 0.25 bar/g) and the catalyst bed, equilibrated at 25 °C, subjected to a period of solvent pre-treatment, which varied between 0 min and 180 min, (this period of pre-treatment was occasionally increased or omitted to observe its effect on the reaction) at a concurrent flow rate of 1 ml. min^{-1}, and a contact time of 150 s, delivered to the catalyst bed by means of a Beckman HPLC pump. Reaction commenced with the introduction of a feedstock of dissolved reagents. The timing of their introduction was controlled by a three way tap positioned between the HPLC pump and stock solutions of solvent and reagent. Ethyl and methyl pyruvate esters were used in 25 mM concentrations when fed separately to the reactor, when the feedstock contained both ethyl and methyl pyruvate the concentration of the individual esters was halved to 12.5 mM to ensure comparability between reactions. Racemic, [*R*], or [*S*] enantiomers of methyl or ethyl lactate were occasionally co-fed with the pyruvate esters in 25 mM concentration. The time on line for the majority of reactions was 2 h, occasionally longer.

2.7.4 UV/Vis spectroscopic analysis of CFR eluent

UV analysis was employed to determine the amount of cinchonidine leached from a catalyst bed that contained a known amount of pre-adsorbed cinchonidine, when operating under standard reaction conditions. A constant sample volume (1 cm^3) of reactor eluent was collected at regular time intervals and their spectra recorded on a

Perkin Elmer Lambda UV/Visible spectrometer using a quartz cell of path length 0.5 cm. Absorbance measurements were taken at a wavelength of 288 nm, this value being the maximum absorbance observed in the UV/Visible spectrum of cinchonidine in dichloromethane over the range 250 nm – 650 nm (Figure 2.9).

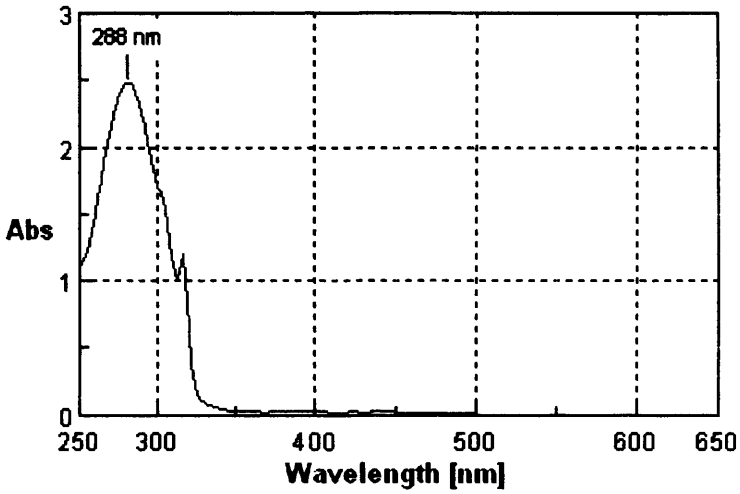

Figure 2.9 The UV/Vis spectrum of cinchonidine.

To obtain a correlation between the experimental absorbance values and cinchonidine concentration, absorbance measurements were recorded for a range of standard solutions (0 mM to 0.5 mM) of known concentration to generate a calibration curve (Figure 2.10) from which the concentration of cinchonidine present in the reactor samples could be calculated.

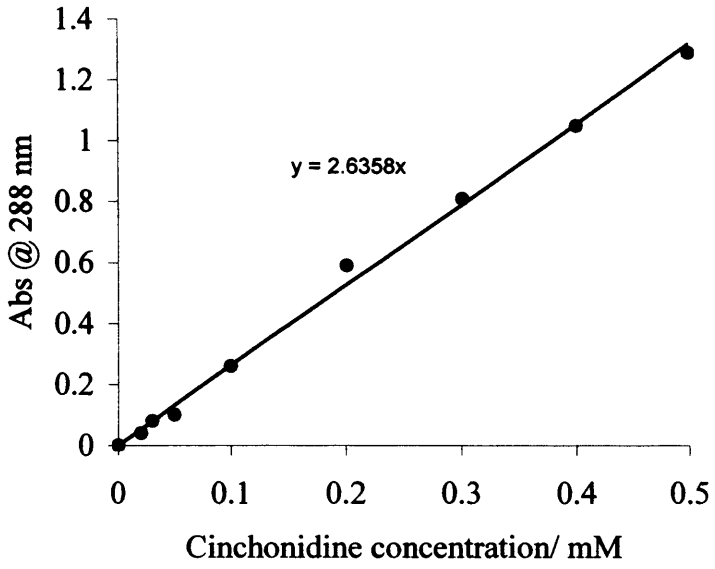

Figure 2.10 UV/Vis cinchonidine calibration curve.

2.7.5 Product recovery and analysis

The eluent from the reaction was sampled at regular time intervals during the time the reactor was on line using a two-way tap positioned at the outlet of the reactor. Enantiomeric excess and conversion to products was determined using off line chiral gas chromatography employing the same experimental conditions reported earlier in section 2.5.2. Reactants and products were of a concentration that did not require solvent dilution prior to analysis.

2.8 Hydrogenation of ethyl pyruvate over platinum modified hydroquinidine and hydroquinine derivatives of cinchonidine in batch reactor

2.8.1 Catalysts

The catalysts used in this study were 5% Pt/γ-Al_2O_3, 5% Pt/C and 2.5% Pt/SiO_2 all of which were manufactured and supplied by Johnson Matthey.

2.8.2 Catalyst Reduction

All catalysts were subjected to a reductive pre-treatment prior to their introduction to the autoclave using the apparatus described earlier in section 2.2.5.2. The catalysts were heated in a flow of 5% H_2/Ar (1 ml. min^{-1}) at a rate of 10 °C /min from 298 K to the desired final temperature between 373 K and 673 K. The catalyst was maintained at this temperature for a further 2 h before being allowed to cool to ambient in the 5% H_2/Ar flow. The catalyst was transferred to a desiccator where it was stored prior to its use.

2.8.3 Catalytic Testing

All catalytic reactions involving hydroquinidine and hydroquinine derivatives were carried out using the autoclave apparatus described earlier in section 2.4. Hydroquinidine or hydroquinine cinchonidine derivatives of varying concentration (1 mg to 100 mg, 0.17 mM to 8.5 mM) and ethyl pyruvate (7.66 g, 66 mmol) was charged to the reactor, which contained the freshly reduced platinum catalyst (0.25 g) suspended typically in dichloromethane, acetic acid or toluene (12.5 cm^3).

The autoclave was sealed and purged three times with hydrogen (30 bar) to remove any residual air from the reactor, then pressurised to the experimental operating pressure (50 bar). The contents of the autoclave were cooled to 296 K using an ice bath prior to the start of the reaction.

The reaction was initiated on commencement of stirring (1200 rpm); the temperature, H_2 pressure and stirring rate were maintained throughout the course of the reaction. The reaction was allowed to proceed for 1 h after which the hydrogen pressure was released and the contents of the autoclave analysed using chiral gas chromatography.

2.8.4 Nuclear Magnetic Resonance ^{1}H NMR

Proton NMR was used to investigate the possible hydrolysis of hydroquinidine-4-chlorobenzoate in solution. A series of proton NMR experiments were recorded for 0.5 cm^3 solutions of CD_2Cl_2 and CD_3COOD containing varying amounts of hydroquinidine-4-chlorobenzoate (7.3 μmol - 0.1μmol) in the presence of excess water (1 μl, 55 mmol). The spectra were recorded using a Bruker Avance multinuclear 400 MHz NMR spectrometer. The spectrometer was configured to lock automatically on the deuterium signal of the solvent, which also acted as an internal reference.

2.9 References

1 S.S. Kim, W. Zhang and T. J. Pinnavaia, *Catal. Lett.*, **43** (1997) 149.

2 S.J. Gregg and K.S.W. Sing, *Adsorption, Surface Area and Porosity*, Academic Press, (1982).

3 G. Englehardt and D. Michel, *High Resolution Solid State NMR of Silicates and Zeolites,* J. Wiley and Sons (1997), 50.

4 G. Perego, *Catal, Today.*, **41** (1998) 251.

5 J.W. Niemantsverdriet, *Spectroscopy in Catalysis*, VCH Publishing.

6 A.K.E Jarvis, A.L. Gray and R.S. Houk, 1992. *Handbook of Inductively Coupled Plasma Mass Spectrometry.*

Chapter Three

Chapter Three MCM-41, A Support for Platinum Catalysed Enantioselective Hydrogenation

3.1 Introduction

3.1.1 History and Definition of Zeolites

The Swedish mineralogist Axel Cronstedt first described zeolites as a mineral group in 1756 [1]. Cronstedt observed that if the mineral stilbite was heated it hissed and bubbled as if it were boiling, he denoted this material "zeolite" taken from the Greek words *zeo*, to boil and *lithos*, stone.

Zeolites are a class of alumosilicates based on a rigid anionic framework with well-defined channels and cavities. The primary building units of zeolites are $[SiO_4]^{4-}$ and $[AlO_4]^{5-}$ which adopt a tetrahedral geometry linked together by corner-sharing to form bent oxygen bridges. It is possible for these tetrahedra to link by sharing two, three or all four corners, providing a variety of diverse structures as illustrated in Figure 3.1. Silicon-oxygen tetrahedra are electrically neutral when connected together in a three dimensional network as can be observed in quartz and SiO_2, however, the substitution of Si by Al in such structures creates an electrical imbalance. To preserve overall electrical neutrality each $[AlO_4]^{5-}$ tetrahedron requires a balancing positive charge, which is provided by exchangeable cations held electrostatically within the zeolite.

Chemically, zeolites can be represented by the formula: $xM_{2/n}O{:}xAl_2O_3{:}ySiO_2{:}wH_2O$ where M can be elements in groups IA or IIA or an organic cation, while n is the cation valence, and w represents the number of water molecules contained within the zeolite pores.

The rapid evolution of zeolite science has expanded the definition of zeolites to a variety of non-silicate materials, such as aluminophosphates ($AlPO_4$) and metal aluminophosphates (*M*APO) [2] the metal species *M* can be divalent forms of Co, Fe, Mg, Mn and Zn as well as trivalent Fe.

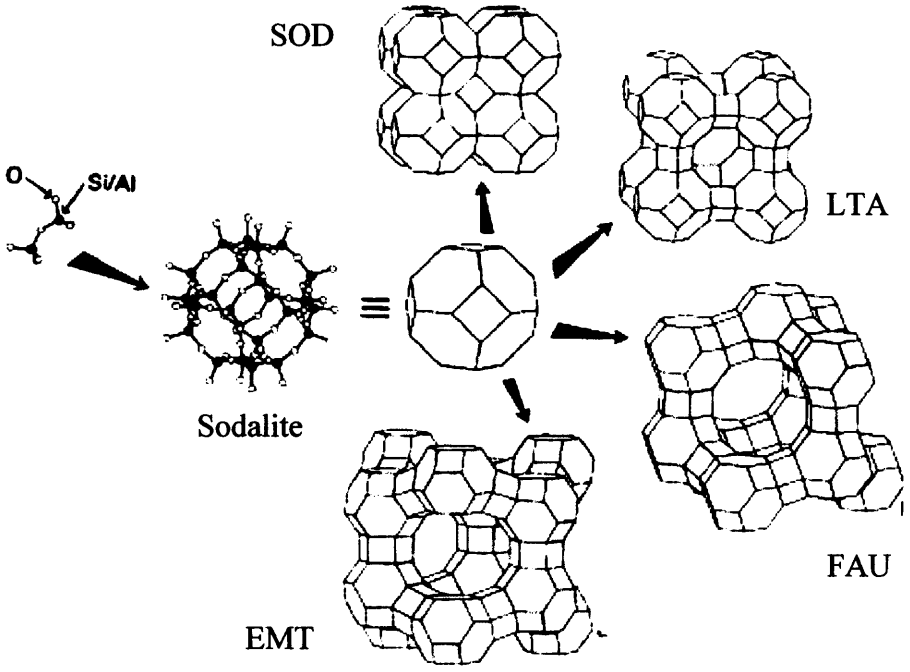

Figure 3.1 Various zeolite structures, based on the sodalite cage [3]

For many years zeolites have been widely used as detergent builders, cation exchange materials and adsorbents [4]. More recently research has focused on their ability to act as catalysts in a wide variety of industrial processes [5], many of which are highly specific. Approximately 60 naturally occurring zeolites have been successfully characterised [6], yet in the quest for more efficient and selective catalysts more than 130 entirely new synthetic structures have been developed [7].

Until recently, all zeolites reported had pores in the microporous range, (0.2 to 2.0 nm), the maximum being 0.75 nm as found in faujasite, (zeolite Y) [8]. The requirement to

process molecules that are too large to access the pores of conventional zeolites has led to a search for materials which have pore sizes in the mesoporous range (2 to 50 nm). The most commonly used catalyst supports such as silica and alumina have pores in this range yet these are irregular, non-uniform and of a broad size distribution.

3.1.2 Mesoporous Materials

Research into supramolecular templated mesoporous materials [9] began in the early 1990's with the discovery of the M41S family of mesoporous materials by researchers at Mobil. Several reviews of the general properties, methods of synthesis and their potential uses have been reported in the literature [10]. To date, three distinct mesophases (Figure 3.2) have been identified within this family of materials: lamellar MCM-50 [11] cubic MCM-48 [12] and hexagonal MCM-41 [13].

These mesoporous (alumino) silicate materials, with uniform pore sizes of 1.5-10 nm break past the pore-size constraints of microporous zeolites.

The extremely high surface area (> 1000 m^2g^{-1}) and the ability to precisely tune the pore volume are among the many desirable properties that have made these materials the focus of great interest in heterogeneous catalysis.

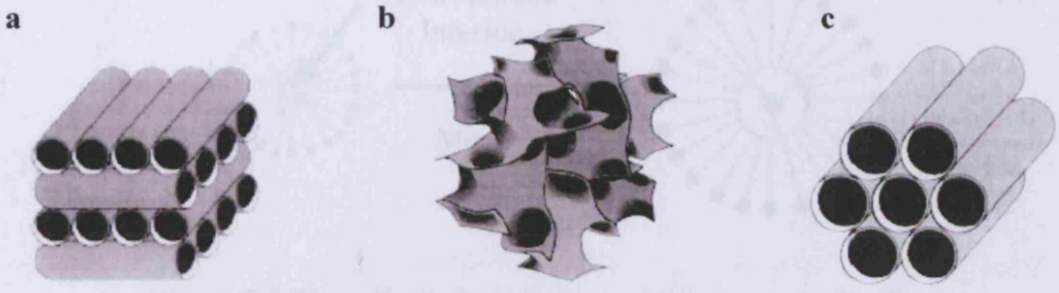

Figure 3.2 The M41S family of mesoporous materials. **a**) lamellar MCM-50, **b**) cubic MCM-48, **c**) hexagonal MCM-41.

3.1.3 Synthesis of MCM-41 Materials

Mesoporous MCM-41 materials are synthesised using liquid surfactant templates. Generally the surfactants are quaternary ammonium compounds of general formula $C_nH_{2n+1}(CH_3)_3N^+$, where *n* is an alkyl chain typically between 10 and 20 carbon atoms in length. Variation of the alkyl chain length [14] allows the control of pore size in the MCM-41 material.

Table 3.1 The effect of surfactant alkyl chain length on the pore diameter of MCM-41.

$C_nH_{2n+1}(CH_3)_3N^+$ (*n*)	Pore diameter (nm)
12	3.1
14	3.4
16	3.9

The pore diameter of these materials can be further increased by the addition of an auxiliary hydrocarbon [15] such as mesitylene during synthesis. The mesitylene molecules are solubilised within the centre of the micelle, causing the surfactant assembly to swell and generate materials with pore diameters of up to 10 nm as illustrated in Figure 3.3.

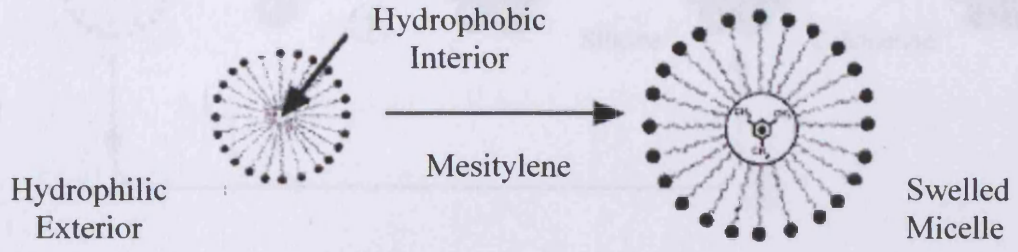

Figure 3.3 The effect of mesitylene addition on micelle diameter.

3.1.4 Mechanism of MCM-41 Formation

In the formation of zeolites the dominant process of structural growth is the condensation of alumosilicate material around single template molecules. In contrast it is thought that the growth of MCM-41 is facilitated by a liquid crystal templating (LCT) mechanism, in which the surfactant forms liquid crystalline micelles which serve as an organic template for the growth of MCM-41. The micelles take the form of rods, which stack together to form a close packed hexagonal array (Figure 3.4). In the LCT mechanism, originally postulated by Beck *et al*, two possible mechanistic formation pathways have been proposed which are consistent with the observed structures [16].

Pathway **1**; the liquid crystal hexagonal phase forms first, prior to silicate deposition occurring.

Pathway 2; silicate deposition takes place about a single rod, which induces the ordering of the liquid crystal phase into the desired hexagonal structure.

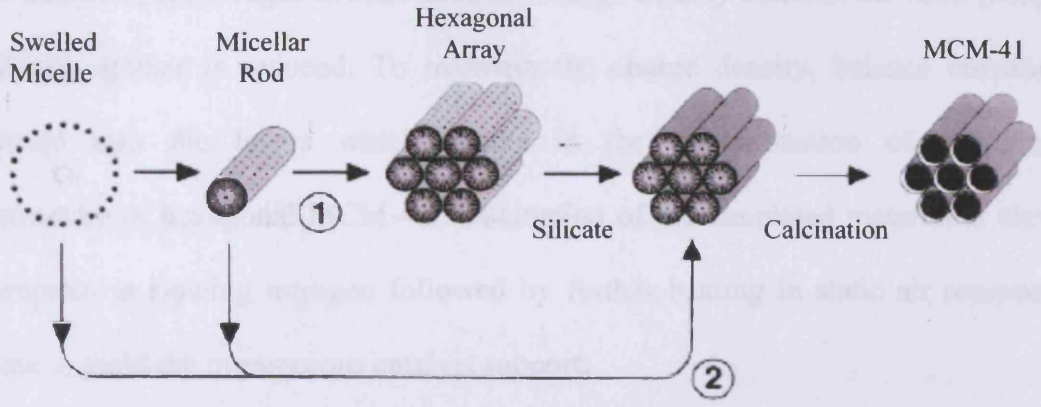

Figure 3.4 possible mechanistic pathways for the formation of the hexagonal phase MCM-41: **1** the liquid crystal initiated pathway and **2** the silicate anion initiated pathway.

A second mechanistic model based on charge density matching was proposed by Stucky [17, 18], which suggested that MCM-41 is derived from a lamellar phase. Using XRD Stucky observed the initial phase of the reaction mixture was layered and formed *via* the electrostatic attraction between the anionic silicates and the cationic surfactant head groups as shown in Figure 3.5.

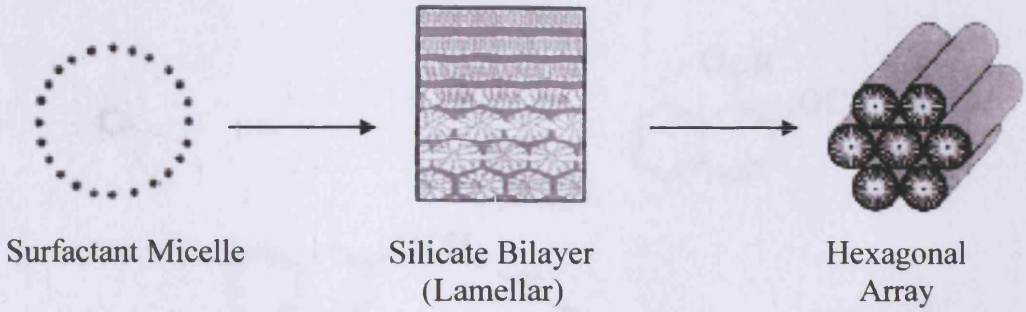

Figure 3.5 Schematic representation of the mechanism proposed by Stucky *et al.* for the transformation of lamellar to hexagonal MCM-41.

As the silicate species begin to condense, the charge density between the head group and the silicate species is reduced. To maintain the charge density, balance curvature is introduced into the layers which results in the transformation of the lamellar mesostructure to hexagonal MCM-41. Calcination of the templated material at elevated temperatures in flowing nitrogen followed by further heating in static air removes the template to yield the mesoporous catalyst support.

3.1.5 Catalytic Applications of MCM-41

The first catalytic studies with mesoporous molecular sieves focused on metal substituted MCM-41 materials in which the active species was incorporated into the silicate matrix

during synthesis or deposited within the pore structure post process calcinations [19]. The reactions studied were mainly oxidation and acid catalysed. As an acid catalyst aluminosilicate MCM-41 has found application in Friedel-Crafts acylations [20]. Gunnewegh *et al.* observed that the reaction between 2-methoxynaphthalene and acetic anhydride within the pores of H-MCM-41 at a temperature of 100 °C, was regiospecific giving the 1-acylated product exclusively [21] (Figure 3.6.).

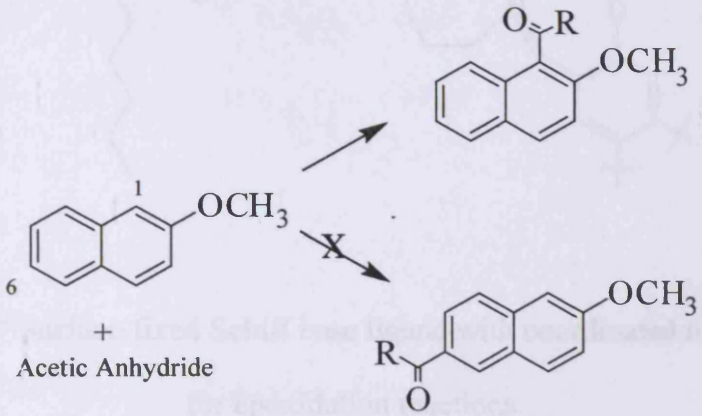

Figure 3.6 Acid catalysed acylation of 2-methoxynaphthalene over H-MCM-41.

As an oxidation catalyst, Ti-MCM-41 has shown superior activity to that of its zeolite counterparts in the oxidation of bulky hydrocarbons such as norbornene in the presence of *t*-butylhydroperoxide. The mesoporous catalyst showed a 90% selectivity for epoxides while the same reaction carried out over Ti containing ZSM-5 showed little activity [22]. Recent research has centred on the immobilisation of catalytically active complexes onto the inner walls of the MCM-41 porous framework, thus combining the advantages of homogeneous catalysis with a high surface area heterogeneous catalyst support. Sutra and Burenel [23] successfully immobilised a homogeneous epoxidation catalyst within the MCM-41 mesopore (Figure 3.7), which facilitated increased selectivity in

epoxidation processes and eased problems associated with catalyst separation and regeneration.

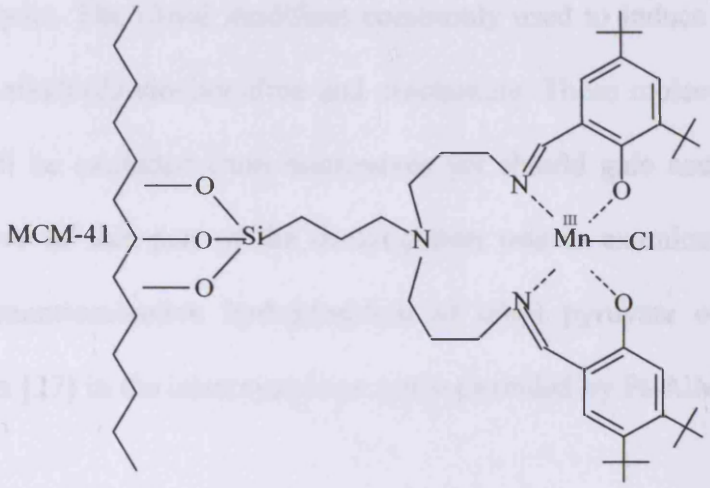

Figure 3.7 Surface-fixed Schiff base ligand with coordinated manganese for epoxidation reactions.

MCM-41 materials have also found application as hydrogenation catalysts. Pt-MCM-41 has been used to hydrogenate geraniol [24] in a manner that exploits the geometry of the mesoporous solid. Use of Ru-MCM-41 [25] has also been described as a catalyst in the hydrogenation of prostaglandin intermediates. Significantly, the mesoporous environment is conducive to enantioselective reaction; for example, the ephedrine-catalysed condensation of benzaldehyde and diethyl zinc in the pores of MCM-41 has been shown to give an enantiomeric excess in the resultant 1-phenylpropan-1-ol twice that obtained for the same reaction at a silica-gel surface [26].

3.1.6 Aim of investigation

Enantioselective hydrogenation of pyruvate esters over chirally modified platinum (the Orito reaction) is a reaction that could benefit from the development of suitable mesoporous catalysts. The chiral modifiers commonly used to induce enantioselectivity are the cinchona alkaloids cinchonidine and cinchonine. These molecules are of such a size that they will be excluded from micropores yet should gain access to mesopores. Thus, the objective of this part of the investigation was to examine the feasibility of conducting the enantioselective hydrogenation of ethyl pyruvate over cinchonidine-modified platinum [27] in the intracrystalline space provided by Pt-AlMCM-41.

3.2 Results

3.2.1 Preparation of AlMCM-41 catalyst support materials

3.2.1.1 Preparation of *C16* AlMCM-41 using cetyltrimethylammonium bromide as a template

C16 AlMCM-41 was prepared using cetyltrimethylammonium bromide as a liquid template following the procedure outlined in section 2.2.1. The template containing material was calcined following the procedure outlined in section 2.2.3. The X-ray diffraction pattern of the calcined material (Figure 3.8) consisted of a sharp feature at 2θ 2.6° together with a broad feature at 2θ 4.05°. HRTEM images showed mesopores in hexagonal arrays throughout the fields of view [16] (Figure 3.9).

Thermal gravimetric analysis (TGA) was used to determine the optimum calcination temperature and the effectiveness of the calcination process (Figure 3.10 and 3.11). The Si:Al ratio of the final material was 100:8 as determined by ICP-MS. The surface area of

the calcined material was 990 m^2g^{-1}. Adsorption measurements estimate the mean pore size of the material to be 2.3 nm in diameter.

^{27}Al MAS-NMR spectra of the pre-calcined material (Figure 3.12, **a**), showed a single resonance at 54.3 ppm. The chemical shift of this resonance remained unchanged on calcination, however, a new resonance of notable intensity appeared at -0.4 ppm (Figure 3.12 **b**), indicating a change in the distribution and nature of aluminium present within the material.

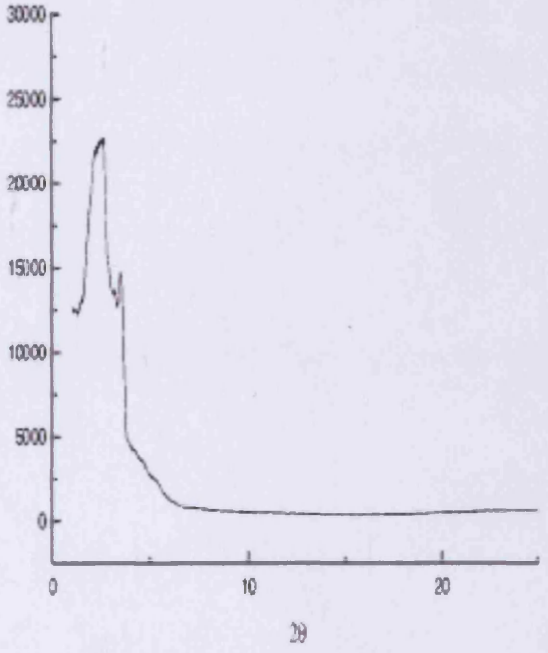

Figure 3.8 Powder XRD pattern of calcined *C16* AlMCM-41.

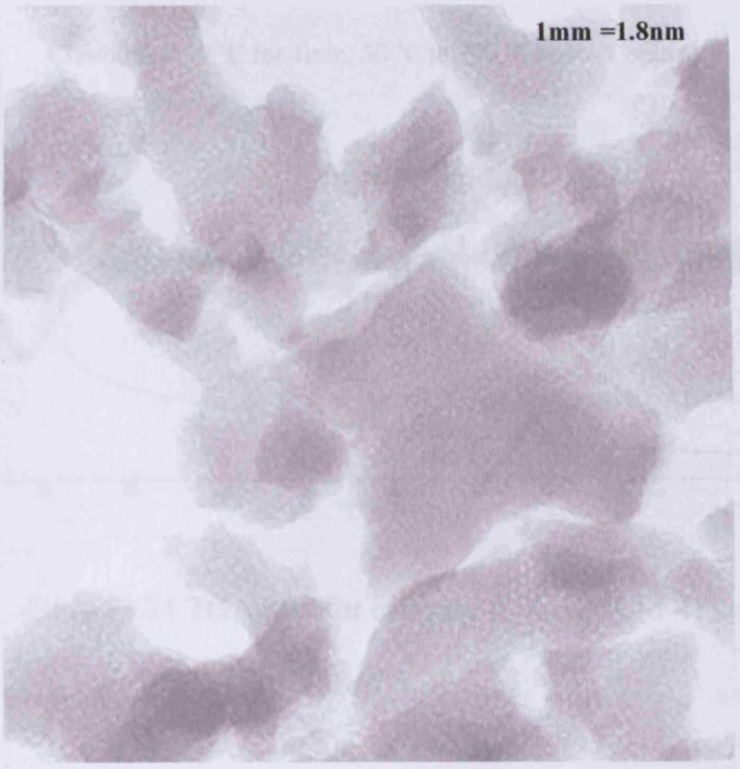

Figure 3.9 HRTEM micrograph of calcined *C16* AlMCM-41 viewed down the pore axis.

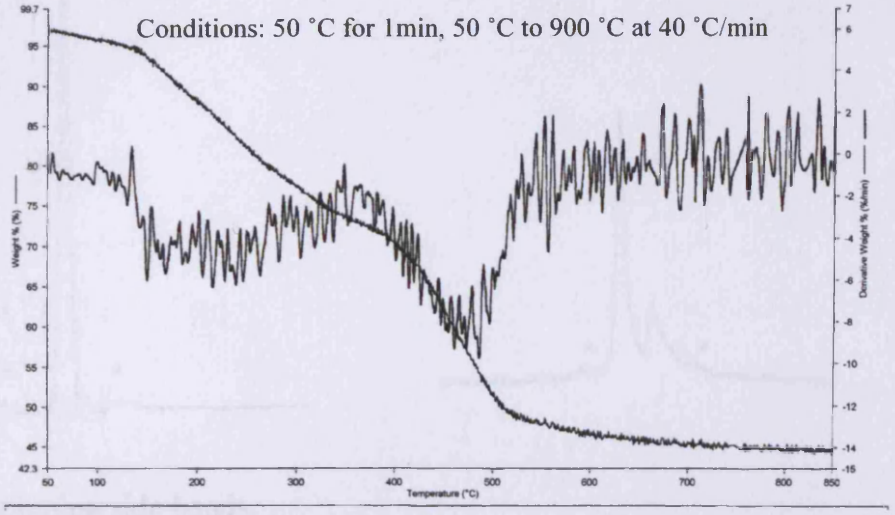

Figure 3.10 TGA plot for uncalcined *C16* AlMCM-41.

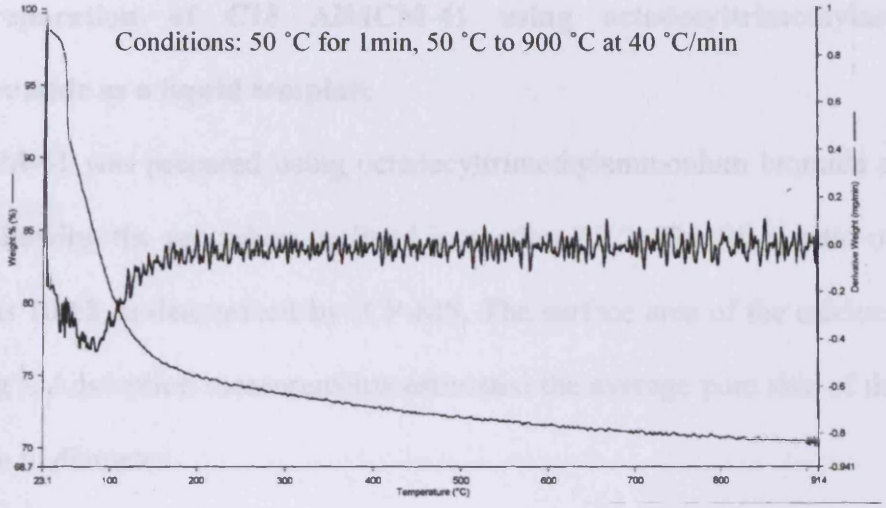

Figure 3.11 TGA plot for calcined *C16* AlMCM-41.

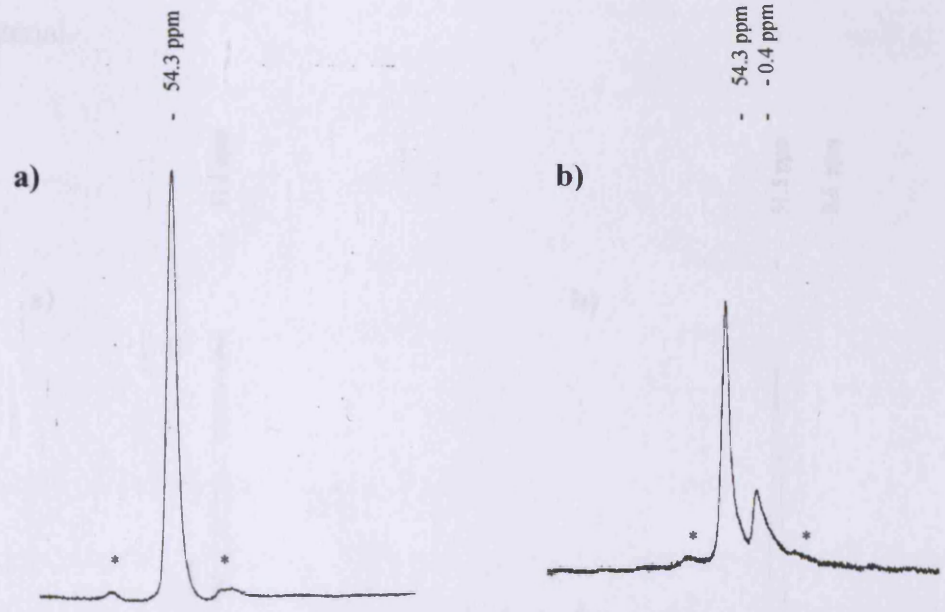

* Denotes spinning side bands.

Figure 3.12 ^{27}Al MAS NMR spectra of the *C16* derived (**a**) uncalcined and (**b**) calcined AlMCM-41materials.

3.2.1.2 Preparation of *C18* AlMCM-41 using octadecyltrimethylammonium bromide as a liquid template

C18 AlMCM-41 was prepared using octadecyltrimethylammonium bromide as a liquid template following the procedure outlined in section 2.2.2. The Si:Al ratio of the final material was 100:8 as determined by ICP-MS. The surface area of the calcined material was $992 m^2 g^{-1}$. Adsorption measurements estimated the average pore size of the material to be 3.1 nm in diameter.

Figure 3.13 shows the ^{27}Al MAS-NMR spectra of the uncalcined (**a**) and calcined (**b**) materials. The uncalcined spectrum shows a single resonance at 51.2 ppm. On calcination a new resonance is observed at -0.4 ppm signifying a distributional change in the type of aluminium present in the material. No HRTEM analysis was carried out on the *C18* material.

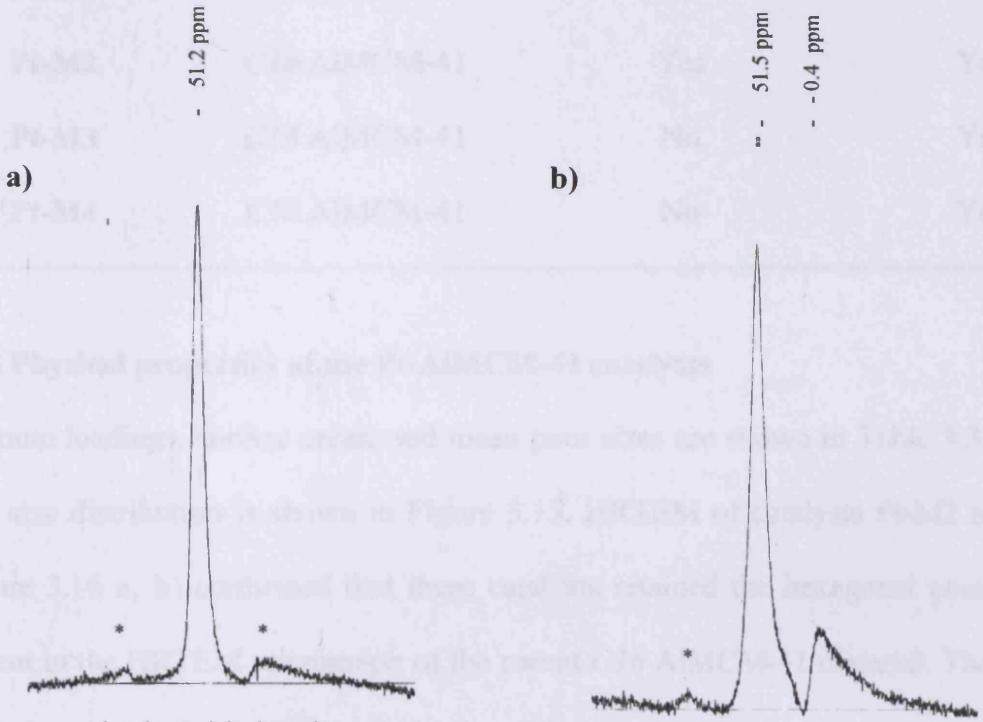

* Denotes spinning side bands.

Figure 3.13 ^{27}Al MAS NMR spectra of the *C18* derived uncalcined (**a**) and calcined (**b**) AlMCM-41materials

3.2.2 Formation of Pt-AlMCM-41

An ion exchange strategy was adopted for the preparation of Pt^{2+}AlMCM-41 precursors (section 2.2.4); a procedure analogous to that used in the formation of Pt clusters in the supercages of zeolite NaY [28]. The calcined *C16* or *C18* AlMCM-41 materials were slurried for 1 h at room temperature with a 0.105 mmol solution of $Pt(NH_3)_4(NO_3)_2$. The sample was washed, filtered and air dried. The Pt^{2+}AlMCM-41 materials were converted to catalysts Pt-M2 to Pt-M4 by subsequent activation in dry flowing oxygen and/or hydrogen (99.9%) (Table 3.2). Catalyst Pt-M1 was prepared *via* the Pt^{2+} ion exchange of uncalcined *C16* AlMCM-41. The catalyst activation step for catalyst Pt-M1 was omitted.

Table 3.2 Summary of the activation process for each of the catalysts tested

Catalyst	Parent material	Catalyst activation	
		Oxidation	Reduction
Pt-M1	*C16* AlMCM-41	No	No
Pt-M2	*C16* AlMCM-41	Yes	Yes
Pt-M3	*C16* AlMCM-41	No	Yes
Pt-M4	*C18* AlMCM-41	No	Yes

3.2.3 Physical properties of the Pt-AlMCM-41 catalysts

Platinum loadings, surface areas, and mean pore sizes are shown in Table 3.3, a plot of pore size distribution is shown in Figure 3.15. HRTEM of catalysts Pt-M2 and Pt-M3 (Figure 3.16 **a**, **b**) confirmed that these catalysts retained the hexagonal pore structure evident in the HRTEM micrograph of the parent *C16* AlMCM-41 material. The majority of platinum crystallites visible within these images were present within the pores of the AlMCM-41 material. ^{27}Al NMR spectra for catalysts Pt-M2 to Pt-M4 are shown in Figure 3.14.

Table 3.3 Physical properties of the active Pt-AlMCM41 catalyst

Catalyst	Platinum loading (%)	Surface area (m^2g^{-1}) Total	Mesopore	Mean pore size (nm)
Pt-M1	-	10	-	-
Pt-M2	1.6	786	684	2.3
Pt-M3	1.6	920	840	2.3
Pt-M4	1.7	992	945	3.1

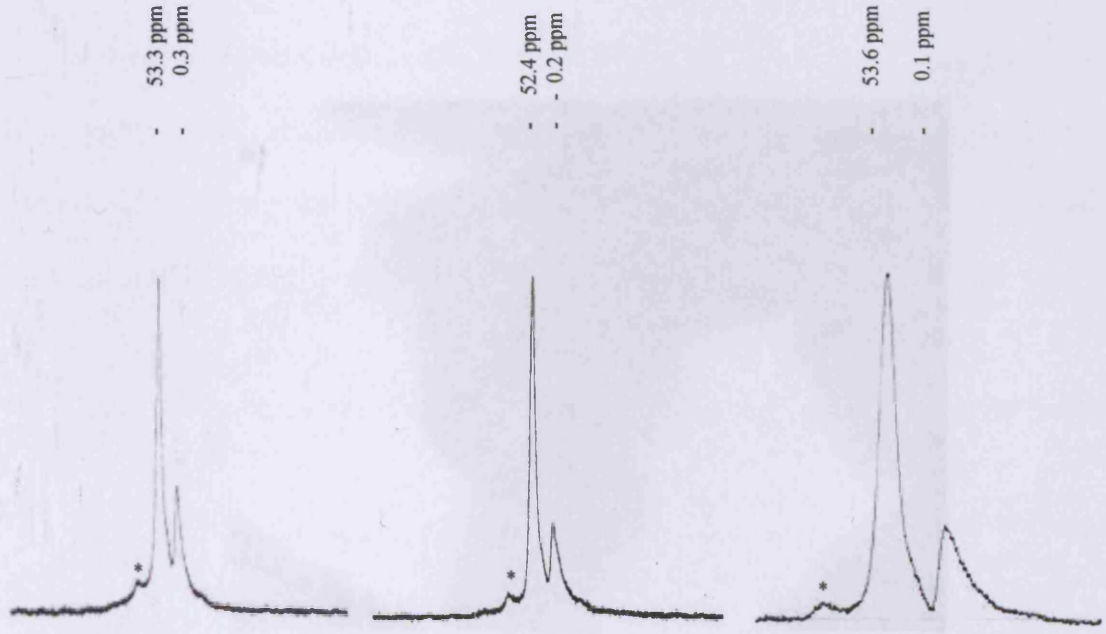

Pt-M2 Pt-M3 Pt-M4

* Denotes spinning side bands.

Figure 3.14 ^{27}Al NMR spectra of Pt-AlMCM-41 catalysts Pt-M2, M3 and M4.

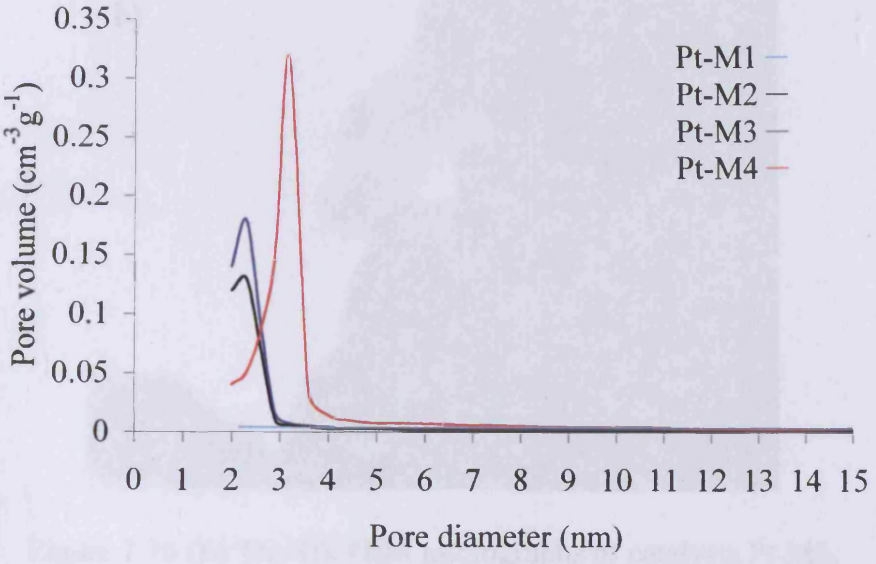

Figure 3.15 Pore size distribution plots for catalysts Pt-M1, Pt-M2, Pt-M3 and Pt-M4.

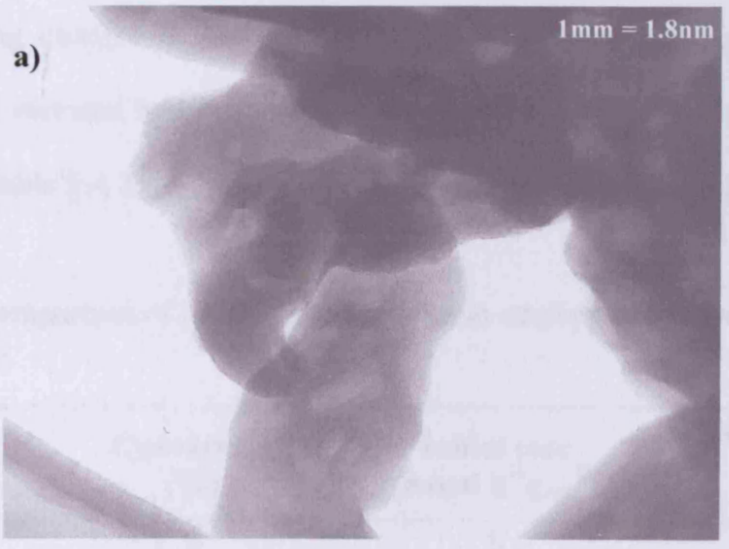

Figure 3.16 (**a**) The HRTEM micrographs of catalysts Pt-M2.

Figure 3.16 (**b**) The HRTEM micrographs of catalysts Pt-M3.

3.2.4 Enantioselective hydrogenation of ethyl pyruvate catalysed by Pt-AlMCM-41

All catalysts were modified *in-situ*, with cinchonidine, dichloromethane, pyruvate ester, and catalyst being charged to the reactor in that order (section 2.5). Reactions were carried out under elevated hydrogen pressures (70 bar) at 293 K. Catalyst performances are compared in table 3.4. Hydrogen uptake curves are shown in Figure 3.17.

Table 3.4 Comparison of catalyst performance in ethyl pyruvate hydrogenation

Catalyst	Conversion (%)	Initial rate (mmol $h^{-1}g_{cat}^{-1}$)	Enantiomeric excess (%)/(*R*)
Pt-M1	5	8	14
Pt-M2	50	190	36
Pt-M3	62	218	64
Pt-M4	100	402	40

70 bar hydrogen, catalyst 0.1 g, ethyl pyruvate 66 mmol, cinchonidine 0.17 mmol, 12.5 cm^3 dichloromethane, stirring rate 1200 rpm, e.e. and conversion measured after 2 hours.

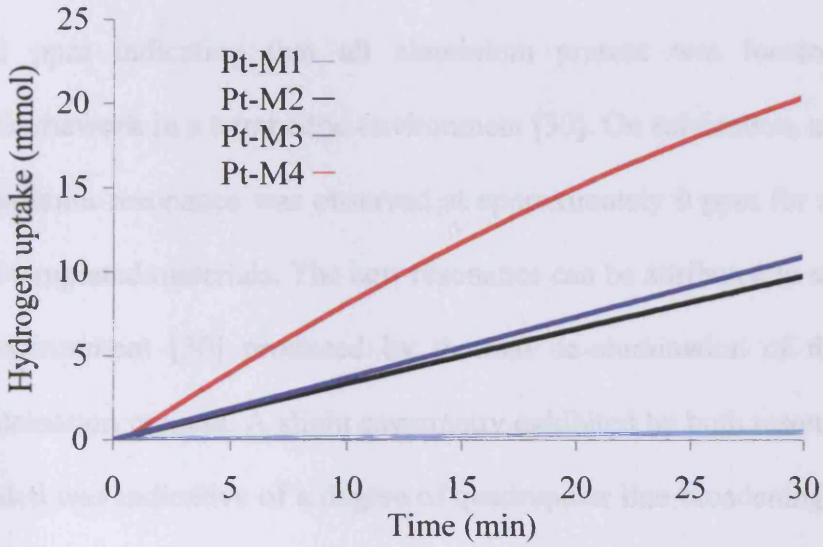

Figure 3.17 Hydrogen uptake curves for catalysts Pt-M1 to Pt-M4.

3.3 Discussion

3.3.1 Physical properties of the catalysts

Micrographs of the final catalysts Pt-M2 and Pt-M3 showed the expected hexagonal arrays associated with the pores of MCM-41 viewed in cross section; other areas showed the pores in longitudinal section (side view). When the pore structure was imaged in cross section as hexagonal arrays, the pores appeared light and the framework dark, as previously reported [29]. For catalyst Pt-M2 and Pt-M3 the mid-pore to mid-pore distance determined from these images was 3.1 nm, which, allowing for wall thickness, is consistent with the estimation of pore diameter of 2.3 nm by adsorption measurements (table 3.3). The adsorption measurements of catalyst Pt-M4 estimate the pore diameter to be 3.1 nm, 0.8 nm wider than those catalysts derived from the *C16* AlMCM-41 material. This was expected as this catalyst was synthesised using the longer *C18* alkyl chain template. Where platinum particles were present on the external surface they were easily distinguished; they were mostly large (5-25 nm) and frequently faceted. Both *C16* and

C18 uncalcined materials had similar ^{27}Al NMR spectra with a strong single resonance at approx. 51.2 ppm indicating that all aluminium present was located within the mesoporous framework in a tetrahedral environment [30]. On calcination, a second lower intensity aluminium resonance was observed at approximately 0 ppm for stocks of both *C16* and *C18* templated materials. The new resonance can be attributed to aluminium in a octahedral environment [30] produced by thermal de-alumination of the framework during the calcination process. A slight asymmetry exhibited by both resonances in those spectra recorded was indicative of a degree of quadrupolar line broadening [31]. The ion exchange of Pt^{2+} of *C16* AlMCM41 and its subsequent activation had only a small effect on the appearance of the ^{27}Al spectra (Figure 3.14). Comparison of the spectra for reduced Pt-M3 and Pt-M2 revealed a slight increase in the proportion of extra framework Al present in Pt-M2. The additional oxidation step therefore appears to remove additional framework aluminium from the structure. The ^{27}Al NMR spectra of catalyst Pt-M4 gave resonances at chemical shift values almost identical to that observed for the *C16* templated catalysts. The ratio of framework to extra framework aluminium was calculated as being 4:1.

3.3.2 Chemical properties of the catalysts

The catalysts examined provided a wide range of activities and enantioselectivities. For Pt-M2 and Pt-M3, all of the Pt active phase was contained within the mesopores of the support, although HRTEM microscopy of Pt-M4 would be desirable it was deemed unnecessary as it has been shown through the images of catalysts Pt-M2 and Pt M3, that the methodology employed in catalyst synthesis was sound. The turnover frequencies for enantioselective hydrogenation, based on the rate measured early in the reaction, at 293 K and 70 bar were 0.8 x 10^{-19} molecules $s^{-1}mg^{-1}_{Pt}$ for Pt-M2 and 1.0 x 10^{-19} molecules s^{-}

$^{1}mg^{-1}_{Pt}$ for Pt-M3. By comparison, the standard reference catalyst EUROPT-1 (6.3% Pt/silica), in which all of the Pt active phase is on the external surface of the catalyst support, shows a turnover frequency of 2.8 x 10^{-19} molecules $s^{-1}mg^{-1}_{Pt}$ when reacted under similar conditions [32]. Thus, confinement of the Pt particles to the mesopores in the *C16* materials reduced the rate of reaction by a factor of three. In contrast, the larger pore *C18* catalyst Pt-M4, showed a greater activity (conversion 100%) to that of the narrower pored *C16* analogues, with a turnover frequency of 1.3 x 10^{-19} molecules $s^{-1}mg^{-1}_{Pt}$. This difference in activity highlights the potential problems associated with the diffusion of reagents to the active platinum site within the narrower pores of catalysts Pt-M2 and Pt-M3. A contributing factor to this observation may be the partial blocking of the catalyst pores by high molecular weight lactate polymer by-products catalysed by unmodified cinchonidine platinum [33]. Catalyst Pt-M1 was the least effective catalyst investigated in both activity (conversion, 5%) and enantioselectivity (e.e. 14%). This material was uncalcined, thus, the only possible site for Pt exchange was at the outer surface of the support with activation of the Pt precursor being restricted to *in-situ* reduction during the course of the hydrogenation reaction.

The enantiomeric excess recorded for Pt-M2 was 36%, while catalyst Pt-M3 generated an e.e. of 64% both in favour of the (*R*)-lactate enantiomer (Table 3.4); these are non-optimised values. The corresponding non-optimised value for reaction over EUROPT-1 is 70% to the (*R*)-enantiomer at 100% conversion [32]. This performance demonstrates that effective modification of the Pt active phase can be achieved in a mesoporous environment. The inferior enantiomeric excess provided by Pt-M2 cannot be attributed to inefficient modification because the conditions of the experiment and the structure of the mesoporous support were identical. The only clear difference between Pt-M2 and Pt-M3 assuming no migration of the Pt in to the structure was the Pt particle size distribution. In

Pt-M3 visible platinum particles appeared as circular in cross section and ranged in diameter from 0.8 to 3.0 nm with a majority being about 2 nm in diameter. For Pt-M2 the largest visible particles in the mesopores were 1.8 nm in diameter, the majority being about 0.8 nm which was close to the limit of resolution of the microscope for samples of this type. Ryoo [34] has demonstrated that oxidation of Pt^{2+} to PtO increases the interaction between metal and support preventing the formation of large Pt agglomerates which occur upon direct reduction of $Pt(NH_3)^{2+}$. It has been reported that Pt/silica and Pt/γ-Al_2O_3 catalysts having a majority of Pt particles below 1 nm in size perform badly as enantioselective hydrogenation catalysts [35] as the necessary adjacent adsorption of modifier and reactant cannot occur on such small particles. Thus, the most likely interpretation of the poorer performance of Pt-M3, by comparison with that of Pt-M2, is that it contained a larger fraction of Pt particles in such a highly dispersed state that it was not as efficiently modified by the alkaloid. Catalyst Pt-M4 was poor as an enantioselective catalyst, which was surprising as the catalyst underwent the same ion exchange and activation procedure as Pt-M2 (the best performing catalyst in the study) and accordingly was expected to exhibit comparable enantioselectivity. The only major difference between the two catalysts was the greater pore size of catalyst Pt-M4. It is known that the pore size of a catalyst support is an important factor in determining the migratory ability of a metal phase and so influence the final size and distribution of the metal crystallites. Therefore the larger pores of catalyst Pt-M4 could facilitate the formation of larger platinum particles and a lower dispersed platinum catalyst (HTREM studies would be required to confirm this) resulting in lower enantioselectivity. Attard has shown that thermal sintering of graphite supported platinum catalysts to manufacture large platinum particles is detrimental to enantioselectivity, observing a bimodal

relationship between enantioselectivity and platinum particle size in the hydrogenation of ethyl pyruvate over cinchonidine modified platinum [36].

Another plausible explanation to account for the inferior enantioselective performance of Pt-M4 is that any possible beneficial steric interaction between the platinum adsorbed modifier and the support within the smaller pores of Pt-M3 in conceivably influencing the diastereoselective transition-state complex or inducing a restricted environment, which can impact on the stereoconfiguration of the products is absent in the larger pored catalyst. Examples of this 'confinement effect' on enantioselectivity have been previously reported. Raja *et al* [37] utilised a non-covalent approach to immobilise a chiral rhodium complex within the pores of a series of desiccant silicas, which had pore sizes that ranged between 3.8 and 25 nm. The catalysts were used in the asymmetric hydrogenation of ethyl benzoylformate. The greatest enantioselectivity was observed for those catalysts that held the complex in the most constrained environment. Other catalysts in the series provided e.e. values that decreased with increasing pore size, reflecting the declining influence of the spatial constraint of the pore.

3.4 Conclusion

The work presented in this chapter is the first to demonstrate that enantioselective hydrogenation of the α-ketoester ethyl pyruvate over cinchonidine modified platinum nano particles supported within the pores of AlMCM-41 is possible with activities comparable to that achieved with the standard catalyst EUROPT-1 (6.3% Pt/SiO_2). By tailoring the pore size of the support and with careful choice of modifier it may now be possible to expand the scope of the enantioselective hydrogenation of pro-chiral compounds which may be of interest to the pharmaceutical and fine chemical industries.

3.5 References

1 A.F. Cronstedt, *Adak. Handal. Stockholm,* **17** (1756) 120.

2 J. A. Martens and P.A. Jacobs, *Stud. Surf. Science and Catal.,* **85** (1994) 653.

3 M. Mabilia, R.A. Pearlstein and A.J. Hopfinger, *J. Am. Chem. Soc.,* **109** (1987) 7960.

4 F. Schueth, K.S.W. Sing and J. Weitkamp, *Handbook of Porous Solids,* **2** (2002) 1058.

5 A. Dyer, *Introduction to Molecular Sieves, Wiley, UK,* 1998.

6 www. ISA-Stugcture.org/databases

7 S.L. Suib, *Chem. Rev.,* **93** 803 (1993).

8 J.E. Naber, K.P. de Jong, W.H.J. Stork, H.P.C.E. Kuipers and M.F.M. Post, *Stud. Surf. Sci. Catal.,* **84**, 1994, 2197.

9 C.T. Kresge, M.E. Leonowicz, W.J. Roth, J.C. Vartuli and J.S. Beck, *Nature,* **359** (1992) 710.

10 A. Sayari, *Chem. Mater.,* **8** (1996) 135.

11 M. Dubois, T.H. Gulik-kryzywicki and B. Cabane, *Langmuir.,* **9** (1993) 673.

12 J.C. Vartuli, K.D. Schmitt, C.T. Kresge, W.J. Roth, M.E. Leonowicz, S.B. McCullen, S.D. Hellring, J.S. Beck, J.L. Schlenker, D.H. Olsen and E.W. Sheppard, *Chem. Mater.,* **6** (1994) 2317.

13. C.T. Kresge, M.E. Leonowicz, W.J. Roth, J.C. Vartuli and J.S. Beck, *Nature,* **359** (1992) 710.

14 J.S. Beck, J.C. Vartuli, W.J. Roth, M.E. Leonowicz, C. T. Kresge, C.T-W. Chu, D.H. Olsen, E.W. Sheppard, S.B. McCullen, J.B. Higgins, K.D. Schmitt and J. L. Schlenker, *J. Am. Chem. Soc.,* **114** (1992) 10834.

15 Y. Liang and R. Anwander *Microporous and mesoporous materials,* **72** (2004) 153.

16 C.T. Kresge, M.E. Leonowicz, W.J. Roth, J.C. Vartuli and J.S. Beck, *Nature,* **359** (1992) 710.

17 A. Monnier, F. Schuth, Q. Huo, D. Kumar, D. Margolese, R.S. Maxwell, G.D. Stucky, M. Krishnamurty, P. Petroff, A. Firouzi, M. Janicke and B.F. Chmelka, *Science,* **261** (1993) 1299.

18 A. Firouzi, D. Kumar, L.M. Bull, T. Besier, P. Sleger, Q. Huo, S.A. Walker, J.A. Zasadzinski, C. Glinka, J. Nicol, D. Margolese, G. D. Stucky and B.F. Chmelka, *Science,* **267** (1995) 1138.

19 P.T. Tanev, M. Chibwe and T.J. Pinnavaia, *Nature,* **368** (1994) 321.

20 E. Armengol, M.L. Cano, A. Corma, H. Garcia and M.T. Navarro, *J. Chem. Soc., Chem. Commun.,* (199) 519.

21 E.A. Gunnewegh, S.S. Gopie and H. van Bekkum, *J. Mol. Catal.,* **106** (1996) 151.

22 A. Corma, M.T. Navarro and J. Perez Pariente, *J. Chem. Soc., Chem. Commun.,* (1994) 147.

23 P. Sultra and D. Brunel, *Chem., Commun.,* (1996) 2485.

24 D. Tas, R.F. Parton, K. Vercruysse and P.A. Jacobs, *Stud. Surf. Sci. Catal.,* **105** (1997) 1261.

25 S. Coman, F. Cocu, J.F. Roux, V.I. Parvulescu and S. Kaliaguine, *Stud. Surf. Sci. Catal.,* **117** (1998) 501.

26 N. Bellocq, D. Brunel, M. Lasperas and P. Moreau, *Stud. Surf. Sci. Catal.,* **108** (1997) 485.

27 P.B. Wells and A.J. Wilkinson, *Topics Catal.,* **5** (1998) 39.

28 L.C. de Menorval, J.P. Fraissard and T. Ito, *J. Chem., Soc., Faraday Trans.,* **178** (1982) 403.

29 T. Kresge, M.E. Leonowicz, W.J. Roth, J.C. Vartuli and J.S. Beck, *Nature,* **359** (1992) 710.

30 J. Klinowski, *Chem. Rev.,* **91** (1991) 1459.

31 A. Medek, L. Marinelli and L. Frydman, in: *Solid State NMR Spectroscopy of inorganic materials.*

32 M. Sutherland, A. Ibbotson, R.B. Moyes and P.B. Wells, *J. Catal.*, **125** (1990) 77.

33 G. A. Attard, *Personal Communication.*

34 R. Ryoo, C.H. Ko, J.M. Kim and R. Howe, Cat. Lett., **37** (1996) 29.

35 S.D. Jackson, M.B.T. Keegan, G.D. McLellan, P.A. Meheux, R.B. Moyes, G. Webb, P.B. Wells, R. Whyman and J. Willis, *Preparation and Characterisation of Catalysts,* (1991) 135.

36 G.A. Attard, K.G. Griffin, D.J. Jenkins, P. Johnston and P.B. Wells *Catalysis Today,* **114** (2006) 346.

37 R. Raja, J.M. Thomas, M.D. Jones, B.F.G. Johnson and D.E.W. Johnson, *J. Am. Chem. Soc.*, **125** (2003) 14982.

Chapter Four

Chapter Four Enantioselective Hydrogenation of Pyruvate Esters in a Continuous Flow Reactor (CFR)

4.1 Introduction

The synthesis of complex chiral molecules in optically pure form is a hugely demanding task which requires new and efficient catalyst technologies. The majority of catalytically prepared compounds are synthesised by homogeneous methods. There are relatively few heterogeneous systems which afford high enantioselectivities. One heterogeneous system that has been studied extensively is the asymmetric hydrogenation of α-ketoesters using supported platinum nanoparticles modified with cinchona alkaloids, which is known as the Orito reaction [1].

To date, most Orito reactions have been carried out using an *in-situ* modification procedure in which the cinchona alkaloid, catalyst, substrate and solvent are stirred together in an autoclave batch reactor. Although the use of batch reactors has proved to be a useful tool to study the chemistry of this complex reaction, industrial operation would be more efficient in a continuous flow reactor (CFR). There are a number of reasons; (i) it engenders process simplification and intensification, since continuous operation negates the need to remove the catalyst at the end of the reaction, thus reducing downtime, (ii) it alleviates the problems associated with catalyst abrasion, (iii) it avoids an unavoidable problem in batch operation in that products remain in contact with the catalyst for long periods of time which can facilitate by-product formation.

Pioneering studies by Baiker and co-workers [2] have shown the feasibility of continuous flow reactors operating at high pressure in the enantioselective hydrogenation of activated ketones including ethyl pyruvate and α-ketopantolactone. More recently, Toukoniitty *et al.* [3] have utilised the same methodology in the enantioselective

hydrogenation of 1-phenyl-1,2-propanedione. For each of these continuous flow reactions the cinchona alkaloid has been continuously fed into the reactor in order to sustain high enantioselectivity, which presents a disadvantage to this improved methodology. Within this chapter the use of pre-modified cinchonidine platinum catalysts in the enantioselective hydrogenation of ethyl pyruvate using a CFR reactor operating under ambient conditions and at low hydrogen pressures is described. The advantages of adopting pre-modified catalysts in the CFR reactor as a means to investigate this fascinating and little understood enantioselective reaction are also discussed.

4.2 Results

4.2.1 Pre-modification optimisation

A number of ethyl pyruvate enantioselective hydrogenation reactions were carried out over a series of 5% Pt/γ-Al_2O_3 catalysts which had previously been pre-modified with varying amounts of cinchonidine, following the procedure outlined in section 2.7.2.2.

A 0.4 g portion of each of the pre-modified catalysts was diluted with silicon carbide fines and charged to a glass reactor as previously described in section 2.8, to give a bed depth of 12 mm. The reactor was sealed and the catalyst bed subjected to a concurrent downward flow of dichloromethane (1 ml. min^{-1}) and hydrogen (300 ml. min^{-1}, 0.25 bar/g) for a 30 min period prior to the introduction of the ethyl pyruvate solution (25 mM DCM @ 1 ml. min^{-1}) to the reactor. The reaction temperature was maintained at 25 °C using a thermostatic jacket. The liquid contact time for each reaction was approx. 2 min.

The results in Figure 4.1 illustrate that a sufficient modifier concentration is a prerequisite for sustained and meaningful enantioselectivity in the hydrogenation of ethyl

pyruvate to (*R*)-ethyl lactate. The catalyst modified with the lowest amount of cinchonidine (0.17 mM) performed badly as an enantioselective catalyst giving a disappointing 2% enantiomeric excess in favour of the (*R*)-enantiomer.

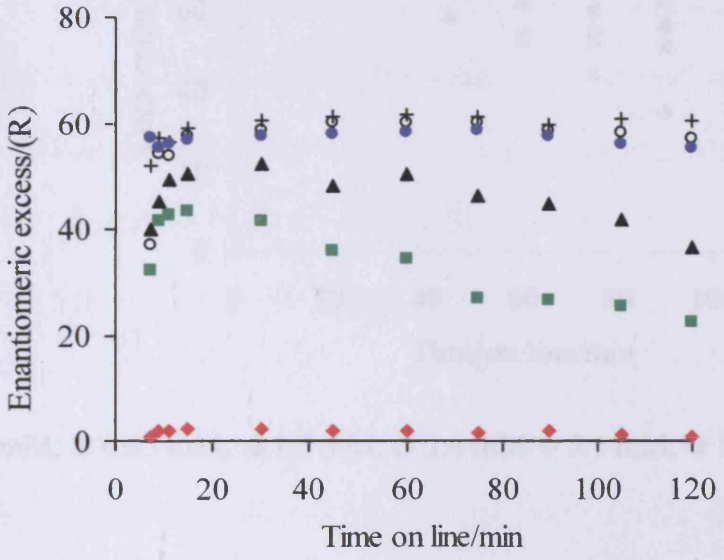

◆ 0.17 mM, ■ 0.85 mM, ▲1.7 mM, ○ 3.4 mM, + 5.1 mM, ● 8.5 mM.

[0.4 g catalyst; 25 mM ethyl pyruvate in DCM @ 1 ml. min^{-1}; 0.25 bar/g H_2 pressure; GHSV 2250h^{-1}; T = 25 ± 1 °C]

Figure 4.1 The effect on enantiomeric excess in the hydrogenation of ethyl pyruvate on varying the concentration of cinchonidine used in the pre-modification of 5% Pt/γ-Al_2O_3

As the concentration of cinchonidine used in pre-modificaton was increased from 0.17 mM to 1.7 mM, the enantiomeric excess was observed to increase dramatically. Maximum enantioselectivity and system sustainability were observed when the cinchonidine solution concentration used for pre-modification reached 3.4 mM. A further increase in the concentration of cinchonidine (8.5 mM) used in catalyst pre-modification

resulted in a slight decrease in the observed enantioselectivity.

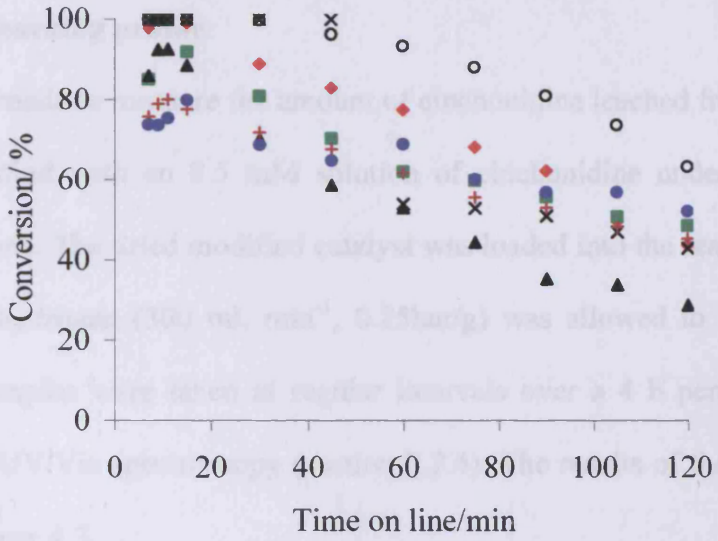

◆ 0.17 mM, ■ 0.85 mM, ▲1.7 mM, ○ 3.4 mM + 5.1 mM, ● 8.5 mM, x no cinchonidine

[0.4 g catalyst; 25 mM ethyl pyruvate in DCM @ 1 ml. min^{-1}; 0.25 bar/g H_2 pressure; GHSV 2250 h^{-1}; T = 25 ± 1 °C]

Figure 4.2 The effect on conversion in the hydrogenation of ethyl pyruvate upon varying the concentration of cinchonidine used in the pre-modification of 5% Pt/γ-Al_2O_3.

All catalysts were found to deactivate, in terms of conversion, with time on line (Figure 4.2), whatever the concentration of cinchonidine used in catalyst modification. In the early part of the reaction a clear relationship was observed between catalyst activity and the amount of cinchonidine used in pre-modification. Those catalysts modified with the least amount of cinchonidine showed the greatest activity. The only catalyst to give 100% conversion to products for a sustained period was the un-modified catalyst, which gave complete conversion for the first 45 min of the reaction before following the same

deactivation trend observed for the cinchonidine modified catalysts.

4.2.2 Modifier leaching profile

An attempt was made to measure the amount of cinchonidine leached from a catalyst bed previously modified with an 8.5 mM solution of cinchonidine under simulated CFR reaction conditions. The dried modified catalyst was loaded into the reactor and DCM (1 ml. min^{-1}) and hydrogen (300 ml. min^{-1}, 0.25bar/g) was allowed to flow through the catalyst bed. Samples were taken at regular intervals over a 4 h period and analysed undiluted using UV/Vis spectroscopy (section 2.7.4). The results of the experiments are illustrated in Figure 4.3.

The concentration of cinchonidine removed from the bed follows an exponential decay curve, with 20 wt/% of the cinchonidine leached from the catalyst bed in the first 30 minutes, following which there was a very slow loss of cinchonidine for the remainder of the time on line.

4.2.3 Catalyst bed pre-treatment

A number of ethyl pyruvate enantioselective hydrogenation reactions were carried out over a series of 5% $Pt/\gamma\text{-}Al_2O_3$ catalysts previously pre-modified with a 5.1 mM solution of cinchonidine. The aim of this sequence of experiments was to investigate the effect of different periods of solvent and hydrogen pre-treatment on enantioselectivity and activity for the hydrogenation of ethyl pyruvate.

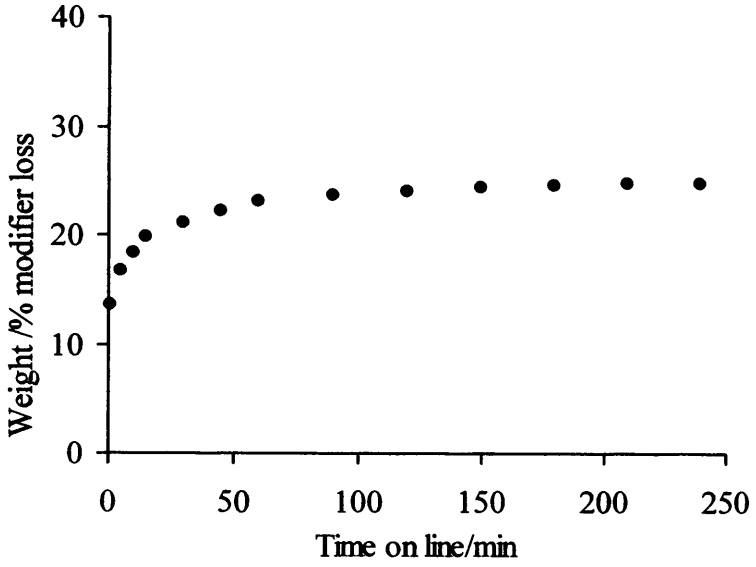

[0.4 g catalyst; DCM @ 1 ml. min^{-1}; 0.25 bar/g H_2 pressure; GHSV 2250 h^{-1}; T = 25 ± 1°C]

Figure 4.3 Loss of cinchonidine from a pre-modified catalyst bed under flowing dichloromethane in the presence of hydrogen.

A 0.4g portion of the pre-modified catalyst was diluted with silicon carbide fines and charged to a glass trickle bed reactor, as described in section 2.7.3. The reactor was sealed and the catalyst bed subjected to a downward flow of dichloromethane (1 ml. min^{-1}) accompanied with a concurrent flow of hydrogen (300 ml. min^{-1}, 0.25 bar/g). The period of pre-treatment was varied between 0 h and 3 h prior to the introduction of the ethyl pyruvate solution (25 mM in DCM @ 1 ml. min^{-1}) to the catalyst bed. The benefit of solvent pre-treatment on enantioselectivity is shown in Figure 4.4. The non pre-treated catalyst gave an average enantiomeric excess of 40% in favour of the (*R*)-enantiomer over the 2 h period on line. Catalysts pre-treated for periods of between 0.5h and 2h were the most efficient with the maximum enantiomeric excess observed being 72% to the (*R*)-

enantiomer for the catalyst pre-treated for 0.5 h. If the period of pre-treatment was extended to 3 h it was found to be detrimental to enantioselectivity, with the average enantiomeric excess observed for this catalyst being 56%.

All catalysts were seen to deactivate with increasing time on line whatever the period of pre-treatment (Figure 4.5). A clear relationship between catalyst activity and the period of pre-treatment was observed in the early part of the reaction, with those catalysts subjected to the shortest periods of pre-treatment showing the highest conversion of ethyl pyruvate to lactate.

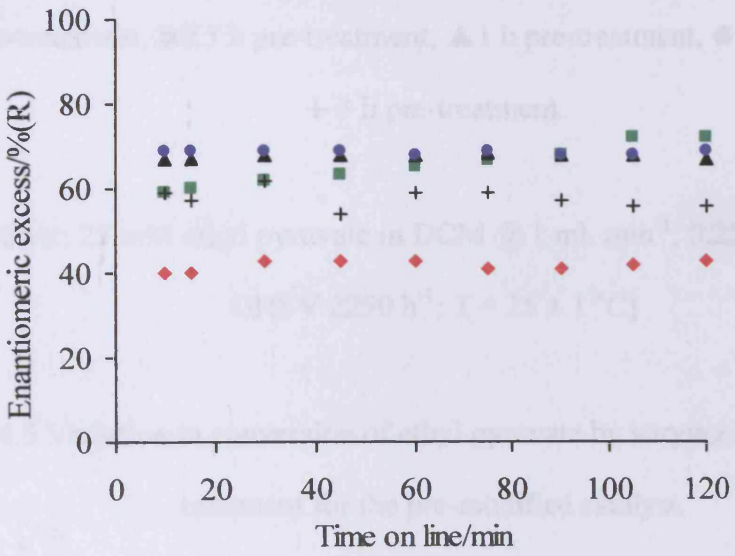

◆0 h pre-treatment, ■0.5 h pre-treatment, ▲1 h pre-treatment, ● 2 h pre-treatment, + 3 h pre-treatment.

[0.4 g catalyst; 25 mM ethyl pyruvate in DCM @ 1 ml. min^{-1}; 0.25 bar/g H_2 pressure; GHSV 2250 h^{-1}; T = 25 ± 1 °C]

Figure 4.4 Variation in e.e. of ethyl pyruvate hydrogenation by varying the period of pre-treatment for the pre-modified catalyst.

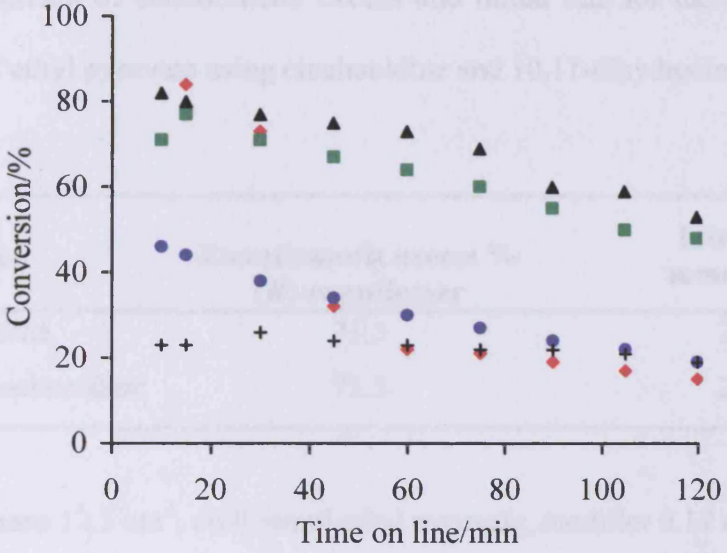

◆0 h pre-treatment, ■0.5 h pre-treatment, ▲1 h pre-treatment, ● 2 h pre-treatment, + 3 h pre-treatment.

[0.4 g catalyst; 25 mM ethyl pyruvate in DCM @ 1 ml. min^{-1}; 0.25 bar/g H_2 pressure; GHSV 2250 h^{-1}; T = 25 ± 1 °C]

Figure 4.5 Variation in conversion of ethyl pyruvate by varying the period of pre-treatment for the pre-modified catalyst.

4.2.4 Autoclave reactions using cinchona modified catalysts

The aim of this set of experiments was to allow a direct comparison between autoclave and CFR reactors in the enantioselective hydrogenation of ethyl pyruvate. The autoclave reactions (section 2.4) were carried out at elevated hydrogen pressure (50 bar) over a 5% Pt/γ-Al_2O_3 catalyst previously modified with cinchona alkaloid (5.1 mM) following the procedure previously described in section 2.3.1. The results of these experiments are shown in table 4.1.

Table 4.1 Comparison of enantiomeric excess and initial rate for the enantioselective hydrogenation of ethyl pyruvate using cinchonidine and 10,11-dihydrocinchonidine as chiral modifiers

Modifier	**Enantiomeric excess % (*R*)-enantiomer**	**Initial rate mmol g^{-1} h^{-1}**
Cinchonidine	71.5	2520
10,11-Dihydrocinchonidine	71.5	2760

[dichloromethane 12.5 cm^3, 66.0 mmol ethyl pyruvate, modifier 0.17 mmol, 0.25 g catalyst, 50 bar hydrogen pressure, stirring rate 1200 rpm, Temp = 20 ± 2 °C. Conversion 100%]

4.2.5 Solvent effects in the CFR

The effect of solvent on ethyl pyruvate hydrogenation in the CFR reactor was investigated using a 5% Pt/γ-Al_2O_3 catalyst pre-modified with a 5.1 mM solution of cinchonidine. A 0.4g portion of the pre-modified catalyst was diluted with silicon carbide fines and charged to a glass reactor as described in section 2.7.3. Ethanol was used to pre-treat the catalyst bed (30min @ 1 ml. min^{-1}) and as the carrier solvent for the ethyl pyruvate (25 mM @ 1 ml. min^{-1}), to allow direct comparison to the equivalent dichloromethane reaction. The results presented in Figure 4.6 show that the choice of reaction solvent has a huge bearing on both enantioselectivity and catalyst efficiency in ethyl pyruvate hydrogenation in the CFR. When ethanol was used as the solvent, conversion to products never fell below 90% during the time the system was on line; in comparison, dichloromethane showed a steady decrease in activity during the reaction with a 50% conversion to product after 2 h on line. Dichloromethane gave the highest

enantioselectivity with a maximum enantiomeric excess of 72%. Ethanol gave a stable enantiomeric excess of 27% during the course of the reaction, a value far below that achieved in dichloromethane.

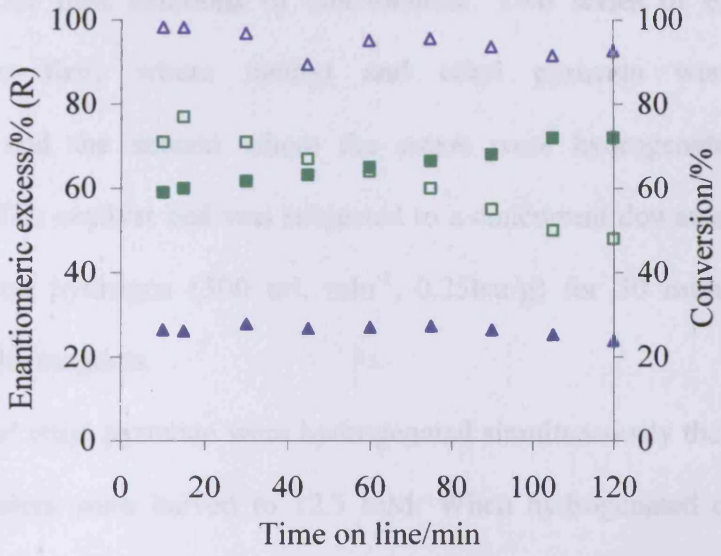

■ e.e. of ethyl lactate using dichloromethane as a reaction solvent.

▲ e.e. of ethyl lactate using ethanol as a reaction solvent.

□ conversion of ethyl pyruvate using dichloromethane as a reaction solvent.

△ conversion of ethyl pyruvate using ethanol as a reaction solvent.

[0.4 g catalyst; 25 mM ethyl pyruvate in DCM/EtOH @ 1 ml. min^{-1}; 0.25 bar/g H_2 pressure; GHSV 2250 h^{-1}; T = 25 ± 1°C]

Figure 4.6 The effect of solvent on enantioselectivity and activity in the hydrogenation of ethyl pyruvate in the CFR.

4.2.6 Simultaneous and sequential hydrogenation of pyruvate esters in the CFR

In order to probe the chiral reaction site generated by cinchonidine on the platinum surface and gain a better insight into the origin of enantioselectivity, a series of hydrogenation reactions were carried out over 5% $Pt/\gamma\text{-}Al_2O_3$ (0.4 g) catalysts pre-modified with 5.1 mM solutions of cinchonidine. Two series of experiments were performed. The first, where methyl and ethyl pyruvate were hydrogenated simultaneously and the second where the esters were hydrogenated consecutively (section 2.7.3). The catalyst bed was subjected to a concurrent downward flow of DCM (1 ml. min^{-1}) and hydrogen (300 ml. min^{-1}, 0.25bar/g) for 30 minutes prior to the introduction of the reagents.

When methyl and ethyl pyruvate were hydrogenated simultaneously the concentration of the individual esters were halved to 12.5 mM. When hydrogenated consecutively the concentration of the pyruvate esters was 25 mM. A three way tap was employed to switch between the individual solutions of ethyl and methyl pyruvate. The flow of reagents into the reactor was set at 1 ml. min^{-1}.

The results for the simultaneous hydrogenation of the ethyl and methyl pyruvate esters are shown in Figure 4.7. The final values of enantiomeric excess for these reactions were lower than those values recorded when the esters were hydrogenated individually. Ethyl pyruvate yielded a final e.e. of 63%, whilst methyl pyruvate gave an e.e. of 57% after 2 h on line, both favouring the (*R*)-enantiomer. Both substrates showed a distinct transient where the e.e. built up over the first 15 min of the reaction. The same conversion deactivation trend observed in the hydrogenation of the individual ester was also observed when the esters were hydrogenated simultaneously, however, deactivation was not so pronounced for methyl pyruvate with conversions typically 10% higher than with the ethyl derivative at the conclusion of the reaction.

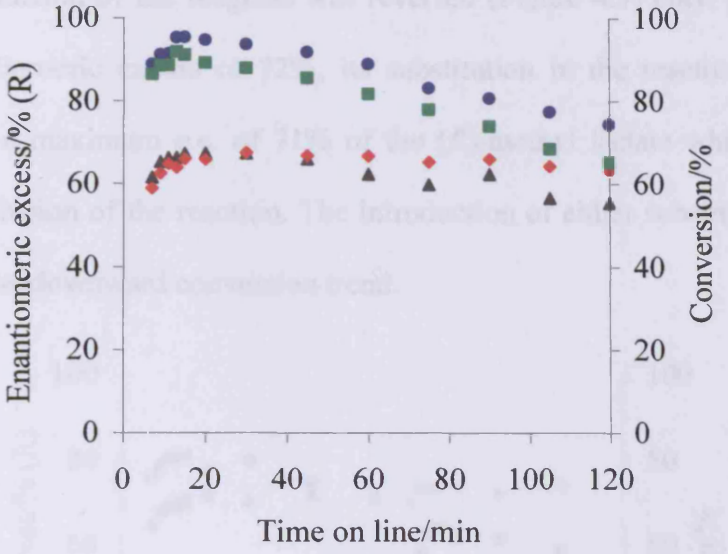

◆ e.e. of ethyl lactate

▲ e.e. of methyl lactate

■ conversion of ethyl pyruvate to ethyl lactate

● conversion of methyl pyruvate to methyl lactate

[0.4 g catalyst; 12.5 mM ethyl pyruvate / 12.5 mM methyl pyruvate in DCM @ 1 ml. min^{-1}; 0.25 bar/g H_2 pressure; GHSV 2250 h^{-1}; T = 25 ± 1 °C]

Figure 4.7 The effect on enantioselectivity and activity in the simultaneous hydrogenation of ethyl and methyl pyruvate esters in the CFR reactor.

The results for the sequential hydrogenation of the pyruvate esters are shown in Figure 4.8 and Figure 4.9. The hydrogenation of methyl pyruvate (Figure 4.8) prior to the introduction of the ethyl pyruvate, showed an enantiomeric excess of 72% for (*R*)-methyl lactate after 60 min on line. The substitution of methyl pyruvate for ethyl pyruvate and its subsequent hydrogenation gave a maximum enantiomeric excess of 73% for the (*R*)-enantiomer, identical to the e.e. observed when the ester was hydrogenated individually.

When the introduction of the reagents was reversed (Figure 4.9) ethyl pyruvate gave a maximum enantiomeric excess of 72%, its substitution in the reactor for the methyl derivative gave a maximum e.e. of 71% of the (*R*)-methyl lactate which decreased to 64% at the conclusion of the reaction. The introduction of either substrate to the reactor did not disturb the downward conversion trend.

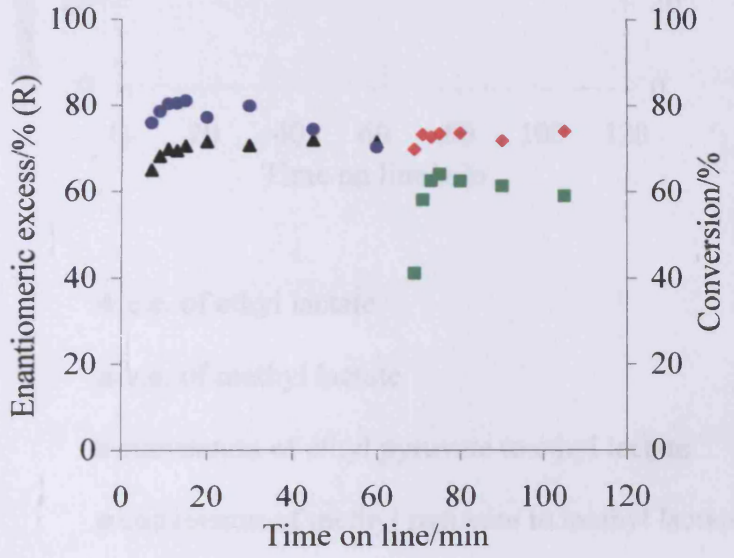

◆ e.e. of ethyl lactate

▲ e.e. of methyl lactate

■ conversion of ethyl pyruvate to ethyl lactate

● conversion of methyl pyruvate to methyl lactate

[0.4 g catalyst; 12.5 mM ethyl pyruvate / 12.5 mM methyl pyruvate in DCM @ 1 ml. min^{-1}; 0.25 bar/g H_2 pressure; GHSV 2250 h^{-1}; T = 25 ± 1 °C]

Figure 4.8 The effect on enantioselectivity and activity in the sequential hydrogenation of methyl and ethyl pyruvate esters.

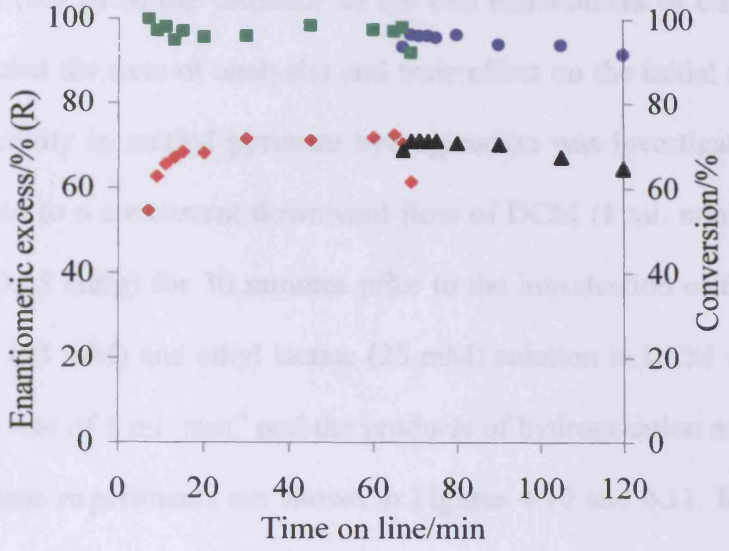

[0.4 g catalyst; 12.5 mM ethyl pyruvate / 12.5 mM methyl pyruvate in DCM @ 1 ml. min^{-1}; 0.25 bar/g H_2 pressure; GHSV 2250 h^{-1}; T = 25 ± 1 °C]

Figure 4.9 The effect on enantioselectivity and activity in the sequential hydrogenation of ethyl and methyl pyruvate.

4.2.7 The enantioselective hydrogenation of methyl pyruvate in the presence of different enantiomers of ethyl lactate

It has been postulated that co-adsorption of products can influence both activity and enantioselectivity of the Orito reaction. [4]. Therefore, a series of methyl pyruvate hydrogenation reactions were conducted over a cinchonidine modified (5.1 mM) 5% Pt/

γ-Al_2O_3 catalyst (0.4 g) in the presence of the two enantiomers of ethyl lactate (ethyl lactate was selected for ease of analysis) and their effect on the initial transient activity and enantioselectivity in methyl pyruvate hydrogenation was investigated. The catalyst bed was subjected to a concurrent downward flow of DCM (1 ml. min^{-1}) and hydrogen (300 ml. min^{-1}, 0.25 bar/g) for 30 minutes prior to the introduction of the reagents. The methyl pyruvate (25 mM) and ethyl lactate (25 mM) solution in DCM were fed into the reactor at a flow rate of 1 ml. min^{-1} and the products of hydrogenation monitored for 2 h. The results of these experiments are shown in Figures 4.10 and 4.11. It is apparent that the presence of ethyl lactate, whatever its stereochemistry, is detrimental to the enantioselectivity of methyl pyruvate hydrogenation. In the absence of ethyl lactate, methyl pyruvate gave a sustained e.e. of greater than 70%. When (*R*)-ethyl lactate was co-fed with methyl pyruvate the maximum e.e. observed was 66%, which falls to 58% at the end of the reaction. When the introduction of methyl pyruvate was delayed by 1 h to the pre-treated (*R*)-ethyl lactate catalyst bed, a further drop in enantioselectivity was observed with the final e.e. a low 52%. When (*S*)-ethyl lactate was fed through the catalyst bed for 1 h prior the introduction of methyl pyruvate the resultant maximum e.e. was 68%, close to the maximum value achieved when methyl pyruvate was hydrogenated individually, and significantly higher than the e.e. value obtained when the reaction was conducted over the (*R*)-ethyl lactate pre-treated bed.

The highest conversion to products, 62% after 2 h on line, was achieved in the absence of ethyl lactate and the results in Figure 4.11 illustrate the detrimental effect ethyl lactate, whatever its stereochemistry, has on catalyst activity in the hydrogenation of methyl pyruvate.

The greatest reduction in catalyst activity was observed when the catalyst bed was pre-treated for 1 h with either (*R*) or (*S*)-ethyl lactate prior to the introduction of methyl

pyruvate, with conversion to products after 2 h on line at 40% and 42% respectively. Catalyst deactivation was not so pronounced when (*R*)-ethyl lactate was co-fed with methyl pyruvate from the start of the reaction with conversion at 48% at the conclusion of the experiment.

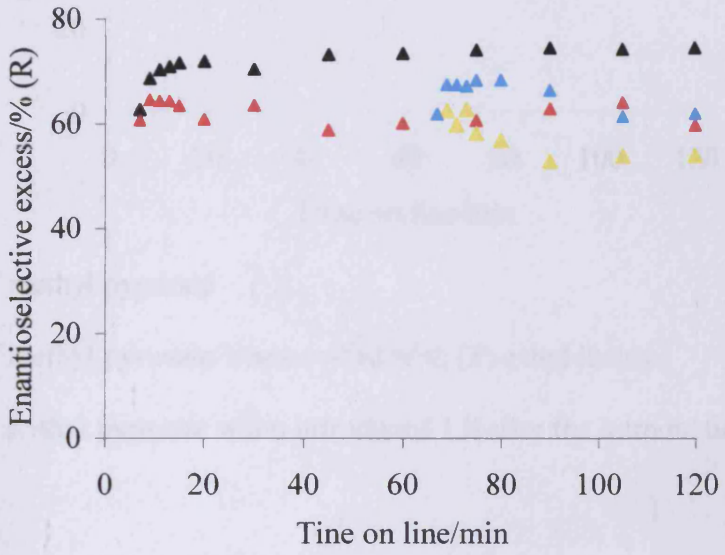

▲ e.e. of methyl lactate.

▲ e.e. of methyl lactate when co-fed with (*R*)-ethyl lactate.

▲ e.e. of methyl lactate when introduced 1 h after the introduction of (*R*)-ethyl lactate.

▲ e.e. of methyl lactate when introduced 1 h after the introduction of (*S*)-ethyl lactate.

[0.4 g catalyst; 25 mM methyl pyruvate / 25 mM ethyl lactate in DCM

@ 1 ml. min^{-1}; 0.25 bar/g H_2 pressure; GHSV 2250 h^{-1}; 25 °C; T = 25 ± 1 °C]

Figure 4.10 The effect on enantioselectivity in the hydrogenation of methyl pyruvate on co-feeding different enantiomers of ethyl lactate.

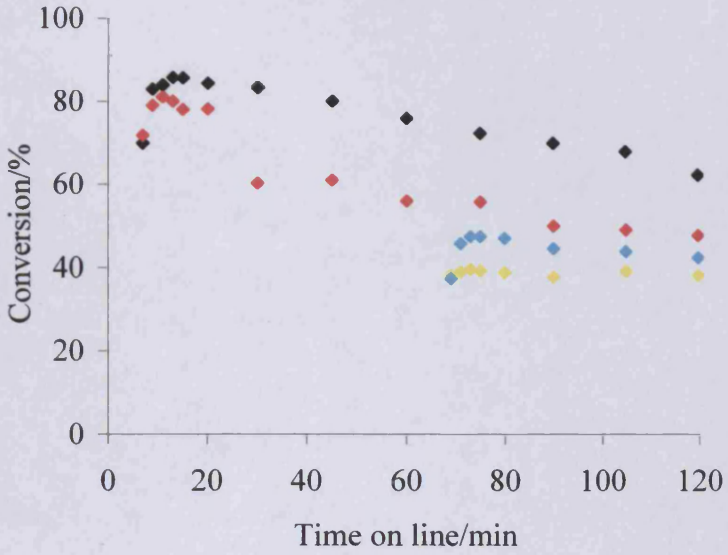

◆ Conversion of methyl pyruvate

◆ Conversion of methyl pyruvate when co-fed with (*R*)-ethyl lactate

◆ Conversion of methyl pyruvate when introduced 1 h after the introduction of (*R*)-ethyl lactate

◆ Conversion of methyl pyruvate when introduced 1 h after the introduction of (*S*)-ethyl lactate

[0.4 g catalyst; 25 mM methyl pyruvate / 25 mM ethyl lactate in DCM @ 1 ml. min^{-1}; 0.25 bar/g H_2 pressure; GHSV 2250 h^{-1}; T = 25 ± 1 °C]

Figure 4.11 The effect on activity in methyl pyruvate hydrogenation on co-feeding different enantiomers of ethyl lactate.

4.3 Discussion

4.3.1 Variation of enantioselectivity and activity with cinchonidine pre-modification concentration and the period of catalyst pre-treatment

The rationale behind the pre-modification of the platinum catalysts prior to their introduction into the reactor was to ensure that the cinchonidine was evenly distributed throughout the catalyst bed. The *in-situ* modification of the catalyst could have potentially resulted in an uneven distribution of cinchonidine down the length of the bed. Analysis of the solvent exiting the catalyst bed previously pre-modified with a 8.5 mM solution of cinchonidine (Figure 4.3), shows 20 Wt% of the modifier to be removed within the first twenty minutes of the experiment being on line. After which there was a very slow loss of cinchonidine for up to 4 h, which became negligible after that with the residual modifier remained adsorbed. The large initial loss of modifier was expected as there were potentially multiple layers of cinchonidine on the platinum surface and catalyst support which were weakly bound and easily removed by the flowing solvent. It is anticipated that the vinyl group of cinchonidine was rapidly hydrogenated under the reaction conditions employed to give 10,11–dihydrocinchonidine. It has been previously shown in autoclave experiments (section 4.2.4) that this reduction is not detrimental to enantioselectivity. Hydrogenation of the aromatic quinoline ring of cinchonidine is not expected under the mild conditions [5].

Variation of enantiomeric excess with the concentration of cinchonidine used in the pre-modification of 5% $Pt/\gamma\text{-}Al_2O_3$ catalysts for the hydrogenation of ethyl pyruvate is illustrated in Figure 4.1. There is a clear correlation between enantioselectivity and the concentration of cinchonidine used in catalyst pre-modification, with enantioselectivity

observed to pass through a maximum with increasing concentration of cinchonidine used in pre-modification.

The optimum enantioselectivity (ca. 70%) was achieved with a cinchonidine modifier solution concentration of 5.1 mM. This value of enantiomeric excess is comparable to the e.e. obtained when the same reaction is conducted in the autoclave reactor at elevated hydrogen pressures. The presence of an optimal modifier concentration suggests that the adsorption of the modifier at the platinum surface is potentially influenced by several different parameters such as platinum surface area, modifier surface coverage and the competitive adsorption of other species.

Cinchonidine is considered to adsorb parallel to the platinum surface through the π-electron system of the quinoline ring [6]. The poor enantioselectivity observed for those catalysts modified with cinchonidine solution of concentration less than 3.4 mM is indicative of insufficient cinchonidine modification of the platinum surface, which leads to the promotion of the racemic hydrogenation of ethyl pyruvate. The drop in e.e. observed when the concentration of cinchonidine used in pre-modification is increased to 8.5 mM is potentially associated with overcrowding of cinchonidine at the platinum surface, which can block the efficient adsorption of ethyl pyruvate at the chiral reaction site and cause the modifier to deviate from the optimum adsorption geometry required for optimal enatioselectivity. Baiker has previously conducted an *in-situ* ATR-IR investigation into the mode of cinchonidine adsorption using a model platinum-alumina catalyst [7]. Three modes of cinchonidine adsorption were identified, the populations of which were dependent upon the level of surface modifier coverage; at low coverage a strongly adsorbed species was identified where the quinoline ring was orientated parallel to the platinum surface. At higher cinchonidine surface coverage, two weakly adsorbed

moieties were observed, where, the quinoline ring was tilted away from the catalyst surface, resulting in reduced enantioselectivity for ethyl pyruvate hydrogenation.

These observations also account for the benefits of catalyst pre-treatment on enantioselectivity. Catalysts treated for between 0.5 h and 2 h prior to reaction provide an approximate 30% improvement in enantioselectivity compared to the untreated system. The pre-treatment step removes excess cinchonidine from the platinum surface, reducing overcrowding and allowing the modifier to adopt its optimum conformation where it adsorbs parallel to the platinum surface. The removal of excess modifier also provides additional beneficial space for the efficient adsorption of the α-ketoester adjacent to the cinchonidine molecule. The low enantioselectivity observed for the catalyst pre-treated for 3 h is the consequence of additional cinchonidine, although small in quantity, being removed from the catalyst bed over this extended period of pre-treatment resulting in insufficient modification of the platinum surface with cinchonidine. Conversion to ethyl lactate was generally observed to decrease with increasing periods of pre-treatment (Figure 4.5). This was contrary to the anticipated outcome as the pre-treatment step removes cinchonidine from the catalyst bed and it has previously been shown that the presence of cinchonidine is detrimental to catalyst activity with the unmodified catalyst being the most active (Figure 4.2). The least active catalyst was the one which had been pre-treated for 3 h prior to reaction, yielding a maximum 25% conversion to product. This catalyst had been treated for 3 h with dichloromethane, plus experienced an additional 2 h of dichloromethane flow during the course of the reaction. It is possible that dichloromethane may contain high molecular weight contaminants which can build up at the platinum surface poisoning the catalyst blocking the efficient adsorption of ethyl pyruvate.

In relation to activity, the presence of cinchonidine in batch reactor systems considerably increases the overall rate of reaction in ethyl pyruvate hydrogenation with up to a 100 fold increase [8] observed when compared to the un-modified reaction. The results presented in Figure 4.2 clearly show that this is not the case in the CFR reactor and that the maximum conversion to products for all catalysts tested, whatever the concentration of cinchonidine used in pre-modification, was achieved in the initial stages of the reaction, after which time the catalyst deactivated rapidly. Murzin has recently reported the continuous enantioselective hydrogenation of ethyl benzoylformate [9] over cinchonidine modified platinum. The reaction was seen to deactivate rapidly with time, the conversion dropping from 60% to 25% after 45 min. Gradual catalyst deactivation in continuous flow reaction systems has also been reported in the hydrogenation of isopropyl-4,4,4-trifluoroacetate [10] and 1-phenyl-1,2-propanedione [3]. Murzin attributed the catalyst deactivation to the low concentrations of ester being hydrogenated, which were similar to the α-ketoester levels used in this study. Deactivation was also observed at low substrate levels when the reaction was conducted in an autoclave reactor which gives strength to Murzin argument.

An other possible explanation for the rate decrease observed in the CFR reactor is that the system does not undergo the same vigorous stirring experienced in the autoclave reactor. This is known to increase the rate of reaction through the more rapid diffusion of hydrogen throughout the liquid phase and its subsequent activation at the platinum surface coupled with the more efficient transportation of reagents and products to and from the catalyst surface. Rapid stirring will also influence the adsorption / desorption equilibrium characteristics of the modifier and hinder the deposition of surface contaminants such as polymers which can build up at the platinum surface and influence conversion.

4.3.2 Solvent effects in the CFR reactor

The influence of reaction solvent in the hydrogenation of ethyl pyruvate in the CFR reactor has been studied.

The solvents investigated, dichloromethane and ethanol, gave markedly contrasting results for both activity and enantioselectivity in the hydrogenation of ethyl pyruvate. Dichloromethane yielded a maximum e.e. of 72% in favour of (*R*)-ethyl lactate whilst conversion was seen to drop steadily from 80% to 50% after 2 h on line. Ethanol gave a maximum e.e. of 27% to the (*R*)-enantiomer, with a sustained 95% conversion to products for the 2h the reaction was on line.

The influences of solvent in α-ketoester hydrogenation have been the subject of numerous studies in batch reactor systems [11], with a clear correlation being made between enantioselectivity and the dielectric constant of the reaction solvent. Baiker reported that solvents of high dielectric constant stabilise the closed conformers of cinchonidine whilst solvents with a low dielectric constant serve to stabilise the '*open 3*' conformation, which is thought by many researchers to be a prerequisite for high enantioselectivity.

^{1}H NMR has been used to determine the conformational distribution of cinchonidine in different solvents. In dichloromethane (dielectric constant 8.93) cinchonidine adopts a 50% *'open 3'* conformation whilst in ethanol (dielectric constant 24.55) the percentage of *'open 3'* conformer found by ^{1}H NMR was 77%. Thus the superior enantioselectivity observed in dichloromethane cannot be attributed to its ability to stabilise the '*open 3*' conformer of cinchonidine better than ethanol.

A factor which could explain the observed difference in enantioselectivity between the two solvent systems is cinchonidine solubility. Cinchonidine is more soluble in ethanol than dichloromethane [12]; therefore ethanol is expected to remove a greater amount of

cinchonidine from the catalyst bed during pre-treatment, leading to a larger number of un-modified platinum sites at which the racemic hydrogenation of the α-ketoester could take place. The more efficient removal of cinchonidine from the catalyst bed by ethanol also explains the greater activity observed in this solvent because as previously illustrated (section 4.2.5) an un-modified catalyst bed gives a higher conversion to ethyl lactate than when conducted in the presence of cinchonidine.

4.3.3 The effect on enantioselectivity in the co-reaction of methyl and ethyl pyruvate esters

The simultaneous hydrogenation of ethyl and methyl pyruvate was undertaken to investigate if the chiral reaction site generated by cinchonidine on the platinum surface was substrate selective.

The results presented in section 4.2.6 illustrate that there was no substrate discrimination in the simultaneous enantioselective hydrogenation of the ethyl and methyl pyruvate esters. The e.e. values obtained (ethyl pyruvate *c.a.* 68% e.e.; methyl pyruvate *c.a.* 67% e.e.) are slightly lower than that observed when the esters are hydrogenated individually. The conversion for both reactions decreases with time on line as previously reported in this study. These results suggest that the cinchonidine generated enantioselective site does not possess a substrate preference in pyruvate ester hydrogenation and the cinchonidine is capable of adapting its conformation on the platinum surface to accept either substrate. The fact that the cinchonidine molecule is continually altering its conformation to accommodate either methyl or ethyl pyruvate may account for the slightly lower enantioselectivity observed in the simultaneous hydrogenation reaction.

Both methyl and ethyl pyruvate exhibit mirror image transients, where enantioselectivity builds up to a steady state value over a 15 min. period. The phenomenon of increasing

enantioselectivity with time in the early part of the reaction was first reported by Wells and co-workers [13, 14] and has recently been the subject of numerous studies [15-18]. At present, there are two hypotheses as to the origin of this intriguing effect. The first proposes the establishment of an optimised chiral surface [16, 17, 19] while the second attributes the effect to the role of impurities at the metal surface [18, 20]and their subsequent removal.

When ethyl pyruvate is hydrogenated prior to the introduction of methyl pyruvate an initial transient of 15 min is observed before the reaction reaches a steady state (*c.a.* 72% e.e.), the switch to methyl pyruvate is seamless with no visible transient observed. The low first e.e. measurement can be potentially attributed to the cinchonidine 'tuning' its conformation to accommodate the new substrate. This data fits in well with earlier observations that α-ketoesters exhibit lower enantioselectivity when hydrogenated simultaneously due to the continuous fluctuations in the cinchonidine conformation. When the introduction of reagents to the reactor is reversed a similar set of data is generated. The methyl pyruvate gave an initial transient and showed a low first e.e. measurement when ethyl pyruvate was introduced. Again this can be attributed to changes in the cinchonidine conformation. These observations indicate that over the initial part of the reaction, *i.e.* the period of the initial transient, the platinum surface undergoes 'cleaning,' with surface blocking impurities such as carbon dioxide removed *via* hydrogenation or being displaced by the stronger adsorbing α-ketoester substrate.

Another plausible explanation for the lag in enantioselectivity is that the substrate and modifier undergo a form of surface equilibration where the cinchonidine and α-ketoester move about the platinum surface in order to obtain optimum coverage and spacing to allow the efficient modifier : substrate interaction necessary for high enantioselectivity. The time taken to achieve this equilibrium will be the length of the initial transient, after

which enantioselectivity reaches a steady state. This theory fits well with the results obtained for the sequential hydrogenation reactions where no initial transient is observed on introduction of the second ester substrate to the reactor as the cinchonidine molecules have already undergone surface equilibrium and established optimum coverage.

4.3.4 The enantioselective hydrogenation of methyl pyruvate in the presence of different enantiomers of ethyl lactate

The results presented in section 4.2.7 illustrate that the hydrogenation of methyl pyruvate in the presence of ethyl lactate is detrimental to both conversion and enatioselectivity, indicating that the lactate product is poisoning the catalyst.

In the absence of ethyl lactate, methyl pyruvate yields a sustained e.e. in excess of 70%. When (*R*)-ethyl lactate is co-fed with methyl pyruvate the maximum e.e. observed was 66%, which fell to 58% at the end of the reaction. The reduction in enantioselectivity can be explained by the fact that under reaction conditions ethyl lactate can potentially undergo reaction with methyl pyruvate to form oligomers and other polymeric species which can adsorb onto the platinum surface, restricting methyl pyruvate ability to adsorb on to the cinchonidine modified platinum surface, resulting in lower conversion and enantioselectivity. Attard has analysed the products of ethyl pyruvate hydrogenation using GC-MS and detected a series of diastereomeric linear and cyclic dimers formed *via* a base catalysed addition of (*R*) and (*S*) ethyl lactate to ethyl pyruvate. Attard postulated that these dimers undergo further reaction to form high molecular weight polymers which coat the platinum surface and remain undetected by GC-MS.

The pre-treatment of the catalyst bed for 1 h with (*R*)-ethyl lactate prior to the introduction of methyl pyruvate led to an 18% reduction in enantioselectivity to (*R*)-methyl lactate and a 30% reduction in conversion to products when compared to the

same reaction conducted in the absence of ethyl lactate. When the bed was treated with (*S*)-ethyl lactate for 1 h prior to the introduction of methyl pyruvate the maximum e.e. observed was 67%, close to the maximum value achieved when methyl pyruvate was hydrogenated individually.

A plausible explanation for the inferior enantiomeric excess observed in the hydrogenation of methyl pyruvate over an ethyl lactate modified bed, is the possible unfavourable interaction between ethyl lactate and modifier. The hydroxyl group of ethyl lactate can readily hydrogen bond to the quinuclidine nitrogen of the modifier; such an interaction blocks access of the substrate to the active site, reducing the enantioselective hydrogenation of methyl pyruvate. The reduction in the observed methyl lactate enantioselectivity was not so pronounced when the reaction was conducted in the presence of (*S*)-ethyl lactate, as this enantiomer does not possess the correct stereochemistry to fit into the 'chiral pocket' generated by cinchonidine (which is configured to generate (*R*)-ethyl lactate) and effectively hydrogen bond to the quinuclidine nitrogen.

4.4 Conclusion

It has been shown that cinchonidine pre-modified catalysts perform well in the enantioselective hydrogenation of ethyl pyruvate in the continuous flow reactor operating under mild conditions, with e.e. values comparable to when the reaction was conducted at elevated hydrogen pressures in the batch reactor using the same solvent. However activity is observed to decrease with time on line contra to the rate acceleration observed in the batch reactor. The absence of a second transient in the sequential hydrogenation of methyl and ethyl pyruvate indicates that the initial transient was the result of system optimisation i.e. surface platinum cleaning. The reactions where lactate product was co-

fed or pre-fed into the catalyst bed resulted in low enantioselectivity and activity implying that the system is self poisoning.

4.5 References

1 Y. Orito, S. Imai and S. Niwa, *J. Chem. Soc. Jpn.*, (1979) 1257.

2 M. Künzle, R. Hess, T. Mallat and A. Baiker, *J. Catal.*, **186** (1999) 239.

3 E. Toukoniitty, P. Mäki-Arvela, A.K. Neyestanaki, T. Salmi, R. Sjöholm, R. Leino, E. Laine, P.J. Kooyman, T. Ollonqvist and J. Väyrynen, *App. Catal. A: Gen.*, **216** (2001) 73.

4 T. Mallat, Z. Bodner, K. Borszeky and A. Baiker, *J. Catal.*, **168** (1997) 183.

5 O.J. Sonderegger, M.W. Gabriel, T. Buergi and A. Baiker, *J. Catal.*, **230** (2005) 499.

6 G. Bond and P.B. Wells, *J. Catal.*, **150** (1994) 329.

7 D. Ferri, T. Bürgi and A. Baiker, *J. Chem. Soc. Chem. Commun.*, (2001) 1172.

8 H.U. Blaser, H.P. Jalett, D.M. Monti, J.F. Reber and J.T. Wehrli, *Stud. Surf. Sci. Catal.*, **41** (1988) 153.

9 E. Toukoniitty, P. Mäki-Arvela, N. Kumar, T. Salmi, and D.Yu. Murzin, *Catal. Lett.*, **95** (2004) 179.

10 N. Künzle, T. Mallat and A. Baiker, App. *Catal. A: Gen.*, **238** (2003) 251.

11 J.T. Wehrli, A. Baiker, D.M. Monti, H-U. Blaser and H.P. Jalett, *J. Mol. Catal.*, **57** (1989) 245.

12 Z. Ma and F. Zaera, *J. Phys. Chem.*, **109** (2005) 406.

13 P. Meheux, A. Ibboston and P.B. Wells, *J. Catal.*, **128** (1991) 441.

14 M. Sutherland, A. Ibboston, R.B. Moyes and P.B. Wells, *J. Catal.*, **125** (1990) 77.

15 J. Margitfalvi, M. Hegedűs and E. Tfirst, *Tetrahedron: Asymmetry*, **7** (1994) 571.

16 Y Sun, J. Wang, C. Le Blond, R.N. Landau and D.G.Blackmond, *J. Catal.*, **161** (1996) 752.

17 Y.Sun, J. Wang, C. Le Blond, R.N. Landau and D.G.Blackmond, *J. Catal.*, **161** (1996) 759.

18 T. Mallat and A. Baiker, *J. Catal.*, **176** (1998) 27.

19 D. G. Blackmond, *J. Catal.*, **176** (1998) 267.

20 T. Mallat, Z. Bodnar, B. Minder, K. Bovszcky and A. Baiker, *J. Catal.*, **168** (1997) 183.

Chapter Five

Chapter Five Inversion of the Sense of Enantioselectivity

5.1 Introduction

In previous studies [1] into the enantioselective hydrogenation of ethyl pyruvate (**I**), it has been established that with cinchonidine and quinine modified platinum catalysts the reaction proceeds to form predominantly (*R*)-ethyl lactate (**II-*R***), whereas with cinchonine and quinidine modified platinum catalysts the reaction forms (*S*)-ethyl lactate (**II-*S***) preferentially (Scheme 5.1).

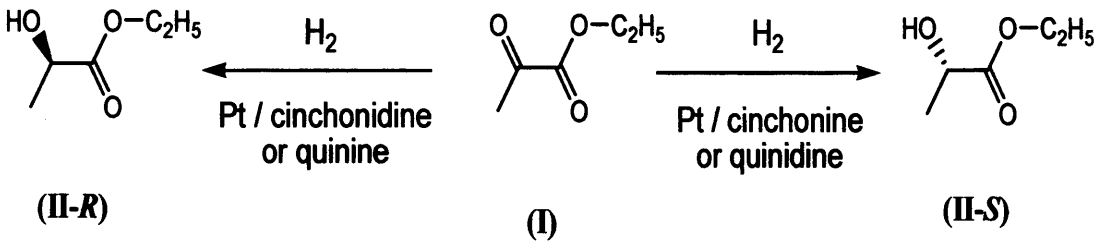

Scheme 5.1 The products of ethyl pyruvate (I) hydrogenation over cinchona modified platinum catalysts.

Considerable effort has been focused on the mechanism of these reactions, and three structural features of the cinchona and related modifiers that ensure they are effective in enantiofacial discrimination have been identified, namely; (i) an aromatic moiety that enables adsorption on the platinum surface, (ii) the absolute configuration at *C8* and *C9* which controls the sense of the enantioselectivity, (iii) a basic nitrogen which is considered to interact with the substrate resulting in a 1:1 complex that is hydrogenated enantioselectively [1].

The reaction is, however, complicated by effects observed in the early part of the reaction where enantioselection increases with conversion [2-4]. Consequently, there has been

limited progress in gaining an understanding of this fascinating reaction at the molecular level.

Recently, Baiker and co-workers [5-7] and Bartók *et al* [8, 9] have shown a further intriguing aspect of this reaction, namely that the sense of the enantioselection can be inverted for specific modifiers by changing the extent of reaction [5], the solvent [8] or the substituent at the *C9* position of the alkaloid [6, 7].

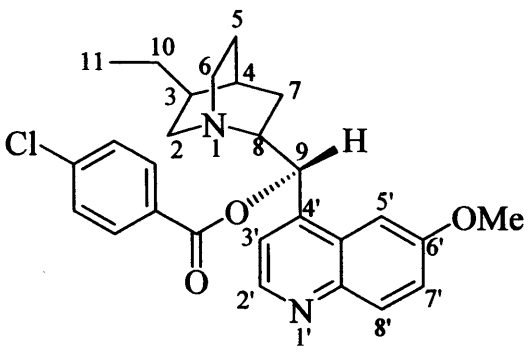

1

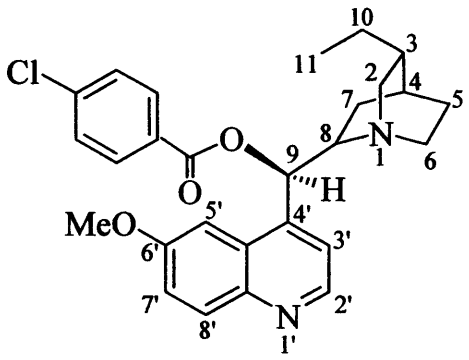

2

Figure 5.1 Hydroquinidine-4-chlorobenzoate **1** and hydroquinine-4-chlorobenzoate **2** modifiers.

In all the above cases the effect is induced by changes in the reaction conditions. In this chapter the findings are presented on how the sense of enantioselectivity can be influenced solely by changing the concentration of 4-chlorobenzoate derivatives of hydroquinine and hydroquinidine (Figure 5.1) used in the reaction.

5.2 Results

5.2.1 Autoclave reaction conditions

All platinum catalysts were modified using an *in-situ* procedure as outlined in section 2.3.2, in which the modifier hydroquinidine-4-chlorobenzoate **1** or hydroquinine-4-chlorobenzoate **2** was added to the autoclave reactor immediately prior to the start of the reaction. Under standard conditions, ethyl pyruvate (66 mmol), solvent (12.5 cm^3), modifier (1-100 mg) and catalyst (0.25 g) were sealed in the autoclave. Hydrogen was admitted to the required reaction pressure of (50 bar) and the reaction initiated with the commencement of stirring (1200 rpm). Reaction temperature was maintained at 20 °C ± 2 °C. This was the standard operating procedure used for the hydrogenation of ethyl pyruvate in the autoclave reactor (Section 2.8.3), unless stated to the contrary.

5.2.2 The effect of solvent and modifier concentration on the enantioselectivity observed in ethyl pyruvate hydrogenation

The enantioselective hydrogenation of ethyl pyruvate was conducted over a 5% Pt/γ-Al_2O_3 catalyst recently reduced at 400 °C, using hydroquinidine-4-chlorobenzoate and hydroquinine-4-chlorobenzoate as modifiers in a range of different solvents, the results of which are shown in Table 5.1. When hydroquinidine-4-chlorobenzoate was used as a modifier in acetic acid the sense of the enantioselectivity was inverted in comparison to when the reaction was conducted in dichloromethane at the same modifier : platinum ratio.

A more intriguing observation was that when the reaction was conducted solely in dichloromethane the sense of enantioselectivity inverted as the concentration of the modifier increased. At a catalyst modifier ratio of 0.18 the observed e.e. was 32% in

favour of (*S*)-ethyl lactate. As the catalyst modifier ratio was increased to 6.3 the e.e. was 8% in favour of the (*R*)-enantiomer. The opposite effect with a similar magnitude was observed when hydroquinine-4-chlorobenzoate was used as a modifier.

Table 5.1 Effect of reaction solvent and modifier concentration on the hydrogenation of ethyl pyruvate.

Modifier (mg/mg_{Pt})	**Solvent**	**Hydroquinidine[a]**		**Hydroquinine[a]**	
		Conversion / %	**e.e. / %**	**Conversion / %**	**e.e. / %**
6.3	acetic acid	47	26 (*S*)	52	25 (*R*)
6.3	Toluene	6	2 (*R*)	19	9 (*R*)
6.3	Dichloromethane	97	8 (*R*)	89	14 (*S*)
1.28	Dichloromethane	100	6 (*S*)	100	21 (*R*)
1.28	Dichloromethane	n/a	n/a	98	20[b](*R*)
0.18	Dichloromethane	100	32 (*S*)	100	20 (*R*)

[**a**] Modifiers used as 4-chlorobenzoate derivative.

[**b**] 1mg (6.4 mmol) 4-chlorobenzoic acid added to reaction.

[Solvent 12.5 cm^3, 66.0 mmol ethyl pyruvate, 0.25 g 5% $Pt/\gamma\text{-}Al_2O_3$, 50 bar hydrogen pressure, stirring rate 1200 rpm, Temp = 20 °C ± 1 °C]

Subsequently, a series of enantioselective hydrogenations were carried out over a 5% $Pt/\gamma\text{-}Al_2O_3$ reduced at 400 °C modified with hydroquinidine 4-chlorobenzoate in which the concentration of the modifier was varied over a range of two orders of magnitude using dichloromethane as a reaction solvent.

The results presented in Figure 5.2 show that the sense of the enantioselection is a function of the modifier concentration and that (*S*)-ethyl lactate is formed (*ca.* 30% e.e.) at low modifier : platinum ratios.

As the concentration of the modifier was increased, the product became racemic and subsequently, at higher modifier concentrations, (*R*)-ethyl lactate was preferentially formed (*ca.* 10% e.e.). The hydrogen uptake curves for each hydrogenation reaction are shown in Figure 5.3.

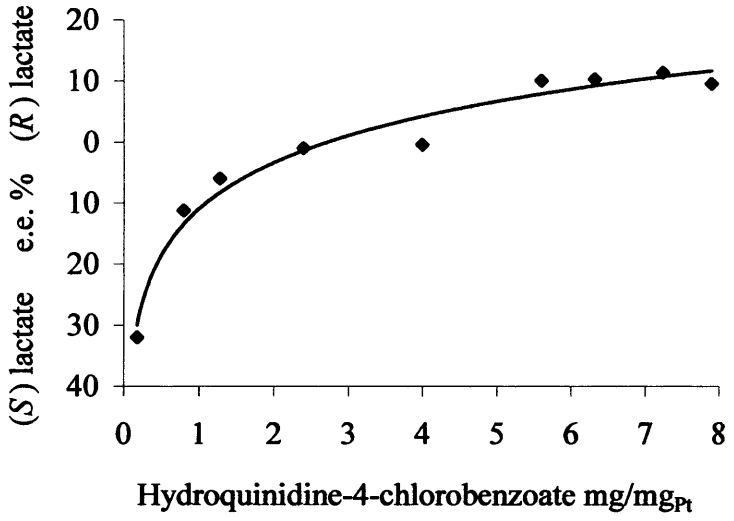

[Solvent 12.5 cm^3, 66.0 mmol ethyl pyruvate, 0.25 g 5% Pt/γ-Al_2O_3, 50 bar hydrogen pressure, stirring rate 1200 rpm, T = 20 °C ± 1 °C.]

Figure 5.2 The effect of modifier concentration on the sense of enantioselectivity in the hydrogenation of ethyl pyruvate over a 5% Pt/γ-Al_2O_3 catalyst reduced at 400 °C in flowing 5% H_2/Ar

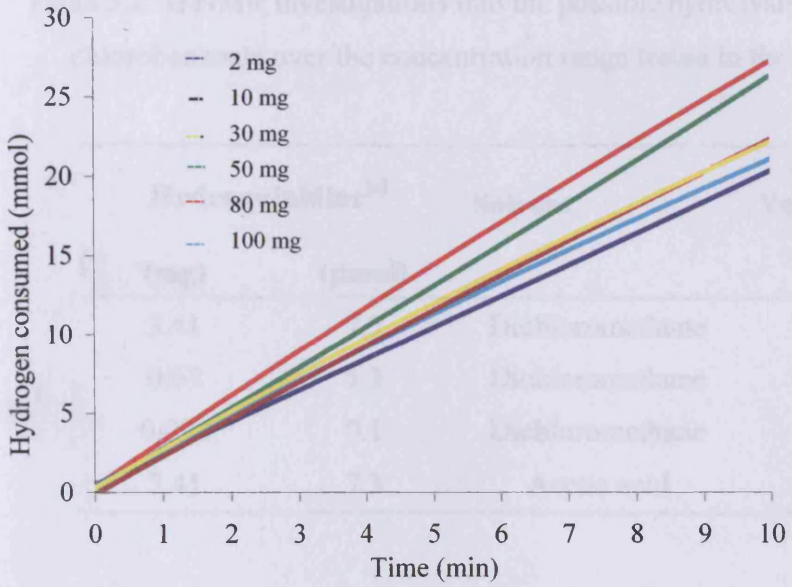

[Solvent 12.5 cm^3, 66.0 mmol ethyl pyruvate, 0.25 g 5% $Pt/\gamma\text{-}Al_2O_3$, 50 bar hydrogen pressure, stirring rate 1200 rpm, T = 20 °C ± 1 °C.

Figure 5.3 Hydrogenation uptake curves for ethyl pyruvate hydrogenation over 5% $Pt/\gamma\text{-}Al_2O_3$ reduced at 400 °C at various hydroquinidine-4-chlorobenzoate modifier concentrations.

5.2.3 Solution stability of hydroquinidine-4-chlorobenzoate

^1H NMR was used to investigate the stability of hydroquinidine-4-chlorobenzoate in both dichloromethane and acetic acid over the concentration range tested in the presence of ethyl pyruvate and water. Special attention was made to the potential appearance of NMR signals associated with the hydrolysis of the modifier hydroquinidine and 4-chlorobenzoic acid. A series of ^1H NMR experiments were recorded in a 0.5 cm^3 CD_2Cl_2 solution and 0.5 cm^3 CD_3COOD containing hydroquinidine-4-chlorobenzoate at the concentrations specified in Table 5.2 in the presence of an excess amount of water (1 µl, 55 mmol).

Table 5.2 ^{1}H NMR investigations into the possible hydrolysis of hydroquinidine-4-chlorobenzoate over the concentration range tested in the presence of water.

Hydroquinidine[a]		**Solvent**	**Vol. Water added (µl)**
(mg)	**(µmol)**		
3.41	7.3	Dichloromethane	1
0.64	1.3	Dichloromethane	1
0.092	0.1	Dichloromethane	1
3.41	7.3	Acetic acid	1

In all cases the structural integrity of the hydroquinidine-4-chlorobenzoate remained intact; no degradation of the modifier was observed and no appearance of peaks related to 4-chlorobenzoic acid was viewed to be present (Figure 5.4).

The spectra of 4-chlorobenzoic acid run in both acetic acid and dichloromethane along with the spectra of hydroquinidine-4-chlorobenzoate (various concentrations) can be viewed in Appendix A,

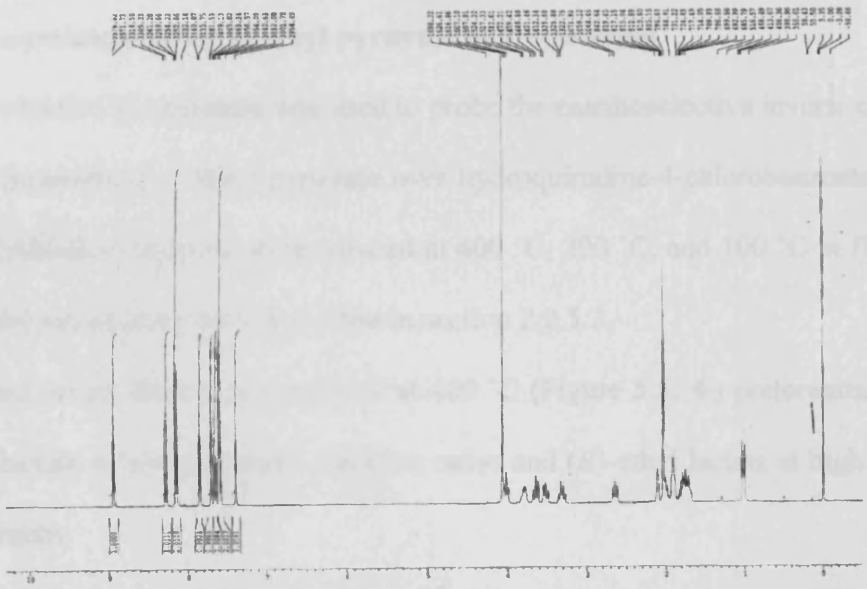

a) ^{1}H NMR spectra of hydroquinidine-4-chlorobenzoate (7.3 μmol) in acetic acid

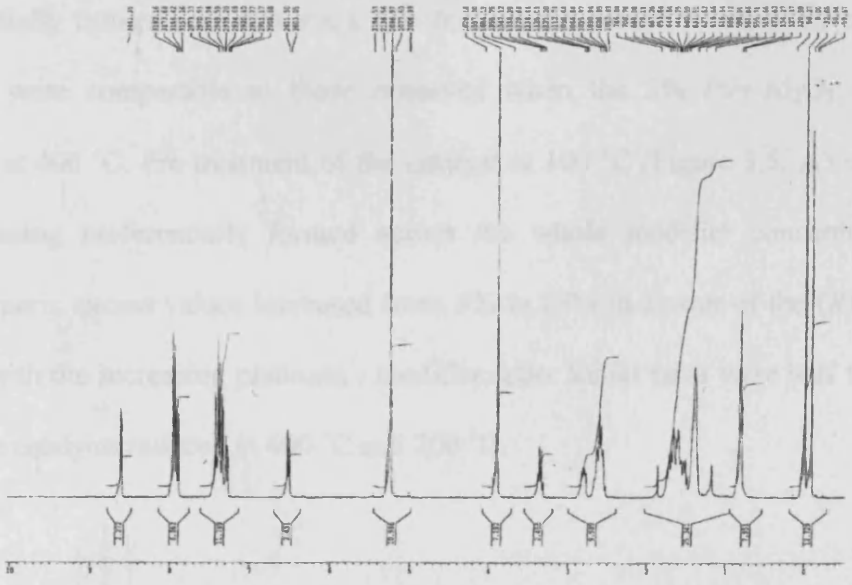

b) ^{1}H NMR spectra of hydroquinidine-4-chlorobenzoate (7.3 μmol) in dichloromethane

Figure 5.4 Comparison of the ^{1}H NMR spectra of hydroquinidine-4-chlorobenzoate in acetic acid and dichloromethane

5.2.4 The effect of reduction temperature on 5% Pt/γ-Al_2O_3 catalysts and its effect on enantioselectivity in ethyl pyruvate hydrogenation

Catalyst reduction temperature was used to probe the enantioselective inversion observed in the hydrogenation of ethyl pyruvate over hydroquinidine-4-chlorobenzoate modified platinum. Alumina catalysts were reduced at 400 °C, 200 °C, and 100 °C in flowing 5% H_2/Ar hydrogen as previously described in section 2.2.5.2.

As reported earlier the catalyst reduced at 400 °C (Figure 5.5, ◆) preferentially formed (*S*)-ethyl lactate at low platinum : modifier ratios and (*R*)-ethyl lactate at high platinum : modifier ratios.

When the catalyst was reduced at 200 °C (Figure 5.5, ■) a comparable trend was observed with the reaction proceeding racemically at low platinum : modifier ratios and enantioselectively at higher platinum : modifier ratios with (*R*)-ethyl lactate being preferentially formed (*ca.* 10% e.e.). The initial rates across the modifier range for this catalyst were comparable to those observed when the 5% Pt/γ-Al_2O_3 catalyst was reduced at 400 °C. Pre-treatment of the catalyst at 100 °C (Figure 5.5, ▲) saw (*R*)-ethyl lactate being preferentially formed across the whole modifier concentration range. Enantiomeric excess values increased from 6% to 23% in favour of the (*R*)-enantiomer, in line with the increasing platinum : modifier ratio. Initial rates were half that observed for those catalysts reduced at 400 °C and 200 °C.

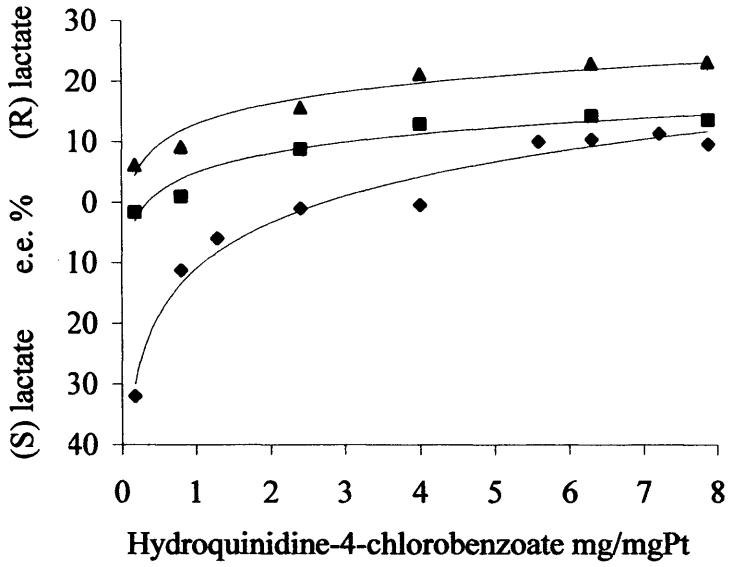

[Solvent 12.5 cm^3, 66.0 mmol ethyl pyruvate, 0.25 g 5% $Pt/\gamma\text{-}Al_2O_3$, 50 bar hydrogen pressure, stirring rate 1200 rpm, T = 20 °C ± 1 °C]

Figure 5.5 The effect of catalyst reduction temperature on the enantioselective hydrogenation of ethyl pyruvate using hydroquinidine-4-chlorobenzoate as a chiral modifier. ◆ 400 °C, ■ 200 °C, ▲ 100 °C, 5% $Pt/\gamma\text{-}Al_2O_3$.

Table 5.3 Initial rate data for the 5% Pt/γ-Al_2O_3 catalysts reduced at different temperatures

Hydroquinidine[a] /Pt ratio (mg/mgPt)	**400 °C Initial rate (mmol $g^{-1}h^{-1}$)**	**200 °C Initial rate (mmol $g^{-1}h^{-1}$)**	**100 °C Initial rate (mmol $g^{-1}h^{-1}$)**
0.18	492	602	243
0.8	540	550	381
2.4	535	562	-
4	631	550	360
6.3	654	600	376
7.9	516	586	400

[a] 4-chlorobenzoate derivative

[Solvent 12.5 cm^3, 66.0 mmol ethyl pyruvate, 0.25 g 5% Pt/γ-Al_2O_3, 50 bar hydrogen pressure, stirring rate 1200 rpm, T = 20 °C ± 1 °C]

5.2.5 Catalyst support effects

The effect of catalyst support on the hydrogenation of ethyl pyruvate over hydroquinidine-4-chlorobenzoate modified platinum was investigated. A 2.5% Pt/SiO_2 and a 5% Pt/C catalyst were both reduced at 400 °C following the same reduction procedure used for those 5% Pt/γ-Al_2O_3 catalysts previously examined. The results illustrated in Figure 5.6 demonstrate that the silica and carbon supported platinum catalysts solely favour the (*R*)-ethyl lactate enantiomer at all modifier : platinum ratios tested, contrary to the inversion of enantioselectivity observed when the reaction is carried out over the alumina supported platinum catalyst reduced at 400 °C. Comparison of initial rate measurements show the Pt/γ-Al_2O_3 catalyst to be the most active catalyst, with initial rate values approximately four times that observed to when the platinum was

supported on silica. The least active support was graphite with the maximum rate for this support being achieved at the highest modifier : platinum ratio investigated.

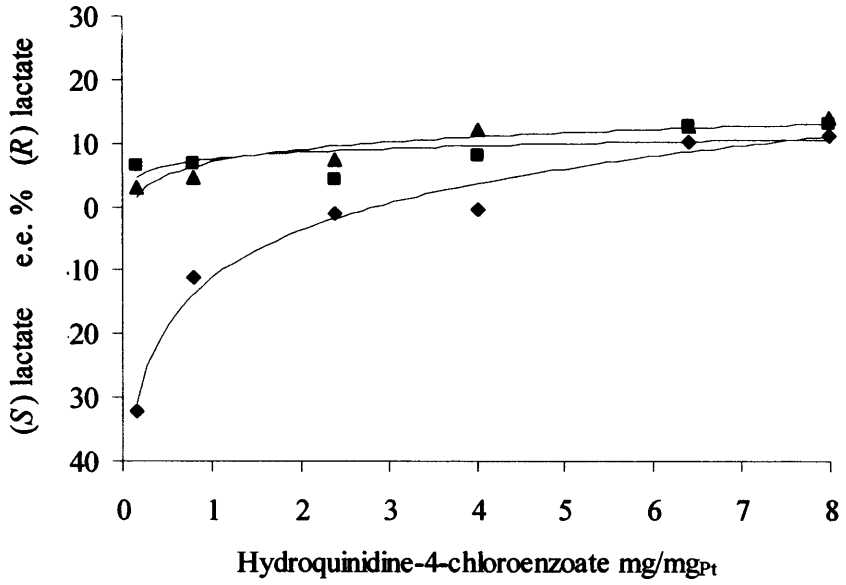

[Solvent 12.5 cm^3, 66.0 mmol ethyl pyruvate, 0.25 g 5% $Pt/\gamma\text{-}Al_2O_3$, 50 bar hydrogen pressure, stirring rate 1200 rpm, T = 20 °C ± 2 °C]

Figure 5.6 The effect of catalyst support on the enantioselective hydrogenation of ethyl pyruvate using hydroquinidine-4-chlorobenzoate as a chiral modifier.

◆ $Pt/\gamma\text{-}Al_2O_3$, ■ Pt/C, ▲ Pt/SiO_2. All catalysts reduced at 400 °C under 5% H_2/Ar.

Table 5.4 Initial rate data for the three different platinum supported catalysts examined.

Hydroquinidine[a] /Pt ratio (mg/mgPt)	**Pt/γ-Al_2O_3 Initial rate (mmol $g^{-1}h^{-1}$)**	**Pt/SiO_2 Initial rate (mmol $g^{-1}h^{-1}$)**	**Pt/C Initial rate (mmol $g^{-1}h^{-1}$)**
0.16	492	113	66
0.8	540	125	73
2.4	535	139	73
4	631	157	92
6.4	654	165	93
8	516	182	112

[a] 4-chlorobenzoate derivative

[Solvent 12.5 cm^3, 66.0 mmol ethyl pyruvate, 0.25g catalyst, 50 bar hydrogen pressure, stirring rate 1200 rpm, T = 20°C ± 2°C]

5.2.6 HRTEM studies of 5% Pt/γ-Al_2O_3 catalysts

Detailed TEM imaging experiments were conducted on the Pt/γ-Al_2O_3 catalysts reduced over the range 100 - 400 °C to determine if reduction temperature had a bearing on platinum particle size, distribution and morphology. Figure 5.7 (a) and (b) are bright field images of the catalysts reduced at 100 °C and 400 °C respectively, in which the Pt nanoparticles are clearly seen by diffraction contrast to be in the 2–5 nm size range in both cases. HRTEM images of representative metal nanoparticles from each of the reduced samples are shown in Figures 5.8 (**a**) and (**b**). The particles are imaged in profile along the Pt [110] projection and {111} and have {002}-type lattice fringes which are clearly resolved. The particles in both cases have truncated cube-octahedral morphologies and expose low energy {111} and {200} facet planes.

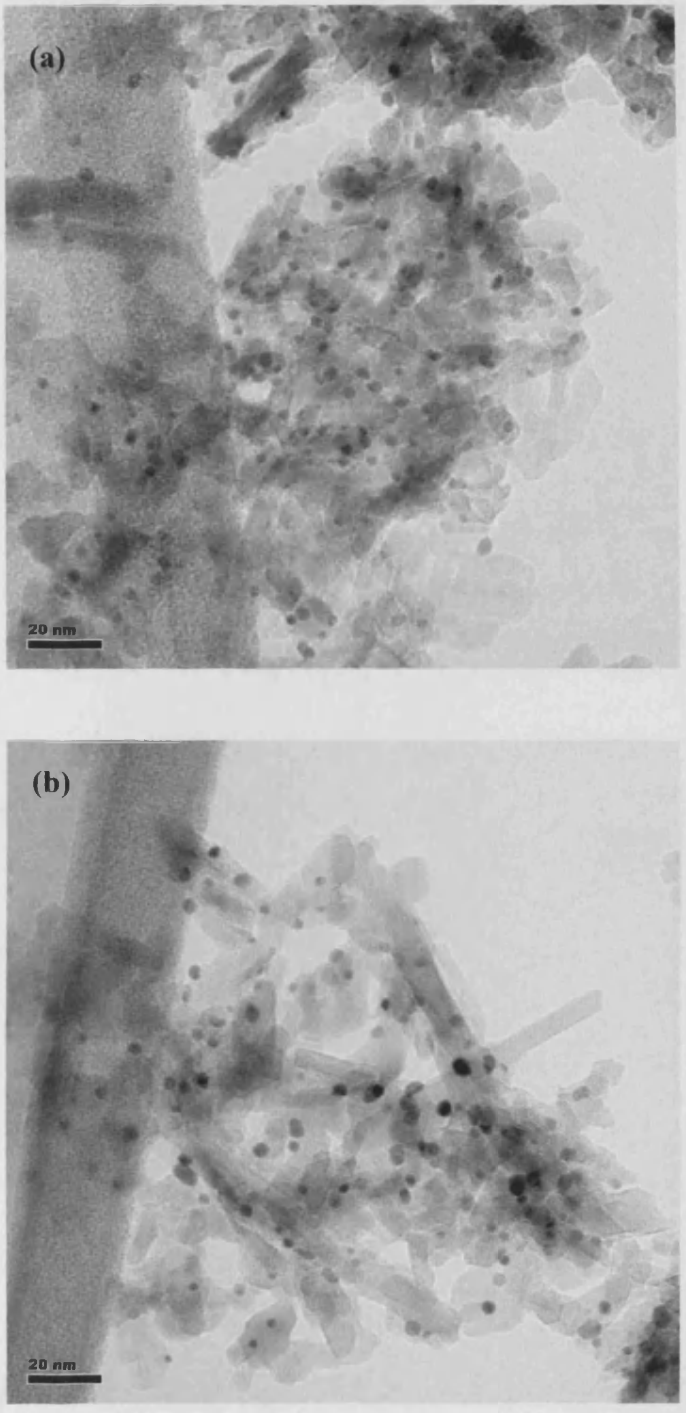

Figure 5.7 Representative bright field electron micrographs of the Pt/γ-Al_2O_3 catalyst materials reduced at (**a**) 100 ˚C and (**b**) 400˚C respectively.

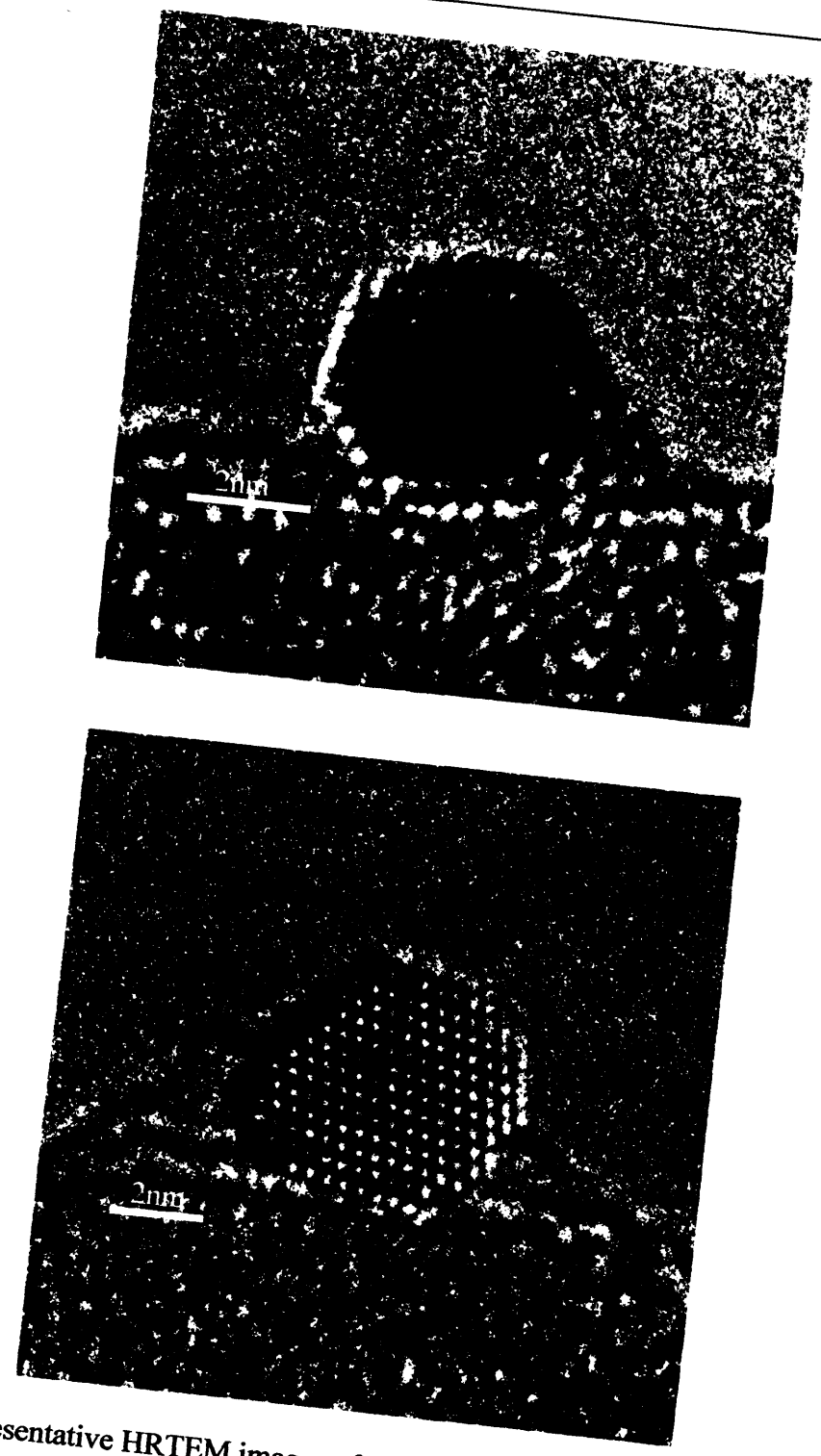

gure 5.8 Representative HRTEM images of Pt nanoparticles in the Pt/γ-Al_2O_3 catalyst materials reduced at (a) 100 °C and (b) 400 °C.

5.3 Discussion

5.3.1 Solvent and modifier concentration effects

The results presented in Table 5.1 illustrate a solvent dependence on the sense of enantioselectivity in the hydrogenation of ethyl pyruvate over hydroquinidine-4-chlorobenzoate modified 5% Pt/γ-Al_2O_3 At a platinum : modifier ratio of 6.3, the reaction showed an e.e. of 26% in favour of the (*S*)-enantiomer when conducted in acetic acid, as expected from the structure of the parent alkaloid. When the reaction was conducted in dichloromethane, at the same modifier : platinum ratio, (*R*)-ethyl lactate was preferentially formed with an e.e. of 8%. The opposite effect with a similar magnitude was observed when hydroquinine-4-chlorobenzoate was used as the chiral modifier. Additional experiments carried out in dichloromethane at hydroquinidine-4-chlorobenzoate : platinum ratios lower than 4 resulted in the preferential formation of (*S*)-ethyl lactate; analogous to when the reaction was conducted in acetic acid

The low enantioselectivity observed when using hydroquinidine-4-chlorobenzoate as a modifier in the hydrogenation of ethyl pyruvate regardless of the reaction solvent may be associated with the introduction of the strongly electron withdrawing 4-chlorobenzoate group at the *C9* position.

As discussed in section 1.6.1 substitution at the *C9* position of cinchonidine can influence the degree of asymmetric induction. Replacement of the hydroxyl group with a methoxy group had no detrimental effect on the enantiomeric excess observed, however, when the substituent at the *C9* position was an electron withdrawing acetyl group there was a dramatic reduction in the enantiomeric excess obtained. Dijkstra's interpretation of the low enantioselectivity observed when these 4-chlorobenzoate derivatives were used as chiral modifiers was based solely on the conformational behaviour of the alkaloid. He

postulated that the *open 3* conformer, thought by many researchers to be a prerequisite for high enantioselectivity in pyruvate ester hydrogenation, was destabilised with the introduction of an electron withdrawing group at the *C9* position of the alkaloid leading to a more closed modifier conformational population.

A similar solvent dependence on the sense of enantioselectivity has been observed by Bartók [8] when using a 1,2-amino alcohol derivative of *L*-tryptophan as a chiral modifier in the hydrogenation of ethyl pyruvate over 5% Pt/γ-Al_2O_3. Bartók observed (*S*)-lactate was preferentially formed when the reaction was conducted in acetic acid and (*R*)-lactate preferentially formed when toluene was the reaction solvent. They attributed the inversion in enantioselectivity to transformations (detected using mass spectrometry) of the modifier in acetic acid, which was not detected when the reaction was conducted in toluene. In light of Bartók's observations it was imperative to determine the stability of the modifier, under the reaction conditions examined.

Detailed ^{1}H NMR experiments were conducted to determine the stability of the modifier in solution with special attention paid to the possible formation of the hydrolysis by-products 4-chlorobenzoic acid and hydroquinidine which can inevitably influence the enantioselective outcome of the reaction. Quinidine is known to preferentially form (*S*)-ethyl lactate in dichloromethane with an e.e. of 56% [10] and would be in direct competition with the hydroquinidine-4-chlorobenzoate modifier. Baiker [11] has carried out detailed studies into the non-linear relationship of enantioselectivity between mixtures of modifiers in the autoclave reactor and determined that a modifier, which is minor in concentration, through more efficient adsorption at the platinum surface, can control the enantioselective outcome of the reaction. The presence of 4-chlorobenzoic acid can also influence the conformational population of the non-hydrolysed modifier through protonation of the quinuclidine nitrogen atom. The ^{1}H NMR results presented in

Figure 5.4 clearly show that hydroquinidine-4-chlorobenzoate was stable in both dichloromethane and acetic acid with no formation of hydrolysis products. An additional experiment where 4-chlorobenzoic acid was added to the reaction did not alter the enantioselection observed in the reaction discounting, any influence this potential product of hydrolysis had on the enantioselective outcome of the reaction. Thus, modifier instability must be considered to be eliminated as an explanation for the enantioinversion observed between reaction solvent and modifier concentration.

It is known that the nature of the solvent can significantly effect the conformation the modifier adopts under reaction conditions [12] through dipolar interactions. Polar solvents serve to stabilise the closed conformer due to inherently larger dipole moments and a shift to a more polar solvent system leads to an increase in the population of closed conformer.

Changes in the appearance of the hydroquinidine-4-chlorobenzoate ^{1}H NMR spectra in acetic acid and dichloromethane are considered to be caused solely by conformational changes to the modifier induced by the solvent analogous to the spectral changes observed for cinchonidine [13]. Potentially the quinuclidine nitrogen atom of the modifier becomes protonated in acetic acid which results in a conformational population shift towards the *open 3* conformer, a conformation which is not so prevalent when the reaction is conducted in dichloromethane. Thus, at the same modifier : platinum ratio the modifier conformational distribution is sufficiently different to yield an excess of (*S*)-lactate in acetic acid while (*R*)-lactate is preferentially formed in dichloromethane. However such different solvent modifier dependent conformational distributions do not explain the modifier concentration dependent inversion in enantioselectivity exhibited when the reaction is conducted solely in dichloromethane.

5.3.2 Catalyst pre-treatment reduction temperature and its effect on enantioselective inversion

There are contradicting opinions on the influence platinum particle size, shape and morphology have on enantioselectivity in the Orito reaction [14-16] yet for certain hydrogen pre-treatment of $Pt/\gamma\text{-}Al_2O_3$ catalysts at elevated temperatures can improve enantioselectivity in the hydrogenation of activated ketones [17, 18]. The results presented in Figure 5.5 clearly show that enantioinversion in ethyl pyruvate hydrogenation is dependent upon the temperature of catalyst pre-treatment, a clear enantiomeric swing (approx. 40%) is observed for the reaction with enantioselectivity switching from (*S*)- to (*R*)-lactate over the range tested when the catalyst was reduced at 400 °C prior to reaction. The catalyst reduced at 200 °C generates racemic lactate at low modifier : platinum ratios and (*R*)-ethyl lactate at higher modifier : platinum ratios where as when the platinum was reduced at 100 °C an excess of (*R*)-ethyl lactate was generated across the whole modifier range tested with the e.e. increasing from 5% to 15%.

In relation to catalyst activity, Table 5.3 indicates that higher pre-treatment temperatures are beneficial to the initial rate of reaction. The initial rate data for the catalysts reduced at 200 °C and 400 °C are comparable across the whole modifier range tested however, when the catalyst was reduced at 100 °C the initial rate was approximately 50% lower. Such an observation would indicate that cleaning of the platinum surface of impurities does not take place at 100 °C and that these surface impurities may block the efficient adsorption of modifier and reagents.

Thermal pre-treatment of $Pt/\gamma\text{-}Al_2O_3$ catalysts at elevated temperatures [19] can lead to sintering of platinum nanoparticles to form larger agglomerates which can be accompanied by the potential restructuring of the platinum surface. Baiker [20] has reported a change in the mode of adsorption of alkaloid modifiers at platinum surfaces

with increasing alkaloid coverage. Such overcrowding can potentially alter the conformation the modifier adopts on the platinum surface; therefore, influence the enantioselectivity of the reaction. The point at which overcrowding alters the adsorption mode of the modifier and its prospective surface conformation is directly linked to the size of the platinum particle and therefore the temperature at which the catalyst was reduced. The platinum catalyst reduced at 400 °C potentially has a larger average platinum particle size than those catalysts reduced at lower temperatures, therefore the modifier concentration at which overcrowding alters the adsorption mode and surface conformation of the modifier is higher than those catalysts reduced at lower temperature. Thus, in the case of the catalyst reduced at 100 °C the average platinum particle size is of a size that alkaloid overcrowding takes place at the lowest modifier concentrations leading to the preferential formation of (*R*)-lactate. For the catalyst reduced at 400 °C at low modifier concentrations (*S*)-lactate is preferentially formed and as the concentration of modifier is increased overcrowding becomes an issue and the modifier is forced to adopt a conformation which preferentially yields an e.e. in favour of the (*R*)-enantiomer. These observations serve as a possible explanation for the enantioselective switch observed at high modifier : platinum ratios when ethyl pyruvate was hydrogenated over the 5% Pt/γ-Al_2O_3 catalyst reduced at 400 °C.

To give credence to the above model, detailed microscopic analysis was carried on the reduced catalyst samples to try and establish a link between modifier concentration dependent enantioinversion and platinum particle size. The microscopic data of the catalysts reduced at 100 °C and 400 °C, are shown in Figure 5.7 are difficult to differentiate in terms of particle size and particle distribution. Figure 5.8 compare a single platinum crystallite of the two catalysts, the particles in both cases have truncated

cube-octahedral morphologies and expose low energy {111} and {200} facet planes, which are indistinguishable.

Significant sintering of platinum nanoparticles at the relatively low reduction temperatures employed was not observed. Platinum is a refractory metal with a melting point (T_m) of 1772 °C. Taking into account the possibility of a significant melting point depression at the nanoscale, the pre-treatment temperature of 400 °C is still probably less than $0.4T_m$. Thus, the enantioinversion observed between the catalysts reduced at 100 °C and 400 °C cannot be related to the sintering of the platinum nanoparticles or morthphological alterations to the platinum crystallites.

It is possible that the temperature of reduction has an effect on the structure of the catalyst support and this has a bearing on the sense of enantioselectivity and the effect of catalyst support is discussed in the following section.

5.3.3 Catalyst support effects

The effect of catalyst support on enantioinversion was investigated. Platinum supported on silica, graphite and alumina were reduced at 400 °C and their effect on enantioinversion investigated at modifier : platinum ratios between 0.18 and 8. The results of these experiments were presented in section 5.2.5. Enantioinversion was only observed for the Pt/γ-Al_2O_3 catalyst with an enantiomeric swing of 43% from the (*S*)- to the (*R*)- enantiomer as the modifier : platinum ratio was increased. Both silica and carbon platinum supported catalysts resulted in the selective formation of (*R*)-lactate whatever the modifier : platinum ratio used.

A catalyst support performs several functions; most importantly, it maximises the surface area of the catalytically active metal phase (*i.e.* platinum) and hinders the sintering of platinum at elevated temperatures. The platinum particles are in close proximity to the

support and can influence the activity of the metal catalyst in one of two ways. Firstly, the interaction between support and platinum can modify the electronic character of the catalyst particles which can affect the adsorption and reaction characteristics at the active site. Secondly, the extent of interaction between support and platinum can influence both shape and geometry of the platinum crystallite. Sintering studies of platinum catalysts in a hydrogen atmosphere [21] indicated that metal - support interaction decreased in the order Al_2O_3 > C > SiO_2 for platinum based catalysts. Previous microscopic studies illustrate that platinum particles on both the silica [22] and alumina support (Figure 5.7) are of similar size and morphology and can also be discounted as the origin of enantioinversion as was the case in the series of Pt/γ-Al_2O_3 catalysts studied.

Therefore, consideration must be given to the adsorption characteristics of the support material which are governed by its surface functionality. Silica is an acidic support rich in hydroxyl groups, while carbon, also acidic in nature, has a surface covered in carboxylic acid and phenolic hydroxyl groups. Both these acidic supports favour interaction with cationic species while γ-alumina is amphoteric. The inferior rate of reaction exhibited by the acidic silica- and carbon- supported platinum catalysts compared to that of alumina, suggests that support functionality has a bearing on both the sense of asymmetric induction and on the rate of reaction. Rate data suggests that larger amounts of modifier are preferentially adsorbed at the surface of these acidic supports, most probably *via* the highly polarised carbonyl carbon atom of hydroquinidine-4-chlorobenzoate, an interaction which appears not to be so prominent with the alumina phase. Such an interaction can potentially explain the failure of these acidic supports to exhibit the same enantioinversion shown by the alumina catalyst. It may be that at low modifier concentrations the modifier preferentially adsorbs at the platinum interface sites which remain under the direct influence of the support dictating the crucial torsion angle

about the *C8-C9* bond, therefore, influencing the surface conformation adopted and having a directing influence on the sense of enantioselectivity. This, in the case of silica and carbon supports, favours the formation of the (*R*)-enantiomer, a conformation which is retained at higher concentration dictating the progress of the reaction.

For the less acidic alumina, the interaction between modifier and support at the edge site may not be so pronounced or of a different type and thus influence the conformation of the modifier in a different manner. This would lead to the preferential formation of the (*S*)-enantiomer at low modifier : platinum ratios. As the amount of hydroquinidine-4-chlorobenzoate is increased, more of the bulk platinum surface becomes modified and the conformation of the alkaloid becomes dictated by the polarity of the solvent and so the influence of the support becomes less pronounced, to the extent where the sense of asymmetric induction observed is inverted.

Such observations may also serve to explain the failure of the alumina catalysts pre-treated at 100 °C and 200 °C to exhibit enantioinversion. It is known that the pre-treatment temperature affects the degree of hydroxylation at the alumina surface. An increase in reduction temperature will reduce the number of hydroxyl groups on the alumina surface, thus, the catalyst reduced at 400 °C will, by definition, have less hydroxyl groups on its surface and the interaction between modifier and alumina at the platinum edge site will be very different to those catalysts reduced at lower temperatures. Such interactions may influence the surface conformation the modifier adopts and explain the enantiomeric switch only observed for those $Pt/\gamma\text{-}Al_2O_3$ catalysts reduced at 400 °C.

5.4 Conclusion

This is the first observation for any heterogeneously catalysed asymmetric reaction where the sense of enantioselectivity is affected solely by changing the concentration of the modifier and is clearly an unprecedented finding given the volume of work conducted on this model reaction. Although the absolute change in e.e. is not particularly high, it is significant and similar in magnitude to the effects observed in previous studies where it is induced by changes in reaction conditions.

Modifier stability, platinum particle size and morphology have been discounted as an explanation for enantioinversion. The effect is only observed for a platinum supported alumina catalyst which had been previously reduced at a temperature of 400C, implying the nature of the catalyst support influences the enantioselective outcome of the reaction. It is possible at low hydroquinidine-4-chlorobenzoate modifier concentrations the modifier preferentially adsorbs at the platinum - support interface site and interact with the surface hydroxyl groups of the support influencing the conformation of the modifier to yield (*S*)-lactate. As the amount of hydroquinidine-4-chlorobenzoate is increased, more of the bulk platinum surface becomes modified and the conformation of the alkaloid becomes dictated by the polarity of the solvent and so the influence of the support becomes less pronounced, to the extent where the sense of asymmetric induction observed is inverted.

5.5 References

1 M. von Arx, T. Mallat and A. Baiker, *Topics Catal.*, **19** (2002) 75.

2 T. Mallat, Z. Bodnar, B. Minder, K. Borszeky and A. Baiker, *J. Catal.*, **168** (1997) 183.

3 D.G. Blackmond, *J. Catal.*, **176** (1998) 267.

4 T. Mallat and A. Baiker, *J. Catal.*, **176** (1998) 271.

5 M. von Arx, T. Mallat and A. Baiker, *Angew. Chem. Int. Ed.*, **40** (2001) 2302.

6 R. Hess, A. Vargas, T. Mallat, T. Bűrgi and A. Baiker, *J. Catal.*, **222** (2004) 117.

7 S. Diezi, A. Szabo, T. Mallat and A. Baiker, *Tetrahedron: Asymm.*, **14** (2003) 2573.

8 M. Bartók, M. Sutyinski, K. Felföldi and G. Szöllósi, *Chem. Commun.*, (2002) 1130.

9 S. Cserényi, K. Felföldi, K. Balázsik, G. Szöllósi, I.Busci and M. Bartók, *J. Molec. Catal., A,* **247** (2006) 108.

10 H.U.Blaser, H.P. Jalett, W.Lottenbach and M. struda, *J. Am. Chem. Soc.*, **122** (2000) 12675.

11 L. Balazs, T. Mallat and A. Baiker, *J. Catal.*, **233** (2005) 327.

12 T. Burgi and A. Baiker, *J. Am. Chem. Soc.*, **120** (1998) 1290.

13 R.P.K. Wells, N.R McGuire, X. Li, R.L. Jenkins, P.J. Collier, R. Whyman and G.J. Hutchings, *Phys. Chem. Chem. Phys.*, **4** (2002) 2839.

14 J. T. Wehrli, A. Baiker, D. M. Monti and H.U. Blaser, *J. Mol. Catal.*, **61** (1990) 207.

15 J.T. Wehrli, A. Baiker, D.M. Monti, H.U. Blaser and H.P. Jalett, *J. Mol. Catal.*, **49** (1989) 195.

16 H. Bonnemann and G.A. Braun, *Angew. Chem. Int. Ed.*, **35** (1996) 1992.

17 Y. Orito, S. Imai and S. Niwa, *J. Chem. Soc. Jpn.*, (1980) 670.

18 H.U. Blaser, H.P. Jalett, D.M. Monti, J.F. Reber and J.T. Wehrli, *Stud. Surf. Sci. Catal.*, **41** (1988) 153.

19 G.A. Attard, K.G. Griffin, D.J. Jenkins, P. Johnston and P.B. Wells, *Catalysis Today,* **114** (2006) 346.

20 D. Ferri, T. Bürgi and A. Baiker, *J. Chem. Soc. Chem. Commun.*, (2001) 1172.

21 R.T. Baker, E.B. Prestridge and R.L. Garten, *J. Catal.,* **56** (1979) 390.

22 N.F. Dummer, R.L. Jenkins, X. Li, S.M. Bawaked, P. McMorn, A. Burrows, C.J. Kiely, D.J. Willock, R.P.K. Wells and G.J. Hutchings, *J. Catal.,* **245** (2007) 487.

Chapter Six

Chapter Six Final Comments and Future Work

6.1 Enantioselective hydrogenation of ethyl pyruvate over cinchonidine modified Pt-AlMCM-41

6.1.1 Final Comments

The lure of working with large molecules of commercial interest has been a driving force in the development of new supports with mesoporous structures that can accommodate larger pro-chiral synthons, which are excluded from the pores of zeolites. It was for this reason that work was undertaken to synthesise a series of AlMCM-41 catalysts as a support for platinum and the subsequent examination of these Pt-AlMCM-41 catalysts, modified with cinchonidine, for the asymmetric hydrogenation of ethyl pyruvate.

Enantioselectivities were observed close to that obtained with the standard reference catalyst EUROPT-1 (6.3% Pt/silica), however reaction rates were lower moderated by an order of magnitude by mass transfer limitations within the mesopore or the potential blocking of the mesopore by platinum which will reduce the available platinum surface area for reaction. However the level of enantioselectivity was impaired when the platinum particle size in the mesopore was of such a size (< 0.7 nm) that there was inefficient modification of the particle and the racemic reaction favoured.

6.1.2 Future work

1 AlMCM-41 is a versatile support that can be tailored to produce materials having various uniform pore sizes. We have found that pore size has a bearing on catalytic activity and enantioselectivity in ethyl pyruvate hydrogenation and is a factor which warrants further investigation.

2 Preliminary studies examined the hydrogenation of ethyl pyruvate, a relatively small molecule for which the pore size will only have a limited influence. In combination with point **1** it may be possible to hydrogenate molecules of larger dimensions for which the pore size and support composition may have a positive influence on the enantioselective outcome of the reaction.

3 Pt-AlMCM-41 was an obvious starting point for an initial investigation as platinum catalysed α-ketoester hydrogenation is well understood. As this has been successfully accomplished, AlMCM-41 warrants further investigation as a support for other metals such as palladium which will allow the enantioselective hydrogenation of C=C containing pro-chiral substrates.

6.2 Enantioselective hydrogenation of pyruvate esters in a continuous flow reactor

6.2.1 Final Comments

It has been shown that cinchonidine pre-modified catalysts perform well in the enantioselective hydrogenation of pyruvate esters in the continuous flow reactor operating under mild conditions, with e.e. values (> 70%) comparable to when the reaction is conducted in the same solvent at elevated hydrogen pressures in an autoclave reactor while higher than the e.e. values (≥ 50%) obtained when the reaction was conducted in the gas phase [1].

Maximum and sustained enantioselectivity is not obtained unless the concentration of cinchonidine used in pre-modification is greater than 3.4 mM. A pre-treatment step where dichloromethane is allowed to flow through the catalyst bed for a minimum of 0.5 h prior to the introduction of reagents to the bed is highly beneficial to the enantioselective outcome of the reaction.

Activity is seen to decrease with time on-line, contrary to the autogeneous system where enantioselectivity and activity rise simultaneously until approx. 40% of conversion to products is reached.

Initial transients are observed for methyl and ethyl pyruvate as reaction substrates which last up to 15 min, yet no such transient is observed when substrates are switched mid reaction, suggesting that the catalytic site is optimized for stable enantioselectivity after this initial period.

The pre-treatment of the catalyst bed with (*R*)-ethyl lactate prior to the introduction of methyl pyruvate is detrimental to the catalytic system with an 18% drop in enantioselectivity, potentially the result of an unfavourable interaction between lactate and modifier or the initiation of polymer formation. Such observations imply that in the CFR reactor the enantioselective hydrogenation of pyruvate esters is self poisoning.

6.2.2 Future work

1 The reaction conditions employed in the continuous flow reactor are mild compared to those found in the literature [2]. Further enhancements in enantioselectivity and activity were not possible with the current experimental equipment. The commissioning of a high pressure continuous flow reactor could prove beneficial to improving enantioselectivity and prolonging catalyst activity.

2 The challenge is to develop new systems and diversify our present knowledge to hydrogenate other pro-chiral functionalities such as C=N and C=C over other metals supported on new catalyst supports; there are no reports of copper, iron or cobalt exhibiting enantioselectivity when modified with cinchona alkaloids.

3 The utilisation of mesoporous materials as a catalyst support, such as the M41S family of materials, with their high surface area and uniform pore structure may increase the contact time between catalyst and substrate and is a line of research worth pursuing.

6.3 Inversion of the sense of enantioselectivity

6.3.1 Final Comments

The ability to alter the sense of enantioselectivity by controlling the amount of alkaloid used in a reaction is a truly intriguing observation. It is generally accepted that enantioselectivity originates from a specific interaction between a cinchona alkaloid modifier and pyruvate or related substrate at a platinum surface.

The results presented in the previous chapter indicate catalyst support, modifier concentration and catalyst pre-treatment all appear to have a bearing on such an interaction and thus on the enantioselective outcome of the reaction. The effect is sensitive to the way in which the $Pt/\gamma\text{-}Al_2O_3$ catalyst is prepared with reduction temperature determining if inversion of enantioselectivity was observed. The same experiments conducted over platinum silica and platinum graphite catalysts failed to demonstrate the same modifier concentration dependence on the sense of enantioselectivity.

NMR has been used to confirm the stability of the modifier when in solution; HRTEM has been used to determine the morphology and size of the platinum particle for the different reduced $Pt/\gamma\text{-}Al_2O_3$ catalysts and were indistinguishable. Thus, the nature of this interaction and the mechanism which leads to enantioinversion is not clear from the work undertaken and certainly warrants further investigation.

6.3.2 Future work

1 The synthesis of hydroquinidine-4-chlorobenzoate analogues, some with fixed conformations, will help in establishing the interaction between modifier, substrate and catalyst and the elucidation of the origin of enantioinversion.

2 The conduction of equivalent experiments over metals other than platinum, for example palladium and iridium, to establish if the phenomenon of enantioinversion is metal specific, would augment this investigation.

3 The initiation of detailed NMR studies using selective NOE experiments and 2D NOESY experiments analogous to those conducted on cinchonidine by Baiker [3] can be used to determine the conformational distribution of the hydroquinidine-4-chlorobenzoate molecules in solution.

4 Computational chemistry calculations can be used to determine the most stable conformation at the platinum surface and determine the interaction of the modifier with the substrate.

6.4 References

1. M. von Arx, N.F. Dummer, D.J. Willock, S.H. Taylor, R.P.K. Wells, P.B. Wells and G.J. Hutchings, *J. Chem. Soc. Chem. Commun.*, (2003) 1926.

2. M Künzle, R. Hess, T. Mallat and A. Baiker, *J. Catal,*. **186** (1999) 239.

3 T. Burgi and A. Baiker, *J. Am. Chem. Soc.*, **120** (1998) 1290.

Appendix A

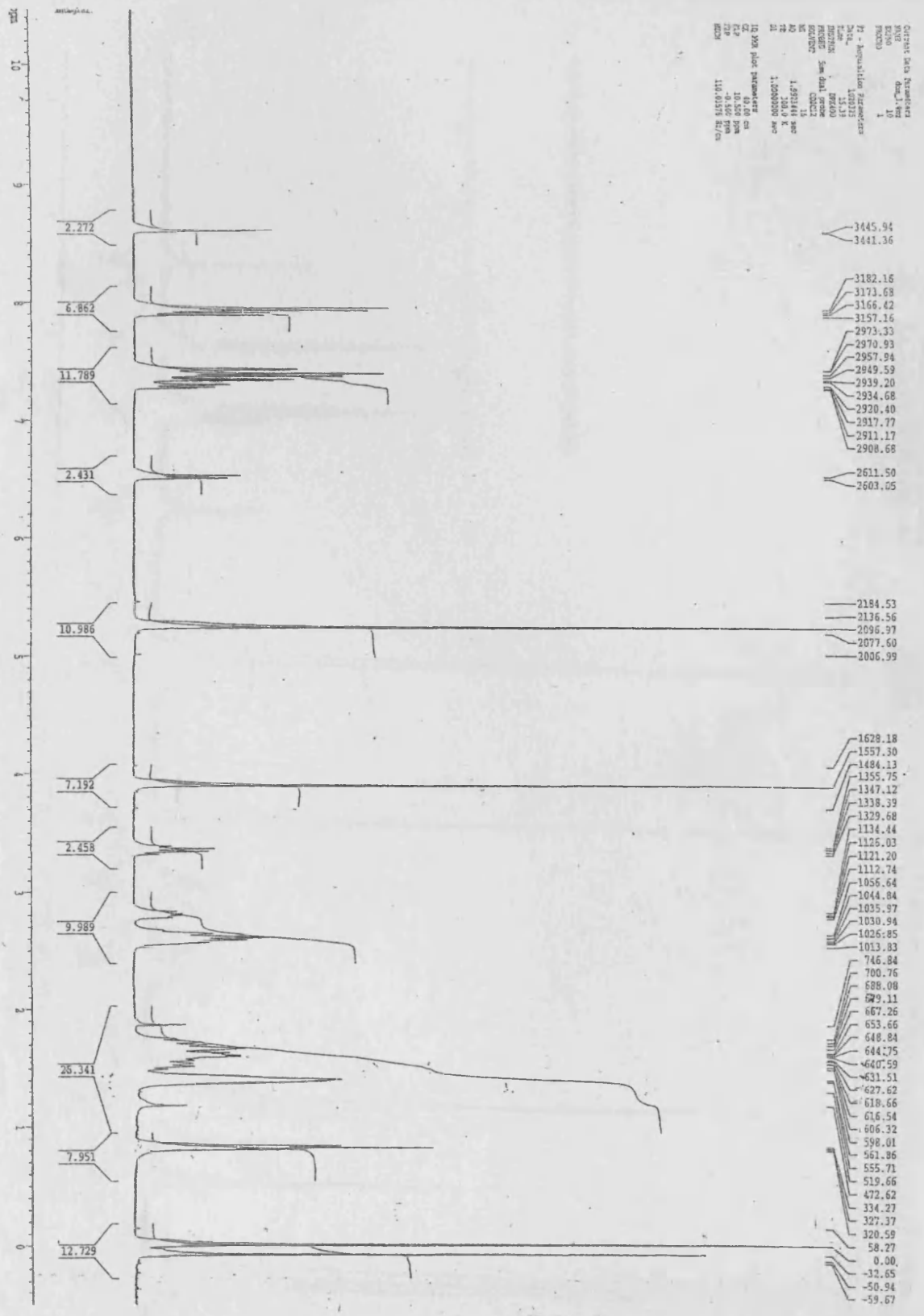

^{1}H NMR spectra of hydroquinidine-4-chlorobenzoate (7.3 μmol) in dichloromethane

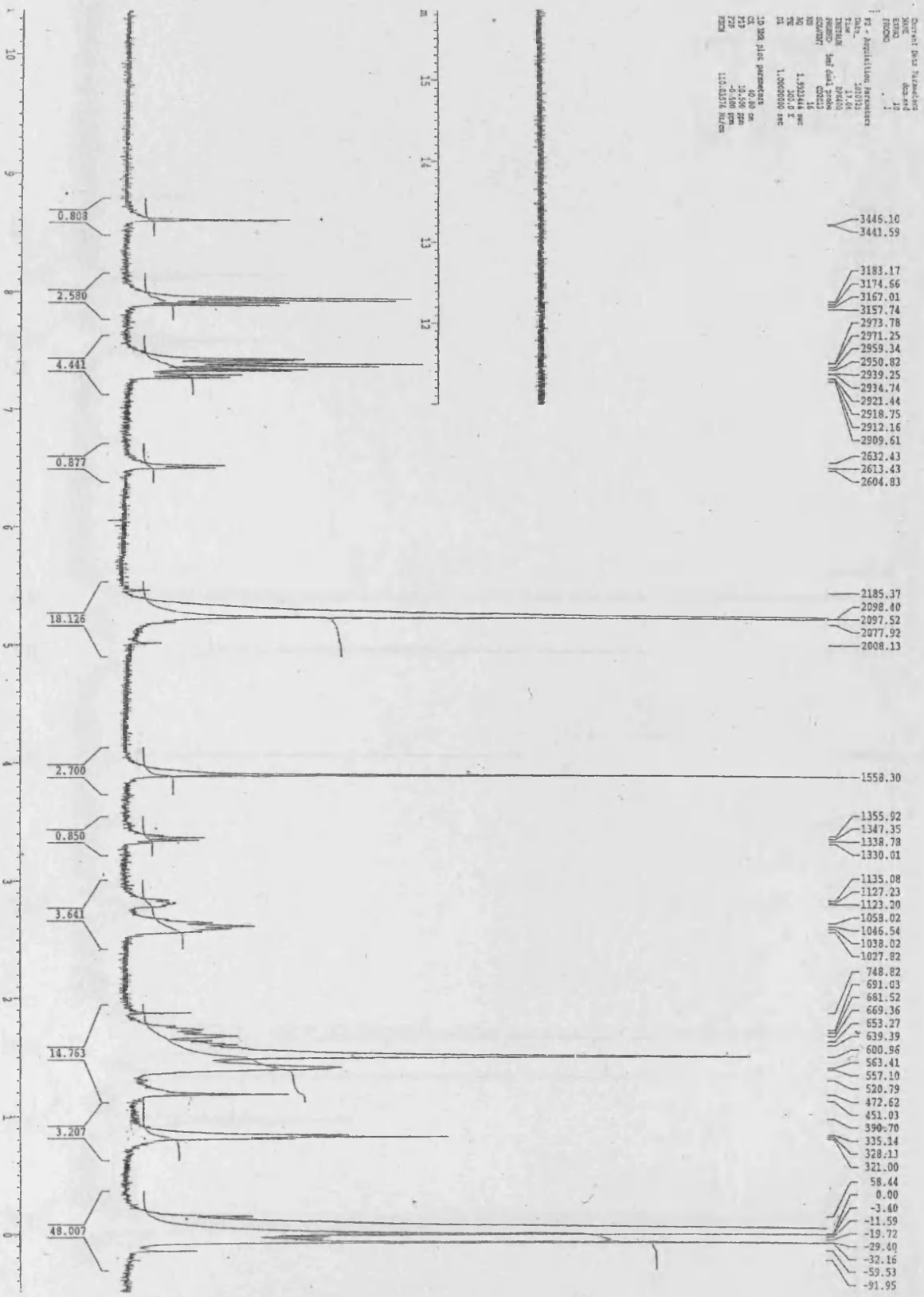

^{1}H NMR spectra of hydroquinidine-4-chlorobenzoate (1.3 μmol) in dichloromethane

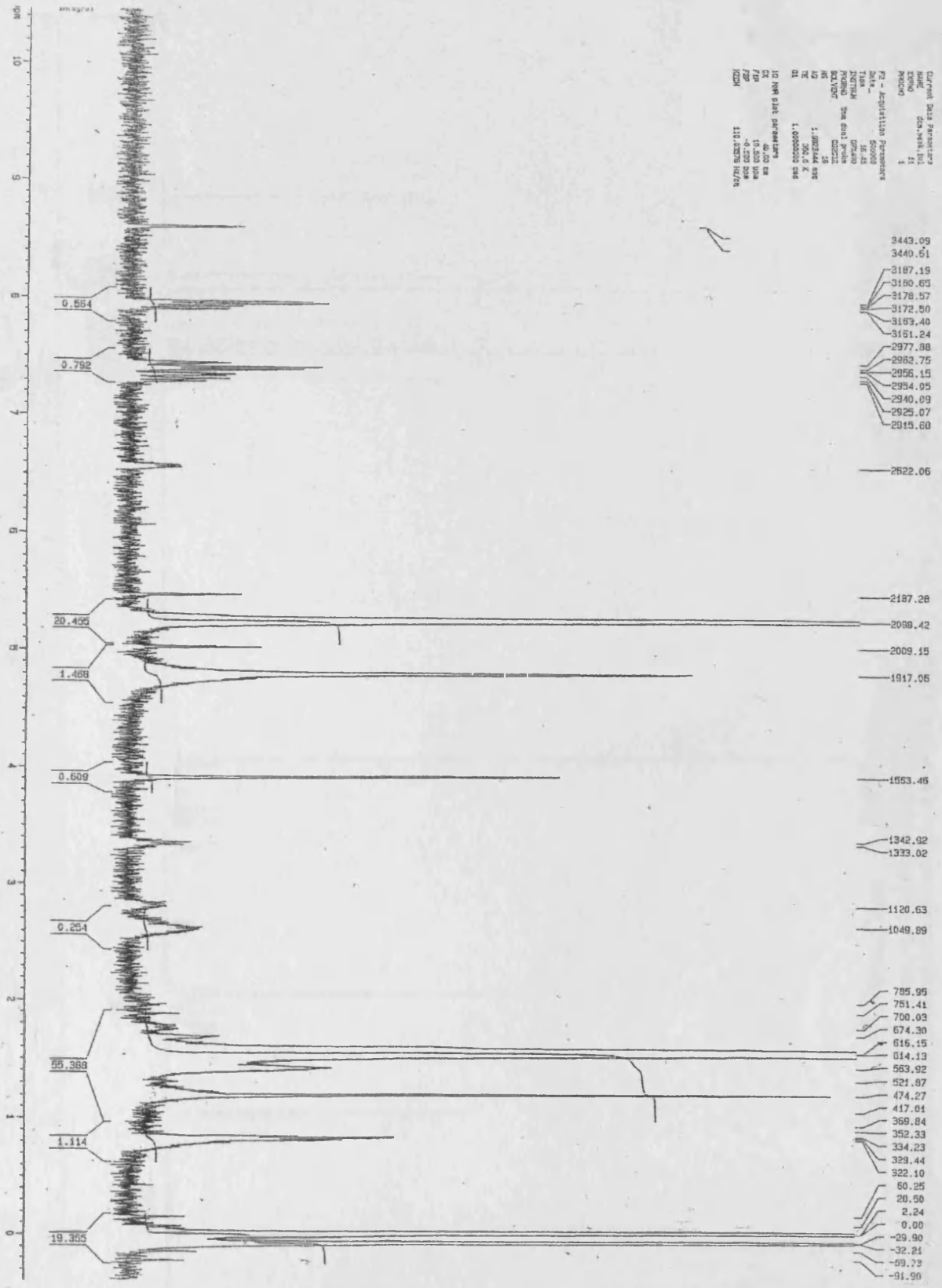

^{1}H NMR spectra of hydroquinidine-4-chlorobenzoate (0.1 μmol) in dichloromethane

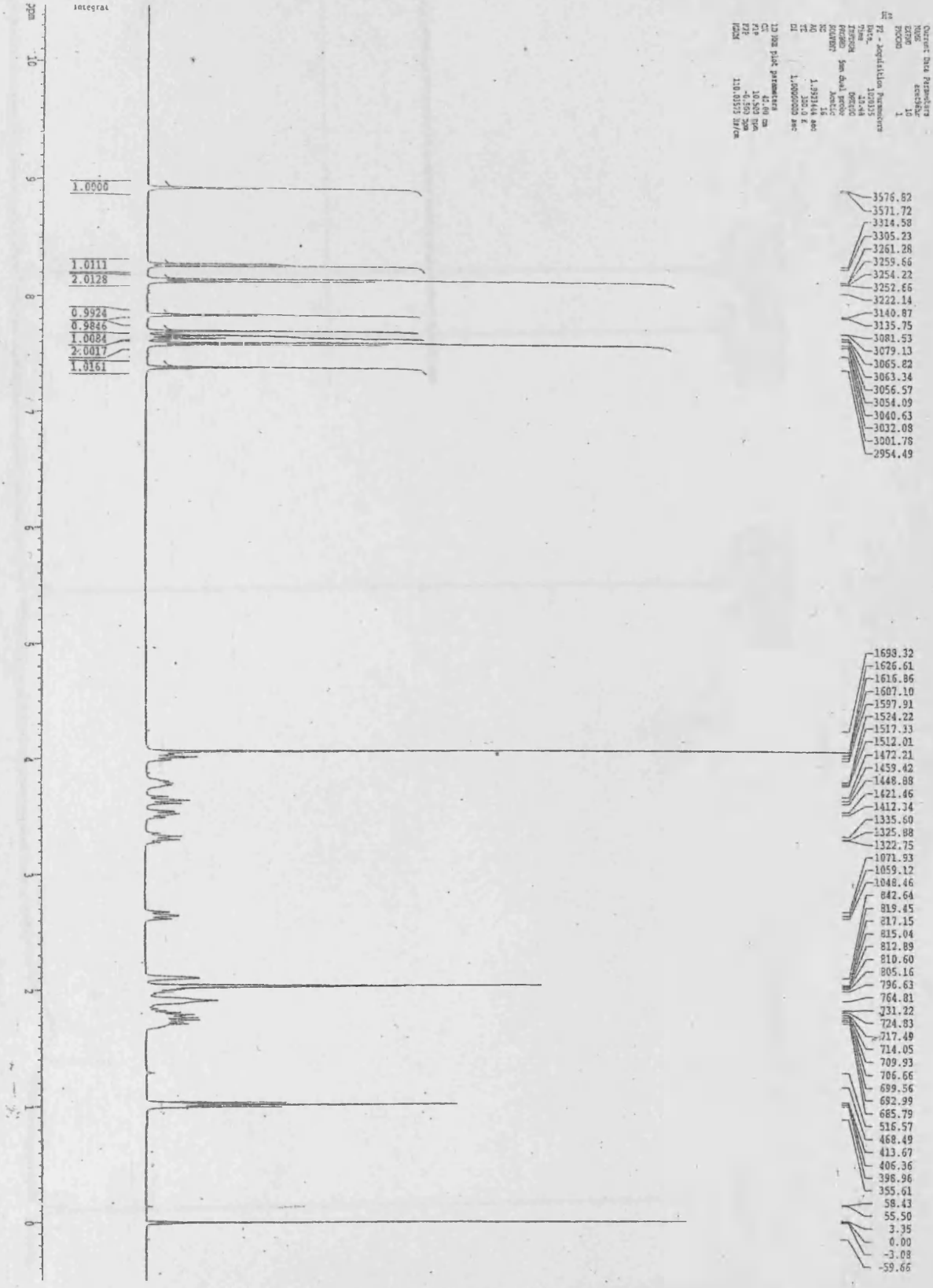

^{1}H NMR spectra of hydroquinidine-4-chlorobenzoate (7.3 μmol) in acetic acid

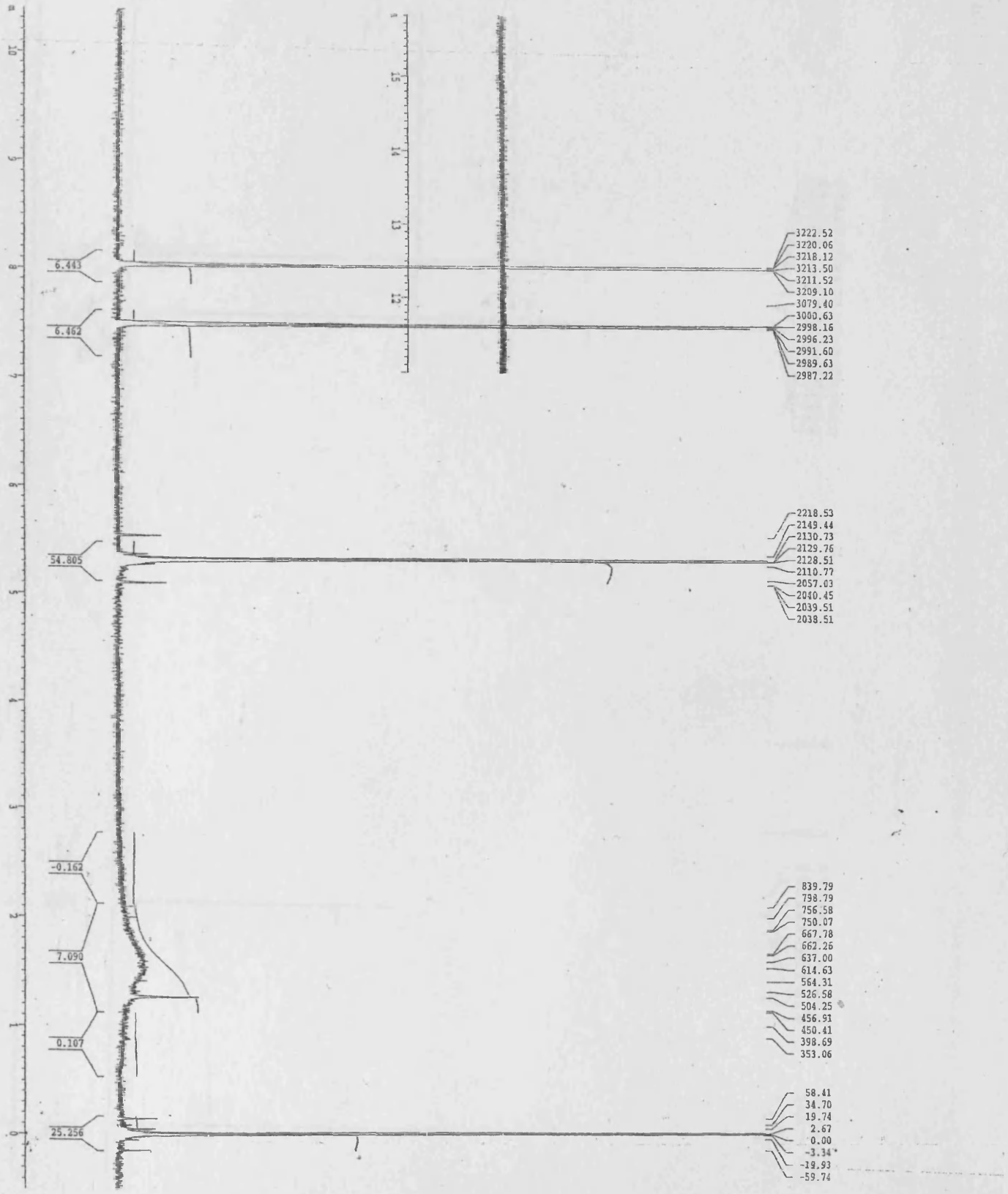

^{1}H NMR spectra of 4-chlorobenzoate in dichloromethane

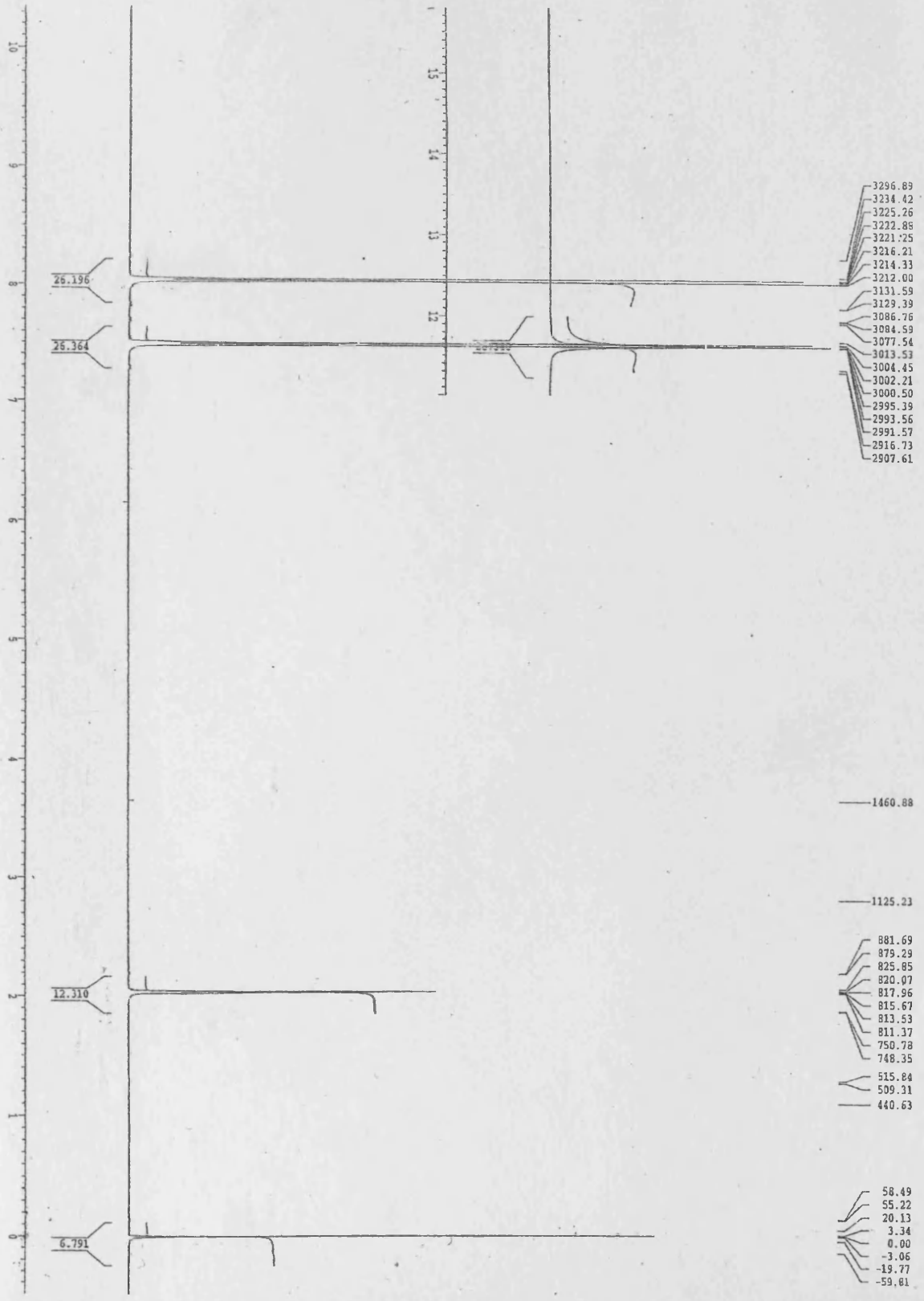

^{1}H NMR spectra of 4-chlorobenzoate in acetic acid